LICENTIATE THESIS

Green Urban Drainage Infrastructure

Hydrology and Modelling of Grass Swales

Hendrik Rujner

Urban Water Engineering

LULEÅ TEKNISKA UNIVERSITET

Green Urban Drainage Infrastructure

Hydrology and Modelling of Grass Swales

Hendrik Rujner

Luleå, 2018

Licentiate thesis

Division of Architecture and Water
Department of Civil, Environmental and Natural Resources Engineering
SE-97187 Luleå University of Technology
Sweden

Printed by Luleå University of Technology, Graphic Production 2018

ISSN 1402-1757
ISBN 978-91-7790-035-1 (print)
ISBN 978-91-7790-036-8 (pdf)

Luleå 2018

www.ltu.se

Acknowledgements

This thesis is based on research that was carried out in the Urban Water Research Group, at the Department of Civil, Environmental and Natural Resources Engineering at Luleå University of Technology (LTU). The studies were conducted within the research cluster Stormwater & Sewers (Dag & Nät), a collaboration between the Urban Water Research Group and the Swedish municipalities of Luleå, Skellefteå, Östersund, Umeå (VAKIN) and Sundsvall (MSVA) which is supported by the Swedish Water and Wastewater Association (Svensk Vatten). The studies were also supported as a part of the project GreenNano (GrönNano), which is funded by VINNOVA and within the projects "ALICE – Attractive Living In Cold Environment" (2015-121) as well as "Reliable modelling of Green Infrastructure in green catchments – Calibration, validation and uncertainty assessment [Swedish: Förbättrad modellering av grön infrastruktur i gröna avrinningsområden] (2015-151) both funded by The Swedish Research Council FORMAS.

The field studies would have been not possible without the help of the staff from Luleå municipality, Department of Urban Planning, Division of Water and Wastewater (Stadsbyggnadsförvaltningen, Avdelning Vatten och Avlopp) who helped me with logistics and equipment and without my PhD colleagues in the Urban Water Research Group who helped during the experiments for which I am grateful. DHI Sweden kindly provided a license for Mike SHE, which facilitated the modelling study. I am also grateful to Stefan Marklund and Fredrik Nyström who helped me with translations and for the kind support from Maria Roldin from DHI Sweden.

I would like to express my thankfulness to my academic supervisors who made this work possible. To my main supervisor Professor Maria Viklander special thanks for your kindness, motivation and scientific guidance, co-supervisor Professor Jiri Marsalek special thanks for your scientific and professional advices and guidance - I learned a lot, thanks to Dr. Anna-Maria Perttu and also particularly Dr. Günther Leonhardt for all the helpful scientific discussions and very kind support. Thanks for your patience; it was an honour to work under your supervision.

Over the years I enjoyed working together with old and new friends and colleagues of the research group. Thanks Shahab and Matthias for the unforgettable time together within and outside the university and for your emotional support. Thank you also Oleksandr and Helen for the shared time and friendship. Brenda, Joel and Youen thank you for taking over. To Inga and Godecke I would also express my sincere appreciation for the time together and all encouraging words.

Finally, I would like to thank my family in Germany and my wonderful girlfriend for always supporting me. Thanks to my parents, grandparents, my sister, Johannes, Christoph and Dilhan and thank you Glacialle for being with me! Without some friends I would not be where I am: My sincere thanks therefore go also to Antje K. and Nigel D.

Thank you all!

Hendrik Rujner Luleå, February 2018

Abstract

The management of urban runoff has evolved along with the advancement of understanding of runoff environmental impacts. Besides the impacts on water quality in the receiving waters, the effects on the urban hydrologic regime include reduced infiltration by the sealing of pervious land, reduced evapotranspiration by removal of vegetation, and the resulting increase of stormwater runoff peaks and volumes causing flooding, and ultimately degradation of receiving waters. In such considerations, urban stormwater management benefits from the implementation of Green Infrastructure which includes decentralized vegetative controls that capture and infiltrate rain where it falls and thus reduce and improve stormwater runoff. An example of small scale elements of Green Infrastructure are traditional grass swales. Through shallow depressions with mild side slopes grass swales collect and infiltrate stormwater from parking lots and roads, while runoff flows are attenuated and further conveyed depending on the hydraulic loading. Grass swales usually operate reliably and their maintenance needs are well understood. Their hydrological performance is, beside their dimensions and the contributing area, determined mainly by hydraulic and soil-related hydrological parameters that change with the intensity of the storm. Yet, because swales discharge to downstream drainage elements, either to the conventional sewer system or to other stormwater management facilities, knowledge of the underlying inter-related processes and influential factors that govern the hydraulic and hydrological performance of grass swales is required.

Against this background, this thesis is devoted to such questions as (i) what are the differences in the hydraulic and hydrological performance of the studied swales, (ii) how do soil characteristics, including the antecedent soil moisture, influence the swale water balance for various hydraulic loadings; and (iii) how can the related hydrological processes be simulated in high-resolution and reliably predicted using a grid-based, distributed model. For this purpose, full-scale studies were performed in three 30-m grass swale sections in Luleå, Northern Sweden, by collecting hydraulic and hydrological data based on routine storm events mimicking block-rainfall storm events of 2 months and 3 years recurrence. The resulting runoff and soil moisture data were used to calculate the swale water balance, to derive event hydrographs and to obtain calibration and validation data for model simulations. The experimental results showed that the relative swale flow volume reduction decreased with an increasing soil moisture and indicated the transition in dominating swale functions: at low initial SWC, runoff was highly attenuated (up to 74%), but for high SWC, the conveyance function dominated (with attenuation as low as 17%). Runoff flow peaks were reduced, proportionally to the volume reductions. Swale outflow hydrograph lag times varied between 5 to 15 minutes and decreased with increasing soil moisture. The swale wetness affected runoff formation, attenuation and subsequent outlet discharge and, for the short-duration events tested, only the top soil layer contributed to these findings. In the three swales tested, soils, initial soil water content, saturated hydraulic conductivity and topography varied spatially significantly. Double-ring infiltrometer measurements resulted in values of 1.78, 4.04 and 9.41 cm/hr (n=9) in the three swales tested and deviated from estimates from averages of spatially integrated infiltration rates. However, with regard to spatial variability, only the topography, described as irregularities in the swale bottom slopes affected the swale runoff dissipation and conveyance in the early phase of the events. Together with estimates of the water stored in the top soil layer, 4-32% of runoff volumes from the mimicked 2-month storm were temporarily stored. The distributed model Mike SHE was found capable of simulating swale drainage processes, when properly calibrated. Close agreement (NSE>0.8) was found not only for the measured and simulated swale outlet hydrographs, but also for the changes of the soil moisture in the top soil layer, which shows rapid increase up to the saturated soil water content, but minor or no progression in depths of 0.2 m. The model output was little sensitive to the initial soil water content, especially for low inflow which resulted in larger residuals in simulated runoff peak flows and volumes. As in field measurements, spatial variability of the initial soil water content had no effect on the swale outflow, but the accuracy of the topographical representation. The thesis findings include several implications regarding effects of the assessed parameters in the application of the model for swale flow simulation and eventually the design of grass swales.

Sammanfattning

Urban dagvattenhantering har utvecklats parallellt med en ökad förståelse för dagvattnets allmänna miljöpåverkan. Utöver ytvattenkvalitén i recipientvatten påverkas även den hydrologiska regimen genom reducerad infiltrationsförmåga i mark orsakad av allt tätare ytskikt samt reducerad evapotranspiration orsakad av minskad vegetationsutbredning. Detta ger både förhöjda toppflöden och avrinningsvolymer, vilket kan resultera i översvämning och slutligen en försämrad ytvattenkvalité i recipienterna. Dagens urbana dagvattensystem förändras mot en högre grad av grön infrastruktur som en central systemkomponent. Decentraliserad omhändertagning av dagvatten såsom svackdiken utjämnar och för bort dagvattensflöden, samtidigt som de fungerar tillförlitligt och deras underhållsåtgärder är välkända. Uppbyggda med små svackor och låglutande slänter samlar svackdiken in och infiltrerar dagvatten från parkeringsytor och vägar. Dessa svackdikens hydrologiska funktion bestäms av en rad faktorer, utöver teknisk dimensionering och avrinningsområdets storlek och hydrologi, även av hydraulik och jordartsrelaterad hydrologi som förändras beroende på respektive nederbördstillfälles intensitet och varaktighet. Eftersom svackdikens utflöde passerar nedströms liggande dagvattentekniker/anordningar, antingen konventionella ledningssystem eller andra teknologier, krävs full förståelse och kunskap om de faktorer som styr svackdikens hydraulik och hydrologi.

Mot denna bakgrund fokuserar avhandlingen på frågorna (i) vilka skillnader finns med avseende på hydraulisk och hydrologisk prestanda för de studerade svackdiken, (ii) i vilken mån påverkar markartsförhållanden, inklusive ingående markfuktighet, svackdikens vattenbalans vid varierande hydraulisk belastning; samt (iii) hur och i vilken mån kan ovanstående simuleras högupplöst och förutsägbart, via den rutnätsbaserade distribuerade modellen Mike SHE. Därför har fullskaliga studier bedrivits i två 30 m långa svackdiken i Luleå kommuns södra stadsområde, där hydrauliska och hydrologiska data insamlats baserat på standardiserade nederbördsförlopp, återskapande blockregn med 2 månaders och 3 års återkomsttid. Data för avrinning och markfukthalter användes för att beräkna svackdikenas vattenbalans, nederbördförloppens hydrografer samt erhålla kalibrering- och valideringsdata för modellsimuleringar. Resultaten från experimenten visade att den volymetriska flödesreduktionen minskade relativt sett med ökande markfukthalt, indikerande en övergång för svackdikets dominerande funktionalitet: vid låga initiala SWC var avrinningen tydligt dämpad (upp till 74%), medan för höga SWC innebar att transportfunktionen dominerade (med dämpningsgrad ner mot 17%). Avrinnande momentana toppflöden reducerades proportionellt mot volymreduktionen. Laggtiden för svackdikets utflödeshydrograf varierade mellan 5 och 15 minuter och reducerades med ökande markfukthalt. Fuktförhållandena i svackdiket påverkade avrinningsförloppet, flödesdämpning och efterföljande utsläpp, och enbart svackdikets översta markskikt berördes under de kortvariga bevattningscyklerna. I de tre testade svackdikena varierade jordart, initial markfukthalt, mättad hydraulisk konduktivitet och topografi signifikant. Mätningar med dubbelrings infiltrometrar gav följande resultat, 1.78, 4.04 samt 9.41 cm/h (n=9), vilket avvek från medelvärdesbaserat estimat från spatialt integrerade infiltrationshastigheter. Med avseende på spatial variabilitet påverkade endast svackdikenas topografi, i form av ojämnheter i och nära dikesbotten, avrinningsförloppen och bortledning under den inledande fasen av regnhändelsen. Sammantaget med uppskattningar av den lagrat vatten i marklagrets toppskikt, bedöms 4-32% av svackdikets ytavrinning från ett simulerade nederbördtillfälle med 2 månaders återkomststid kunna lagras tillfälligt. Mike SHE befanns kapabel att med god noggrannhet kunna reproducera naturbundna dräneringsförlopp och flöden i svackdiken, förutsatt tillbörlig kalibrering. God överensstämmelse (NSE>0.8) framkom inte bara mellan uppmätta och simulerade utgående hydrografer, utan också beträffande ändring av markfukthalt i ytligt marklager med snabb höjning av fukthalt upp emot full vattenmättnad. Däremot framkom endast mindre (eller total frånvaro av) överensstämmelse vad gäller markdjup av 0.2 m. Modellens output uppvisade låg känslighet för ursprunglig markfukthalt, speciellt gällande lågt flöde vilket resulterade i större residualer för simulerade toppflöden och avrinningsvolymer. För fältförsöken framkom att den initiala markfukthaltens spatiala variabilitet inte påverkade utflödet från svackdiket – i motsats till noggrannheten i dikets topografiska representation. Denna uppsats belyser samband och följdverkningar beträffande påverkan från undersökta parametrar på en modell för flödes- och vattenföring i ett svackdike och framledes framtida design av svackdiken.

Table of Contents

List of papers

Paper I Rujner, H. Leonhardt, G., Perttu, A-M., Marsalek, J. and M. Viklander (2016). Advancing green infrastructure design: Field evaluation of grassed urban drainage swales. In Novatech 2016: 9th International Conference on planning and technologies for sustainable management of Water in the City. Lyon, France.

Paper II Rujner, H., Leonhardt, G., Marsalek, J., & M. Viklander (in press). The effects of initial soil moisture conditions on swale flow hydrographs. Hydrological Processes (article in press).

Paper III Rujner, H., Leonhardt, G., Marsalek, J., & M. Viklander (submitted). High-resolution modelling of the grass swale response to runoff inflows with Mike SHE. (submitted to Journal of Hydrology, January 2018).

Table A: Own contribution to above papers.

		Paper I	Paper II	Paper III
Development of research idea		SR	SR	SR
Research study design		SR	SR	SR
Data collection		R	R	R
Data processing and analysis		SR	R	SR
Data interpretation		SR	SR	SR
Publication process	Manuscript preparation for publication	SR	SR	SR
	Responding to reviewers	SR	SR	NA

R: Responsible = develop, consulted (where needed) and implemented a plan for completion of the task
SR: Shared responsibility = made essential contribution towards the task completion in collaboration with other members of the research team
C: contributed = worked on some aspects of the task completion
NC: Not contributed = for valid reasons, has not contributed to compiling the task (e.g. joining the research project after the task completion)
NA: Not applicable

1. Introduction

Stormwater management by effective transport of water from urban areas has been an essential part of urban drainage for centuries. Currently, progressing urbanisation and climate change induced alteration of precipitation patterns and associated urban flooding and pollution of downstream areas, call for adaptation measures serving to mitigate harmful consequences of flooding and degradation of the receiving waters and aquatic habitats, caused by the disconnection of stormwater from the natural hydrological cycle (Fletcher et al., 2013; Semadeni-Davies et al., 2008; Marsalek, 2006; Barrett et al., 1998; U.S. EPA, 1983). Typically, the urban hydrological regime is characterised by increased runoff rates compared to natural catchments, contributing to higher runoff peaks and volumes and, at the same time, a partial loss of infiltration and evapotranspiration abstractions (Fletcher et al., 2013). Whilst traditional design of stormwater management in urban areas uses curbs and gutters, and sewer networks, for efficient transport of surface runoff, currently, such designs are complemented by alternative practises of low impact developments (LIDs) which maintain post-development hydrology of a site close to natural conditions (U.S. EPA, 2000; Coffman, 2002), and urban Green Infrastructure (GI) pronouncing vegetated systems to deliver ecosystem services and stormwater management (U.S. EPA, 2014; Fletcher et al., 2013). Such types of source control measures have in common the ability to reduce the adverse effects of imperviousness by facilitating the reduction of runoff peaks and volumes through retention storage, infiltration, and evapotranspiration, while incorporating aesthetically pleasing amenities into urban drainage. Despite of a growing implementation of such control practices, there are still uncertainties in both, the extent of their possible applications and their hydrological and hydraulic performance (Ackermann and Stein, 2008).

As a more 'traditional' element of urban drainage, widely used grass swales are typically designed to convey, attenuate and treat stormwater runoff from paved areas, and thereby either replace, or supplement, the conventional curb and gutter drainage systems (see Picture 1). Grass swales are often designed with capacities sufficient for handling runoff from severe storms. In the context of integrated stormwater management systems, where grass swales would function as attenuating conveyance structures to other drainage elements, knowledge of the effects of swale design on the swale outflow is of interest. Differences in swale topographies, age, exposure to various hydraulic loads, soil-hydrological properties including the saturated hydraulic conductivity, the size of the connected impervious area, the magnitude of entering runoff loads and antecedent moisture conditions are affecting swale performance and design, and are subject to large uncertainties (Nishat et al., 2010; Dietz et al., 2006; Fletcher et al., 2013).

Consequently, even though a plethora of guidelines and standards for grass swale design exist in various countries and provide recommended values for minimum infiltration rates and prevention of erosion or overflows, they do not sufficiently inform about the boundaries of swale applicability, operation and design, with respect to antecedent soil moisture conditions and design storms, as required for swale planning and design (Nishat et al., 2010).

1.1 Study aim and motivation

Grass swales represent a relatively simple and inexpensive, but effective stormwater control measure to reduce hydraulic and pollution load. Although being a traditional element of urban drainage systems, they earned recent interest in the emergence of urban Green Infrastructure approaches which aim to mitigate the hydrological impacts of urbanisation. Applications of grass swales are therefore likely to expand, yet common practice of swale design and construction results in uncertainties in the estimated drainage capacities, which is of significance where stormwater is conveyed to downstream drainage elements. Beside common parameters used for describing swale hydrological and hydraulic performance, such as the peak flow, volume attenuation and lag time, little has been published on the effects of variation of antecedent moisture conditions (AMC) on such parameters. The primary aim of this thesis is, therefore, to advance the knowledge and understanding of influential factors concerning the formation of swale channel hydrographs, and hydrological and hydraulic performance parameters, and to assess the feasibility of simulating swale flow processes using existing computer models. In particular, the studies described in this thesis address the physical simulation of two selected discrete storm rainfalls under different initial swale conditions, especially two main states of the initial soil water content and its impact on the swale water balance. Consideration is also given to the spatial variability of grass swale physical characteristics like the swale channel topography and the saturated hydraulic conductivity. For this purpose full scale field experiments were conducted focussing on the generation of inflow and outflows in three existing swales together with the measurement of the soil water content, and the analysis of water balance data for two swales. The availability of spatially and temporally detailed data furthermore allowed to investigate the potential of the distributed hydrological model Mike SHE to reproduce observed discharge hydrographs from one selected swale and to determine benefits of data resolution for the predictive model performance.

1.2 Thesis structure

This thesis synthesizes research results of three papers (one refereed conference paper – Paper I, and two submitted journal manuscripts – Papers II and III). The fields covered by the three papers and the relations of the papers among each other are illustrated in Fig.1. Paper I concerns the field procedure for mimicking stormwater runoff by controlled inflow into an urban grass swale and the measurement of soil parameters including the initial soil water content and saturated hydraulic conductivity. The described experiments were extended in Paper II to two more field sites with reliable inflow-outflow measurements allowing the evaluation of outflow hydrographs and the swale water balance. Paper III subsequently reports on the model setup for one selected swale and the event-based calibration against measured discharges. In overall, the thesis comprises six chapters; Chapters 1 and 2 present a brief introduction of the thesis topic describing the significance of the study subject and the study aim, followed by a brief overview of the grass swales as traditional drainage facilities, their design and integration into the current stormwater management planning. Chapter 3 features the descriptions of the experimental field sites and methodologies applied in collecting field data and applying an existing hydrological model to reproduce observed flows and soil water content. In Chapter 4, the main results of the thesis research project are presented,

followed by a discussion of results in Chapter 5. Chapter 6 presents study conclusions. Finally, a list of references cited and the thesis papers are appended.

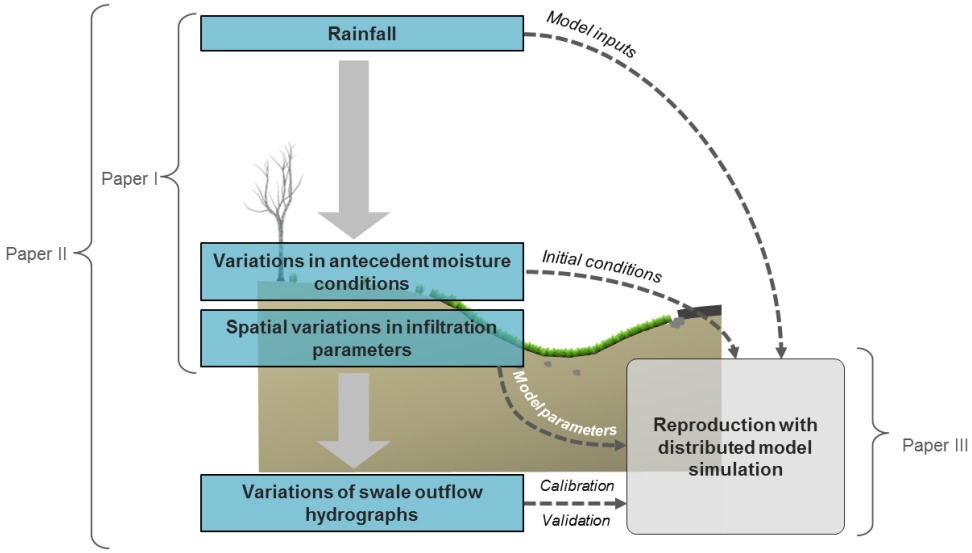

Figure 1: Relationship of the appended thesis papers to each other and to the topics presented in the thesis.

2. Background

This section presents descriptions of the benefits of applications of grass swales in urban drainage and a brief literature review of the concepts, guidelines, and research studies addressing the planning and design of grass swales, including the modelling of swale flow hydrographs.

2.1 Traditional grass swales in urban drainage

Grass swales are shallow linear depressions alongside paved areas, like parking lots and roads. They are typically designed as triangular or trapezoidal channels, with gentle side slopes of different lengths merging with the road shoulder usually on one side and directing the incoming runoff into an inclined swale channel. Swale longitudinal slopes are typically designed in the range from 2 to 5% (UDFCD, 2010; Schueler, 1987); the minimum slopes facilitate positive drainage of swales, the maximum values should prevent soil erosion. In some jurisdictions, mildly sloping swales (< 2%) should include an underdrain to ensure positive drainage (UDFCD, 2010). Other design features improving swale performance in runoff attenuation are cross-check berms increasing infiltration into swale soils (Davis et al., 2012). Traditionally swales were built in places where land was available and the piped stormwater sewer system was not required, or would be rather costly. Currently, grass swales are implemented mostly in suburban industrial and commercial areas and perform such tasks as conveying runoff, reducing runoff peaks and volumes by infiltration, and enhancing the runoff quality by filtration and settling of particles (Caraco and Claytor, 1997; Barrett et al., 1998; Dietz, 2007; Ahiablame et al., 2012). In cold climate grass swales fulfil another important task by providing space for snow storage (Pitt and McLean, 1986; Viklander et al., 2003). In general terms, grass swales are useful for restoring some natural catchment features, including green areas, increased surface roughness, flow detention, disconnection of impervious areas by diverting their runoff to pervious areas, increasing the flow path length and infiltration, and minimizing the amount of runoff flow in closed drainage channels (Prince George´s County, 2014).

2.2 Concepts and guidelines for planning and design of grass swales

Considering the high number of guidelines and standards for LID, and specifically for grass swales design and planning, only a small number of such documents can be discussed here, taking examples from three countries: United States (US), Australia and Sweden. Such a summary focuses on the hydrological and hydraulic aspects of swale design.

In the US various guidelines for (dry) swales exist at different administrative levels: on the national level from the US Environmental Protection Agency, or on the county and city level. According to the 1999 Fact Sheet on Vegetated swales (U.S. EPA, 1999) grass swales should be sized for a six-month- design storm of 24 hours duration and built in soils allowing for a dense vegetative layer and infiltration rates of at least 1.27 cm per hour (0.5 inch/hr). Side slopes are recommended with ratios of less than 1:3 and longitudinal slopes with 2-4%. For the calculation of the swale width the document suggests the usage of various forms of the Manning equation. Prince George´s County (2014) guidelines recommend that grass swales shall be designed for a 1-year 24-hour design storm for stormwater treatment, and with a capacity to carry a 10-year storm with a safe overflow for a

100-year storm. The maximum channel slopes of 4-5%, and max Manning n of 0.15 $s/m^{1/3}$, are recommended in design and analysis aimed at preventing erosion. Both surface storage and soil media storage are considered in the design. For 10-year events the freeboard is recommended with 0.23 m as a maximum. A hydraulic conductivity of at least 1.32 cm/hr is recommended (Prince George´s County, 2014).

For Australian communities, design recommendations for swales are available in documents addressing the Water Sensitive Urban Design (WSUD). For example, the Stormwater management Manual for Western Australia (2004) recommends to design grass swales for three types of storm events: i) frequent storm flows (with 6-month to 1-year average return periods, for water quality treatment; ii) minor storms (up to 5 years return period) for conveyance and prevention of nuisance flooding; and, iii) major flood flows (up to 100 years return period) to control flow velocities and velocity depth criteria during runoff conveyance within the road reserve and freeboard to the adjoining properties (Chalmers and Grey, 2004). Furthermore, swale flow velocities should not exceed 0.5 m/s in order to prevent erosion.

In Sweden, the design guidelines for stormwater control measures are available from two sources: The Swedish Road Administration (Trafikverket) provides regulations for the construction of roads and road drainage, which inform about roadside swale dimensions that the municipalities can voluntarily comply with. The Swedish Water and Wastewater Association (Svensk Vatten) focuses on stormwater drainage controls for urban areas. Municipalities and technical consultants generally comply with both guidelines and adapt them to the local conditions and experience. According to the guideline P110 (Svensk Vatten, 2016) , the design of stormwater control facilities should be based on 10-year design storms for suburban areas, 20-year design storms for high density residential areas, and 30-year design storms for urban centres and commercial areas. For preventing erosion, a maximum flow velocity of 0.25-0.5 m/s is recommended.

2.3 Assessment of swale performance by field experiments

Studies addressing the flow capacity of various drainage elements can be divided into four types: (i) Field assessments for actual rain storms, (ii) field testing for simulated inflows (using irrigation), (iii) laboratory testing in a prototype scale, and (iv) computer modelling. Field measurements addressing grass swale hydrology are relatively uncommon, because of difficulties with controlling experimental conditions, and the fact that generally only larger storms generate measurable flows in swales. Changing weather conditions (wind, sun) in particular impact on the drying and wetting of the surface soils and in irrigation experiments, the rain storms may affect water balance considerations. Furthermore, higher uncertainties in field measurements (Bertrand-Krajewski et al., 2000) and technical and logistical demands have to be taken into account. In Paper II some relevant field studies of grass swales are presented and complement those listed here.

Wanielista et al. (1988) studied five swales in Florida, U.S. to determine their infiltration capacity and flow rates. The study findings with implications for swale design were that runoff increased with lower infiltration rates and higher discharge volumes, and that with increased swale lengths the discharged volume decreased. Bäckström (2002) performed studies on grass swales in Luleå,

Sweden using irrigation to simulate rain runoff. He found that 33% of the pumped inflow infiltrated during the event duration of 30 minutes, with the highest infiltration rates occurring at the beginning of the event. He furthermore observed that there was no runoff generated for minor rains up to 2 mm, for initially dry swales, and concluded that the vegetation layer was a major factor for swale hydraulic retention. Abida and Sabourin (2006) studied the quantitative performance of a 338-m infiltration trench (with sand/silty till) in Canada, by applying a concentrated controlled inflow at the upstream end. The outflow rates and volumes were greatly reduced from 9.8 to 6.3 Ls^{-1} and 53 m^3 to 27 m^3, respectively, during the 1.5 h flow event. The saturated infiltration rate was estimated as 3.5 cm/h in this irrigation experiment. Deletic and Fletcher (2006) assessed a 6.5 m long grass filter strip in Aberdeen, Australia with respect to pollution control and flow characteristics for dry and wet initial soil conditions. They introduced flows of 0.33 to 1.00 Ls^{-1} for one and two hours and calculated flow volume reductions to be between 15-87% depending on the inflow rate and the antecedent soil wetness, which was measured in the range 0.23-0.43 m^3m^{-3}, with the high value assumed to be the saturated water content. They also measured infiltration rates with double-ring infiltrometers in that test site and noted spatially variable values ranging from 0.72 to 7.2 cm/hr. A local decrease of infiltration capacity was assumed to be caused by the clogging of fine soil pores leading to an increase of surface runoff. Davis et al. (2012) evaluated four different swale designs receiving lateral stormwater inflows; some were constructed with filter strips and some with check dams in Maryland, U.S. Based on 52 storm events and considering the initial soil moisture they found that minor storms between 0.3 to 1.5 cm per hour were captured without generating surface runoff. For storms larger than 3.3 cm/hr, the swale was conveying water without significant flow reduction. They concluded that the low storage capacity and the limited length (167-198 m) of the swales tested were responsible for an early excess flow production. They grouped the swale hydrological response into three regimes depending on the severity of the rain event, as minor (no runoff), intermediate (conveyance with substantial volume reductions) and severe (no significant peak flow or volume reductions). Based on their results Davis et al. (2012) proposed two criteria for swale hydrologic design: depths of water that can be infiltrated and depth of water in the swale without significant volume reductions. The former depth is lower and reflects the state when the swales infiltration capacity prevents any runoff; the latter depth corresponds to the state with significant swale discharges, depending on the duration of the storm event, when the swale simply acts as a conveyance channel. Lucke et al. (2014) assessed four swales in Sunshine Coast, Australia based on 24 standardised synthetic runoff simulations to evaluate swale pollutant removal and hydraulic performance. The simulated inflow rates corresponded to one-year storms of 21 and 30 minutes (29.3 mm/h) and varied between 0.5 Ls^{-1} and 2.0 Ls^{-1}, respectively. The initial soil moisture conditions were measured as well as the outlet flow rates using a V-notch weir. To evaluate the hydraulic performance they compared the inlet and outlet hydrographs. Total flow reduction of 52% and peak flow reduction of 61% was calculated as well as lag time of 13 min (measured to the beginning of outflow) and 20 min for peak flow delay. With lower initial soil moisture content, they also demonstrated that the flow reduction was greater. The hydraulic performance of 50 grass swales in Germany constructed 20 years ago were assessed by Kluge et al. (2016). They measured the hydraulic conductivity and compared the results with the German standards. The resulting values were within the recommended range with medians of 1.9 cm/hr for sandy soils and 0.4 cm/hr for silty soils. They also derived spatially averaged K_{sat} values for submerged swales and noted these medians to be higher than measured by double-ring infiltrometers which were as high as 14.3 cm/hr.

At four highways in Minnesota, U.S. García-Serrana et al. (2017a) performed 32 irrigation experiments on grass swale side slopes at four different swales with soil types ranging from sandy loamy sand to clay loam. They computed averaged hydraulic conductivities of 2.8 – 4.9 cm/hr based on 20 measurements, using Modified-Philip-Dunne Infiltrometers. For the three flow rates, 0.07, 0.14 and 0.28 Ls^{-1} introduced at the top of the side slopes, for durations of 15 to 60 min, they found that the average infiltrated water volume was 85% for the low flow, 70% for the medium flow and 47% for the highest inflow rate. They furthermore found that there was a rapid increase in infiltration rates for soil moisture deficits, when above 0.35 m^3m^{-3}. They concluded that beside saturated hydraulic conductivity and side slope length, soil type and vegetation cover would improve infiltration performance. Initial soil water content was found to impact infiltration volumes, which were 12% smaller for wet conditions.

2.4 Assessment by hydrological models

The ability of hydrological models applied in urban stormwater management to simulate LID facilities, including urban grass swales, is a key factor for their future integration into the analysis of urban drainage systems. Planning and design of grass swales require appropriate dimensioning of slopes and channel lengths, and prediction of expected discharges and source control capacities. In this regard several attempts have been undertaken to simulate hydraulic and pollution transport processes in grass swales and grass swale like structures, with conceptual models and more recently with comprehensive urban hydrological model packages. The majority of studies concerned the hydrological/hydraulic performance of LIDs on the urban catchment scale; only few studies address specifically grass swales, and some of those are relevant for describing typical hydrological and hydraulic processes relevant for swale design on a small scale. Some of these studies, summarized below, are complementary to those referred to in the appended Paper III.

2.4.1 Swale and process specific models

Graham (1990) developed a 2D-unsaturated-saturated finite element model coupled to a surface routing model to simulate multiple runoff events into an urban infiltration basin. Results indicated that the antecedent soil moisture condition determined the amount of storage volume available in the UZ (unsaturated zone). The physically-based VFSMOD model which includes an overland flow and infiltration module (the Green-Ampt's equation) was tested by Abu-Zreig et al. (2001) for 20 vegetated filter strips. They estimated the input data from field observations of the strips with varying slopes, length and vegetation cover. Saturated hydraulic conductivity and the initial soil water content were used as inputs. Main findings indicated that the flow width represented by the model was significant for the reproduction of the infiltration volume. Deletic (2001) used experimental data to develop a one-dimensional physically- based model for simulating sediment transport and runoff (TRAVA) if swales. Using the results from the above mentioned field study (section 2.3) of a filter strip and grass swale, Deletic and Fletcher (2006) verified the same model for runoff generation and sediment removal. Most relevant calibration parameter was the hydraulic conductivity. Agreements between the measured and modelled outflow rates were found to be within ±5%. The predictions of flows smaller than 0.05 Ls^{-1} was mentioned to be difficult, assuming that low overland flows are not governed by conventional open channel flow equations, because of

influence of surface tension. Using a 1D-unsaturated zone model (MetaSwap) Geerling (2014) simulated the effects of initial soil water content of a previously investigated grass swale of 36 m length for of a 2-year design storm (60 min/20 mm). The results indicated no effects on the swale water depth, but major effects on the drainage volume and the hydrograph lag time of 10% for soil water contents between very low and very high. Farahi et al. (2017) developed a 1D finite-volume based model that can be used for infiltration trench design. Based on the Richards equation (Richards, 1931) and considering the soil moisture measured with the Time Domain Reflectometry (TDR) probes in a soil column, the water movement through the soil layers could be well simulated and matched with observations. Calculations for dry initial soil conditions showed to be less accurate but the model delivered good approximations under seepage conditions. Garcia-Serrana et al. (2017b) developed and validated a model based on Green-Ampt, Mein-Larson kinematic wave models to quantify the infiltration in roadside swales considering overland flow, infiltration on the side slope and in the channel, as well as the initial soil moisture as described above (Minnesota dry swale calculator). Their modelling results indicate that regardless of K_{sat} and side slope width, more stormwater infiltrated in the side slope (74-97%) than in the swale channel (max. 25%). Given only the lateral inflow from the road and the relatively short inflow events they state that the side slope is typically the primary contributor to runoff loss due to infiltration and that the channel acts as conveyance element for excess flow. The model presented was also sensitive to soil moisture changes (between dry and wet), which affected the early occurrence of excess flow.

2.4.2 Comprehensive urban hydrological models

Using SWMM, Qin et al. (2013) modelled the performance of different urban drainage systems, including grass swales, under various rainfall characteristics. Among others, they investigated the effects on flood volume and the flood reduction by simulating different rainfall return periods, rainfall durations and different time-to-peak-ratios of rainfall hyetographs. They found that the storage layer depth, determined by the soil thickness (here 350 mm) and hydraulic conductivity of the soil layer, are the most sensitive parameters for flood reduction. They also found that compared to the tested permeable pavement or green roof scenarios, the swale option was most effective in flood reduction for heavy and short rainfall events. A review of 150 studies that employed SWMM was performed by Niazi et al. (2017) focussing on water-quality, Green Infrastructure design, and model calibration and verification. They confirmed that SWMM was best suited for medium to large urban scales, but concluded that the model should be improved for incorporation of LID/GI alternatives, in terms of suitable algorithms for hydrological continuity and water quality management in urban areas. SWMM was also used by Flanagan et al. (2017) for multi-year simulations of the treatment performance of a road-side vegetative filter –swale arrangement, with the main soil types of sandy to silty loam. The most sensitive calibration parameter was the hydraulic conductivity, which was previously measured in the field as 0.1 – 3.6 cm/h. Other calibration parameters were depression storage, which changed the runoff volume by 15% of the total rainfall volume for all storms. Only little has been published about high resolution modelling to assess the effects of green infrastructure on small-scale urban hydrology. Helmers and Eisenhauer (2006) applied the distributed, physically-based model Mike SHE, without calibration, to a vegetative filter to analyse the effects of spatial variability in hydraulic properties on the outflow hydrographs, generated by irrigation experiments. They used 26 samples of saturated hydraulic conductivity

ranging from 0.36-13.30 cm/h over an area of 13x15 m and selected the model spatial resolution of 0.76 m, but found no significant impact compared to the spatially uniform soil hydraulic properties. Simulations with higher inflow rates produced better agreements for overland flow (OL) times reaching the outlets. They further explained the representation of micro-topography in the model.

The reviewed literature on experimental and modelling studies of swales in the context of urban stormwater management shows, that there is a continuous and increasing interest in the understanding of grass swale hydrology/hydraulics and performance as an urban stormwater drainage facility. These interests are given by the reconsideration of swales as effective low-cost source control measures, forming a part of the urban green infrastructure, and the need to minimize uncertainties concerning differences in design aspects. Generally, a trend towards modelling LIDs and grass swales for design and planning can be observed, even though there is a lack of detailed temporal and spatial data on operation of such facilities (lack of details on inflow areas, topography and thickness of soil layers). Such information would be required for reliable simulations of various hydrological processes in small-scale LIDs, like grass swales, in order to be able to well design swales for future implementation. So far facility-scale modelling is mainly done by conceptual models, as they are usually more practical for design and planning of stormwater control measures. Distributed hydrological models like Mike SHE, because of their physically-based numerical engines, can compensate for data scarcity, to some extent. However, the majority of their applications deal with water balance simulations of larger-scale catchments and, when used in the urban context, their traditional focus was not concerning small scale processes. To date, relatively little has been published (Helmers and Eisenhauer, 2006) on spatially high-resolution and process oriented modelling with Mike SHE.

3. Methods

Two general research approaches were used to advance the understanding of the hydrology of grass swales: measurements of swale responses to inflows of irrigation water and modelling of such responses with an existing distributed hydrological model (Mike SHE). Field experiments were conducted at three locations in Luleå during the periods August-October 2015 (Swale 3) and August-September 2016 (Swale 1 and Swale 2). Ancillary data collection included the measurement of physical parameters of the swale runoff contributing area, including an elevation survey, soil infiltration rates measured with a double-ring infiltrometer, and textural analysis of soil samples. Such measurements were supplemented by estimations of temporary water storage in surface depressions of the swale channel and the soil matrix of the top soil layer. The distributed physically-based model Mike SHE was used to examine the feasibility of reproducing the relevant swale hydrological processes and identify those processes that are most relevant to swale planning and design. In the following the descriptions of field sites, field measurements and basic computational analyses are presented, and finally, the methodology for the calibration of Mike SHE is also described (for further details, see also Paper II).

3.1 Experimental swale sites

Multiple criteria were applied in the selection of suitable experimental sites, with emphasis on similar physical features of the swales with respect to the channel slope and well-developed and maintained grass cover, the availability of irrigation water, site access and safety of experimental operations. A brief description of the three sites chosen follows.

3.1.1 Swale 1: Örnäset

Swale 1 is located at Örnäset, Luleå and was built in 1956. It drains a two-lane road and has a pine stand on the opposite side. The test section of 30 m (see Fig. 2) was selected at the downstream end of the 200 m swale and drained directly into the storm sewer system. The swale bottom was of 0.2-0.7-m width, the side slopes approximately 1.3-2.0 m wide and the average depths from the road shoulder of 0.6-0.8 m. The side slopes ratios are 1:2 to 1:2.5. The grass cover of Swale 1 was dominated by *Deschampsia flexuosa* (the common name crinkled hair grass) and *Vaccinium vitis-idaea* (the common name lingonberry). Before the irrigation experiments started, the swale vegetation was mowed to an approximate height of 5 cm. Ten soil samples were extracted in Swale 1 and analyzed for grain size distribution (GSD); the results of such analysis are shown in Fig.3. According to the FAO soil classification system (FAO, 2014), the corresponding soil type can be identified as ‘loamy fine sand’. As seen in Fig. 3, soil GSDs varied spatially within the test section. Furthermore, for five of the ten samples collected soil porosities ϕ were determined and are listed in Tab.1.

Table 1 Soil types and porosities for the three tested swales. No statistical significant difference was noted for the measured porosities in Swales 1 and 2.

	Swale 1		Swale 2		Swale 3	
Distance to outlet (m)	Soil texture	Measured ϕ	Soil texture	Measured ϕ	Soil texture	Measured ϕ
1.5	loamy fine sand	0.56	silt loam	0.57		Not measured
4.5						
7.5	fine sand	0.57	fine sand	0.50	Fine sand	
10.8						
14.0	sandy loam	0.54	sandy loam	0.45		
17.5						
21.0	sandy loam	0.42	loamy fine sand	0.43		
24.5						
28.0	sandy loam	0.49	loamy fine sand	0.52		
Average value / category	Loamy fine sand	0.52 ±0.06	Sandy loam	0.50 ±0.05	Fine sand	

3.1.2 Swale 2: Hertsön

The test swale in Hertsön, Luleå, drains a bus lane and on its opposite (eastern) side it is connected to a meadow (Fig. 4). The total swale length is approximately 200 m and the test section of 30 m was just 20 m upstream of the culvert draining to another swale section. The swale bottom was 0.1-0.5 m wide, the side slopes 2.7-3.0 m and the swale depth between 0.8-1.0 m. Side slopes were measured as1:3-1:3.4. Dense grass, which was dominated by *Deschampsia flexuosa* (crinkled hair grass), *Elytrigia repens* (couch grass) and *Phleum pratense* (timothy grass), had to be mowed prior to irrigation experiments. Eleven soil samples were extracted in Swale 2 and analyzed for grain size distribution (GSD); the results of such analysis are shown in Fig. 5. According to the FAO soil classification system (FAO, 2014), the corresponding soil type can be identified as 'sandy loam'. Soil GSDs varied spatially within the test section. Furthermore, for five of the 11 samples collected, soil porosities ϕ were determined and are listed in Tab.1.

Figure 2 Swale 1 in Östermalm, Luleå.

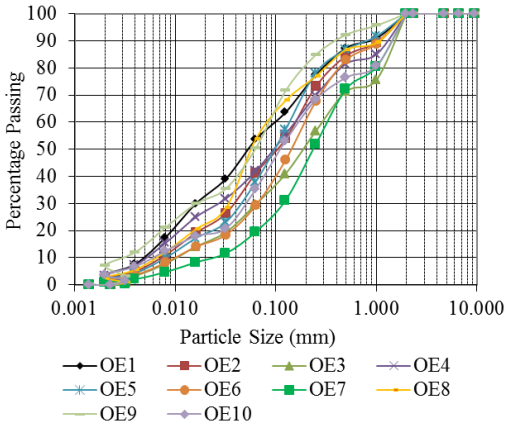

Figure 3 Variance of grain size distributions in ten soil samples from Swale 1 (n=10)

Figure 4 Swale 2 in Hertsön, Luleå.

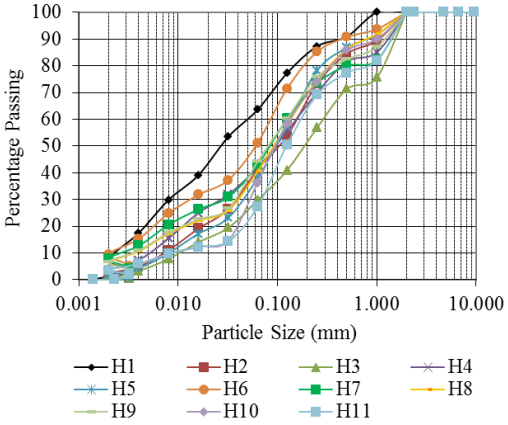

Figure 5 Variance of grain size distributions in 11 soil samples from Swale 2 (n=11)

3.1.3 Swale 3: Östermalm

Swale 3 is located in Östermalm, Luleå, close to Dalagatan street, and drains a bicycle path (Fig. 6). It is shallower than Swale 1 and Swale 2 with depths of 0.3-0.4 m and side slopes of 1:4.5 – 1:5, and shorter with the total length of 55 m. The investigated section had a bottom width of 0.5-0.8 m and side slopes of 1.1-1.6 m. At the downstream end, it drains into a drop structure connected to the storm sewer system. The most abundant grass species in the swale was *Elytrigia repens* (couch grass). The grass height was 5 to 10 cm and did not require cutting. The swale soils are predominantly fine sands (see Fig. 7). Grain sizes of the full spectrum (including clay and smaller silt fractions) were determined for two samples only. Because Swale 3 was accessible from both sides and therefore exposed to pedestrian traffic, its soils showed signs of compaction.

Figure 6 Swale 1 in Östermalm, Luleå.

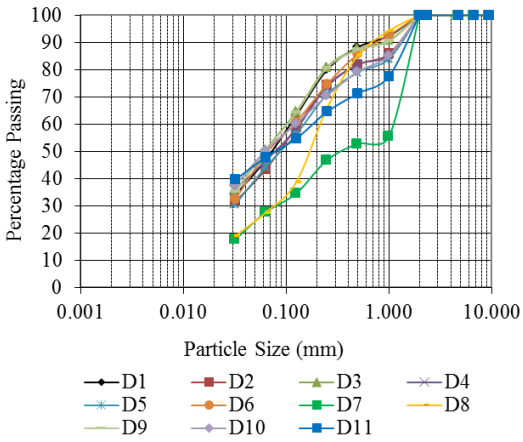

Figure 7 Variance of grain size distribution for soil samples at Swale 1 (n=11)

3.2 Field irrigation experiments

Runoff entry into the swales was simulated by field irrigation with a mobile irrigation system, allowing experimental runs with two equal irrigation inflows: a concentrated longitudinal inflow and a distributed lateral inflow. The water supply system was improved in 2016 for Swale 1 and 2 allowing a better control of the inflow. This included a constant water flow, supplied from municipal drinking water pumping stations, into the water containers, a larger overflow pipe and two instead of three valves at the containers to initiate flow simultaneously (two discharging containers were required for the larger inflow rate). A picture of the main irrigation system elements is displayed in Fig. 8.

3.2.1 Irrigation inflows mimicking selected design storms

Simulated constant inflows of 30 minute durations mimicked runoff from design block rainfalls. Approximate estimations of the recurrence intervals of the applied irrigation flow rates were obtained from the rational method by calculating the rain intensity required to produce runoff flow rates equal to the irrigation flow rates. In such calculations, the runoff contributing swale catchment area was estimated as 450 m^2 for Swales 1 and 2 (with a volumetric runoff coefficient of C=0.75) and 560 m^2 (with C=0.8) for Swale 3. The calculated intensities were then substituted into the intensity-duration-frequency equation for Sweden (Dahlström, 2010) and for the given duration of 30 minutes it was possible to calculate the corresponding frequencies (return periods). In this way, the following return periods were determined for various irrigation flow rates: Swales 1 and 2, 2-months and 3-years, and Swale 3, 0.5, 1, and 2 years.

3.2.2 Selection of antecedent soil moisture conditions for irrigation experiments

Evaluation of the effects of initial soil moisture conditions on swale flow hydrographs was examined for two moisture states, referred to as ´dry´ and ´wet´, respectively. In similar runs, efforts were made to achieve the initial conditions as similar as practically possible, however, this was not always feasible because of changing weather conditions significantly affecting the antecedent 'dry' conditions. Considering the fast drainage of the swale soils tested, for dry condition tests, at least 24 hours with no rain were required. Wet runs were easy to plan – they started within 0-3 hours of completion of the preceding irrigation run. Only in Swale 2 the thresholds for average soil water content from the swale channel (N=5) were used to define subsequent runs start. For Swale 1 and Swale 3 at least one dry day and the 'feel and appearance' method of soil moisture assessment was used to determine the initiation of a dry run.

3.2.3 Flow measurements

For measurements of the swale inflows and outflows, a head-discharge method was selected, using sharp-crested weirs as primary flow measurement elements. For Swales 1 and 2, improved measurement devices were used and consisted of weir boxes with V-notch weirs (45° and 90°) and pressure transducers from the ISCO Area-velocity flow meters for measuring heads in stilling wells attached to the weir boxes (Fig. 9). The arrangement of the irrigation system and measurements used in 2016 differed from those used earlier in 2015. For Swale 3, V-notch weirs inserted into the water supply pipes were used for inflow measurements and the head was measured using the same type of pressure transducer (i.e., as in Swales 1 and 2), located in the pipe 0.8 m upstream of the weir (Fig. 10). The outflow was measured by a compound constriction flow meter consisting of a rectangular weir and an orifice located below the weir crest (Fig. 11). Standard weir equations for the three inflow flume V-notch weirs and the combined rectangular weir-orifice outflow device were used to calculate the flow rates from the measured heads using Matlab. Measurement uncertainties were not determined.

After the 2015 swale water balance calculations revealed serious measurement errors, the flow measurement equipment was improved in time for the 2016 field season by using weir boxes with two standard weirs as can be seen in Fig. 9 for the 90-degree V-Notch weir box combination.

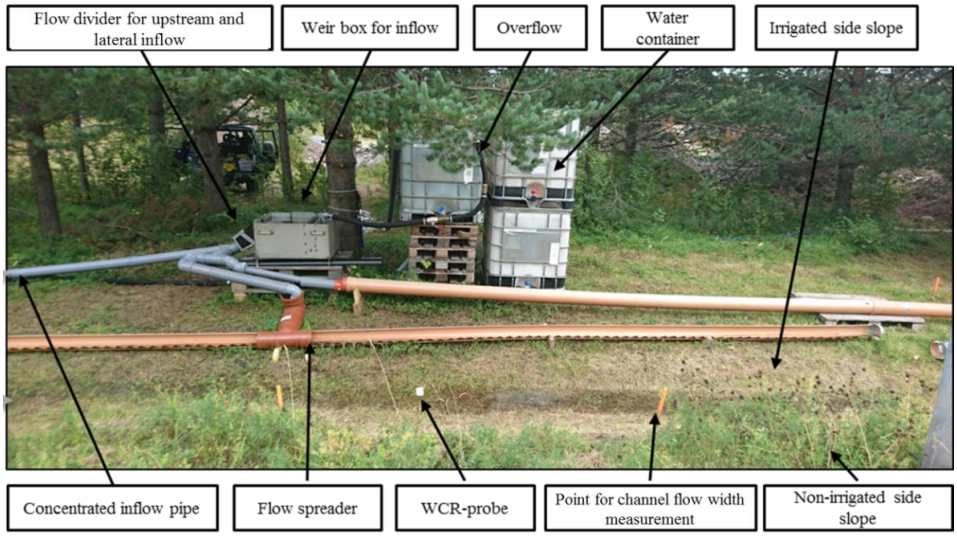

Figure 8 Picture of the water distribution system for near surface irrigation and various measurements.

Figure 9 Stainless steel weir box with 90 -degree V-notch weir attached.

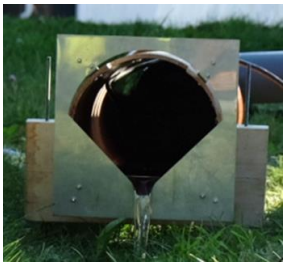

Figure 10 90-degree V-notch weir attached to a pipe channel from experiments in 2015 for inflow measurements.

Figure 13 Double-ring infiltrometer tests conducted every 3 m in the swale channel (n=9).

Figure 11 Compound rectangular-weir-orifice constriction for swale outlet discharge measurements

Figure 12 Near-surface irrigation with a labyrinth weir, producing a lateral inflow to the swale.

The flow rate was calculated from the Kindsvater-Shen equation (Shen, 1981) and compared with volumetric measurements. The Kindsvater-Shen equation allows calculating the weir discharge from the measured hydraulic head:

$$Q = C_e \frac{8}{15}\sqrt{2g}\tan\frac{\theta}{2}h_e^{5/2}$$

Where h_e, the effective head, equals $(h + k_h)$, h is the measured head over the weir notch and k_h is an experimentally determined correction for viscosity and surface tension, C_e = discharge coefficient, θ = notch angle, and g = gravitational acceleration.

The flow rates calculated from the readings of four identical make level sensors (to assess the inter-sensor variability), together with the volumetrically measured flow rates, are plotted in Fig.14 for the 45° V-notch weir. Because of good agreement between the weir and volumetric measurements, there was no need for weir calibration. For the representative ranges of the measured weir heads in the field corresponding to flow rates of 1.06 and 2.65 L/s and the accuracy of the head sensor, which is specified by the manufacturer as ±3 mm, the accuracies of such measurements were estimated as 6-10% for the 45° V-notch and 9-14% for the 90° V-notch weir.

3.2.1 Measurement of the infiltration capacity of swale soils

The saturated hydraulic conductivity was measures with a double-ring infiltrometer at nine points located, every 3 m along the swale bottom, in each of the three tested swales (see Fig. 13). The measurements were performed after the irrigation experiments were completed, in order to prevent flow disturbances which could be caused by ground disruptions resulting from driving infiltrometer rings into the ground.

3.2.2 Soil water content measurements with Water Content Reflectometry

Volumetric soil water content reflectometers (WCR, model CS616 of Campbell Scientific, Inc.) were used to measure soil water content (Fig. 15a). These instruments measure the water content indirectly by sensing the signal propagation velocity of an electronic pulse between two metal rods that changes with the water content (Ruelle and Laurent, 2008). An overview of the locations of the 15 probes in the swale can be seen in Fig. 15b. Five WCR-probes were inserted at an 45° angle into the swale channel at distance of 5 m, four probes (each) were inserted vertically into the irrigated and non-irrigated side slopes at distances of 0.4 m and 0.7 m from the centre of the swale channel and two probes were buried horizontally at 0.3 and 0.6 m below the swale channel bottom, at 1.5 m upstream of the outflow measuring weir box (Fig. 16). Measurements were logged during experimental runs every 30 seconds and such logging lasted anywhere between one hour and several days.

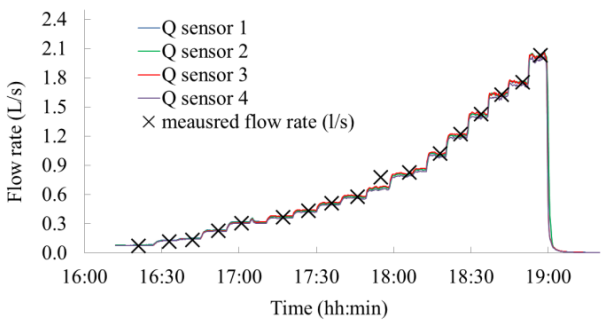

Figure 14 Validation of the Kindsvater-Shen equation for head-discharge measurements by sharp-crested V-notch weirs against the volumetric measurements, and inter-sensor variability of ISCO pressure transducers.

Figure 16 Installation of two WCR-probes for soil water content measurements at 0.3 and 0.6 m depth below the swale channel bottom.

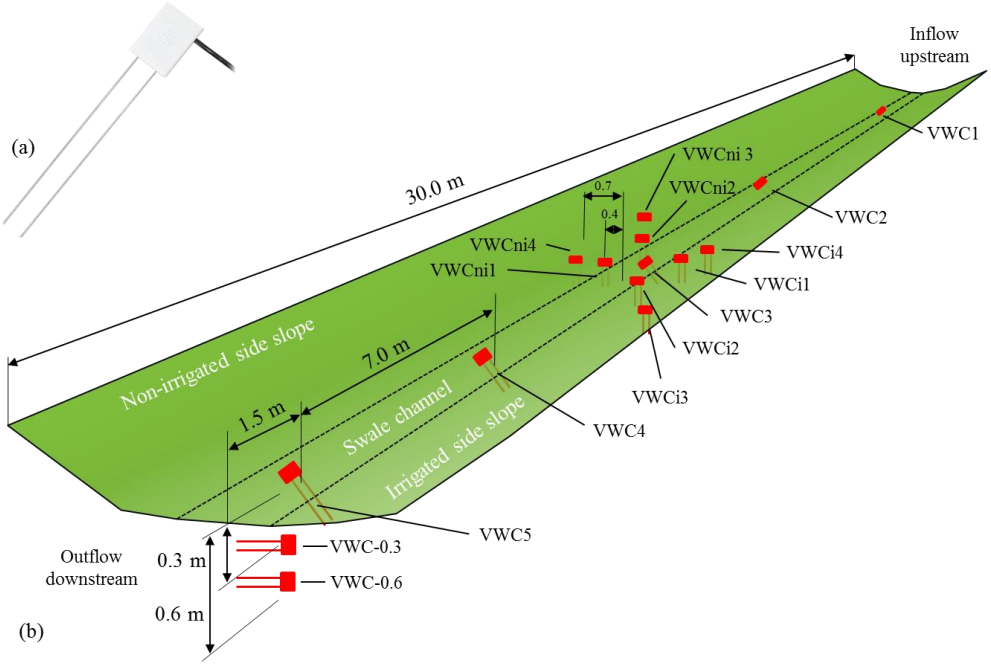

Figure 15 (a) Location and distances of WCR-probes for measurement of the soil water content (red) in the 30-m swale test section. (b) WCR-probe consisting of two metal rods that are inserted into soil and over whose length the soil water content is averaged.

3.2.3 Analysis of experimental data

For the 38 experimental runs meeting the quality control criteria, swale flow hydrographs were produced and the swale water balance calculated. Because of limited durations of experimental runs and major flow conveyance taking place in the channel part of the swale, water balance calculations apply to the swale channel only and evapotranspiration was neglected. Water balance data from the 2015 swale studies were not published, because of measurement errors, and are therefore not included in this thesis. For Swale 1 and Swale 2, 24 runs in total were performed and water balance data (including inflow, infiltrated and outflow volumes) and other calculated parameters (flow volume reduction, peak flow reduction and hydrograph centroid lag time) were presented in Paper II. Inflow and outflow hydrographs were plotted for all the events.

For experimental runs with initial wet conditions, the peak flow reduction, defined as the difference between the inflow and outflow hydrograph peaks, reached quickly quasi-equilibrium and served as a basis for calculating spatially averaged values of K_{sat} denoted with a subscript hyPF. This could be done by using the flow width data, which were collected during the experimental runs, and the subsequent estimation of the spatially averaged infiltration area (A_{inf}) over the test section length of 30 m.

3.3 Modeling of grass swale flow with Mike SHE

The purpose of modelling grass swale flow was to reproduce the hydrological response of the swale to two irrigation inflow rates and for the various initial soil water contents tested in the field. For this task, the distributed, physically-based model Mike SHE was selected, because it can use detailed input topographical data, soil characteristics, and short time steps to simulate continuous time series of water movement and soil water content. For this purpose, the data collected in the Swale 1 study (Paper II) were further processed and applied for model set up, calibration and evaluation. Data processing was accomplished using common software, including MS Excel and ESRI ArcGIS.

3.3.1 Mike SHE configuration

Runoff flow conveyance by, and infiltration in, the swale were considered as the two predominant hydrological processes, which had to be represented well in the model setup. Mike SHE offers several different computational engines for flow simulations, ranging from simple to the distributed physically-based ones. This study focused on both the overland flow (OL) and the unsaturated zone (UZ) modules. For overland flow, the 2D finite difference diffusion wave method was selected, as recommended when dealing with local overland flow and runoff (DHI, 2017). In this method, at each grid point, partial differential equations are discretized and solved by dynamic iteration over time, while the diffusion wave equation describes the depths of flow at each time step.

The unsaturated zone represents a vertical soil profile that interacts with the overland flow, the evapotranspiration model and any saturated zone (Fig. 17). For the vertical movement of water through that profile, the full Richards approach was selected to include soil moisture retention and accurate computation of soil water dynamics.

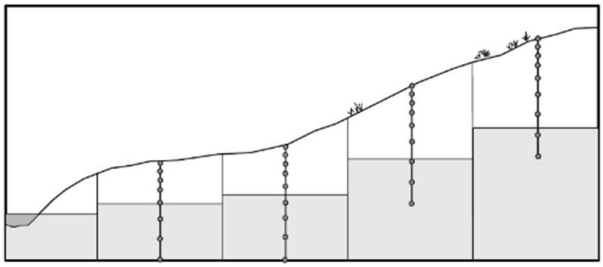

Figure 17 One-dimensional vertical finite difference discretisation for the unsaturated zone in Mike SHE. Vertical dots represent the sample distances of the computational layer increasing with depth. (Source: Beven, 2012)

The soil data are arranged in three soil type layers and within each layer the hydraulic conductivity is calculated using the Van-Genuchten/Mualem function (Van Genuchten, 1980; Mualem, 1976). Accordingly soil data have to be defined for each layer. Considering the two predominant swale flow processes as well as the objective of reproducing field experimental conditions in a 30-m swale section with two main inflow directions, such a set up was represented by a small plot (catchment area) of 307 m^2. The computational grid cell size was 0.2x0.2 m (the total cell number = 40 x 192) and the time intervals in all calculations were set equal to the time interval of logging field measurements, 15 seconds.

3.3.2 Hydrological parameters and input data

Detailed spatial and temporal inputs were required prior to simulation runs. A summary of these inputs is listed in the following table (Tab. 2).

Table 2 Input data for swale flow modelling with Mike SHE

Parameter value	Selected input	Explanation	Units	Mike SHE module
Topography	DEM	based on GPS-measured elevation points		OL
Manning n		Constant throughout the swale	$s/m^{1/3}$	OL
Depression storage		Constant throughout the swale	Mm	OL
Soil characteristics	Saturated soil water content	The maximum SWC value measured in field experiments	m^3m^{-3}	UZ
	Residual water content		m^3m^{-3}	
	Saturated hydraulic conductivity	Measured by the Double-ring Infiltrometer	ms^{-1}	
	Van Genuchten α_c, α_r	Adopted from the literature	1/cm	UZ (relative hydraulic conductivity)
	Van Genuchten n_c, n_r	Adopted from the literature	-	UZ (retention curve)
	Van Genuchten shape factor	Default value	-	UZ (relative hydraulic conductivity and retention curve)
Initial soil water content	Layer file	including spatially averaged initial SWCs for seven swale sections	m^3m^{-3}	UZ
Precipitation	Time-varying spatial layer file	Mimicked by near-surface irrigation	Liters per sec	OL/UZ
Root depth	Spatial layer with three sub-sections	Constant throughout the swale sections	mm	UZ
Leaf area index	Spatial layer with three sub-sections	Constant throughout the swale sections	-	UZ
Reference evaporation		Constant throughout the swale	mm/day	UZ

3.3.3 Model calibration

In total 12 irrigation-discharge events were recorded in Swale 1 (Paper II). Four events with characteristically different initial conditions, described by combinations of low and high inflows, and dry and wet initial soil moisture conditions, were selected for model calibration. Here a systematic manual calibration was applied instead of an automatic calibration because of the interest in effects of soil-water calibration parameters needed to understand the simulation outcome and due to the limited number of calibration parameters and the relatively simple swale structure. Furthermore it was attempted to mitigate the uncertainties associated with modeller´s subjectivity (resulting from the modeller´s selection of parameters, numerical engines and swale representation) by a calibration procedure that uses four representative events to perform event-based calibration.

After the individual inflow and initial SWC parameters were adjusted, the attention switched to adjusting the values of α_r and n_r influencing the soil water retention curve. The values of α_r and n_r were adjusted to obtain an acceptable initial field capacity of the soils, which was not the case when starting this process with the initially chosen values from the literature. The model was then run to

evaluate whether overland flow is generated. Subsequently, the Van Genuchten parameters were changed one-by-one and for each soil layer and the discharge hydrograph, represented by concentrated overland flow at the outlet cell, was evaluated at each time. Finally the Manning n and detention storage were adjusted to achieve an acceptable goodness of fit between the simulated and observed hydrographs. The goodness of fit was evaluated by the Nash-Sutcliffe model efficiency coefficient; the calibration procedure was repeated until the coefficient reached or exceeded the value of 0.95.

3.3.4 Assessment of model performance

The model calibrated for each of the four parameter sets was used to simulate overland flow and infiltration into the unsaturated zone for the eleven remaining events. All resulting discharge hydrographs (4 calibration runs + 4x11 evaluation runs = 48) were plotted together with the observed hydrographs and subject to statistical evaluation. Agreement between the event hydrographs was assessed by statistical analysis of volumetric residuals (i.e., differences between observed and modelled volumes), normalized volumetric residuals, peak flow residuals, normalized peak flow residuals, root mean squared errors and the Nash-Sutcliffe model efficiency coefficient (Nash-Sutcliffe, 1970). As flow reduction by infiltration occurred during the field experiments and in model simulations, the simulated development of the SWC in the top soil layer (0.21 m) was extracted at five measurement points and statistically compared to the measured SWC by means of the RMSE. Further details of these procedures can be found in Paper III.

4. Results

The results section includes the presentation of swale physical characteristics impacting the hydrology, including discharge hydrographs of experimental runs performed at the three test swales, and a comparison to hydrographs simulated with Mike SHE. The water balance analysis is summarized for hydrological/hydraulic performance values (hydraulic conductivity K_{sat}, relative volume reduction ($\Delta V_{peak\ rel}$), relative peak flow reduction ($\Delta Q_{pk\ rel}$), centroid lag time (T_{lag}) as well as the evaluation of measurements of the soil water content in the studied swales).

4.1 Hydrology of grass swales

On the event basis, the hydrology of assessed swales can be described by processes including inflow, infiltration over the side slopes (not measured) and swale channel bottom, storage of water in surface depressions and soil matrix and subsequent conveyance to a discharge point.

4.1.1 Saturated hydraulic conductivity of grass swales measured by DRI

In the three tested swales the DRI tests resulted in K_{sat}-values with significant spatial variability. Swale 1 has the highest infiltration capacities but also the highest spatial variability. Swale 3 soils were more compacted than those of Swales 1 and 2; however its saturated infiltration capacities were higher than those of Swale 2 which was built more recently. Tab. 3 /Fig.18 provides measured K_{sat} values and their standard deviations. For Swale 1 it can be noted that the hydraulic conductivity is lower towards the outlet compared to the rest of the swale bottom.

Table 3 Saturated hydraulic conductivity of three tested grass swales by DRI measurements on the swale bottom and estimated by spatially averaged values during steady peak flow reduction (hyPF).

	Saturated hydraulic conductivity K_{sat} (cm/hr)				
	Swale 1 Örnäset		Swale 2 Hertsön		Swale 3 Östermalm
Distance to outlet (m)	DRI	hyPF	DRI	hyPF	DRI
1.5	7.4	2.78, 3.59, 2.38, 3.38, 3.96, 3.52	2.2	4.60, 4.84, 6.63, 4.63, 3.93, 4.40	2.2
4.5	4.8		4		4.5
7.5	5.6		1.9		1.8
10.8	14.4		1.1		4.8
14	4.4		2.1		3.0
17.5	10.3		0.5		2.9
21	15.4		1.6		6.8
24.5	7.5		2		4.5
28	14.9		0.7		5.9
Average value (St.dev.)	9.41 ± 4.21	3.27 ± 0.58	1.78 ± 0.98	4.84 ± 0.93	4.04 ± 1.69

The saturated hydraulic conductivities calculated from quasi-constant differences in peak flow reductions (due to infiltration) are compared to the DRI measurements in Fig. 18. Except for the Östermalm swale K_{sat} derived by the two methods deviate significantly for Swale 1 and slightly for

Swale 2 while the K_{sat} derived by peak flow differences generate smaller scatter due to spatially averaging. Hydraulic conductivities in the three swales compared show higher variabilities for the DRI method compared to hydrograph-peak flow method.

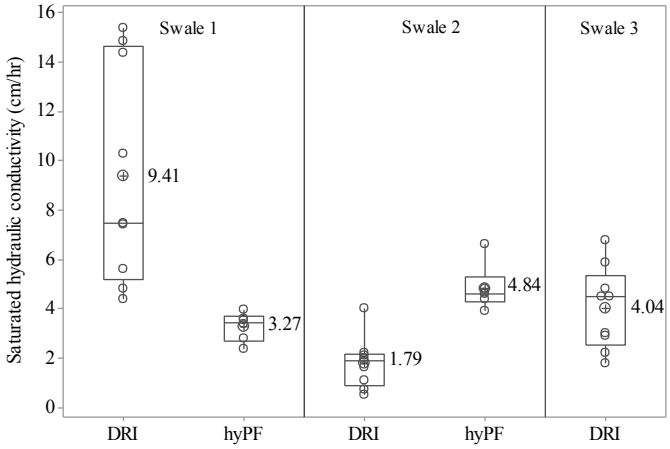

Figure 18 Saturated hydraulic conductivities for swales S1, S2 and S3, represented by DRI measured value plots and by those calculated from swale hydrograph analysis (hyPF).

4.1.2 Swale water storage capacity

Measurement of elevation points were used to illustrate the swales´ topography as digital elevation models, shown in Fig. 19 a-c, and further used to determine the volume of the swale bottom depressions where water ponds.

The differences of the minimum and maximum SWC values measured for the 0.21 m soil layer during the irrigation experiments were used to estimate the water retained in the soil matrix of that layer. Such values are presented together with the volumes of surface depressions in Tab. 4. The estimated values show that Swale 1 and Swale 2 would be able to temporarily retain 1.2 and 1.1 m^3, respectively, which would be 56-61% and 23-25% of the two total irrigation volumes applied, respectively. Swale 3 has the lowest overall storage capacity (in surface depressions and in the soil).

Table 4 Temporary water storage volume of the three swales studied.

	Temporary storage volume (m^3)		
	Swale 1	*Swale 2*	*Swale 3*
Surface depressions	0.35	0.61	0.09
Upper soil matrix	0.04-0.85	0.17-0.46	0.03-0.19
Sum of maxima	**1.20**	**1.07**	**0.28**

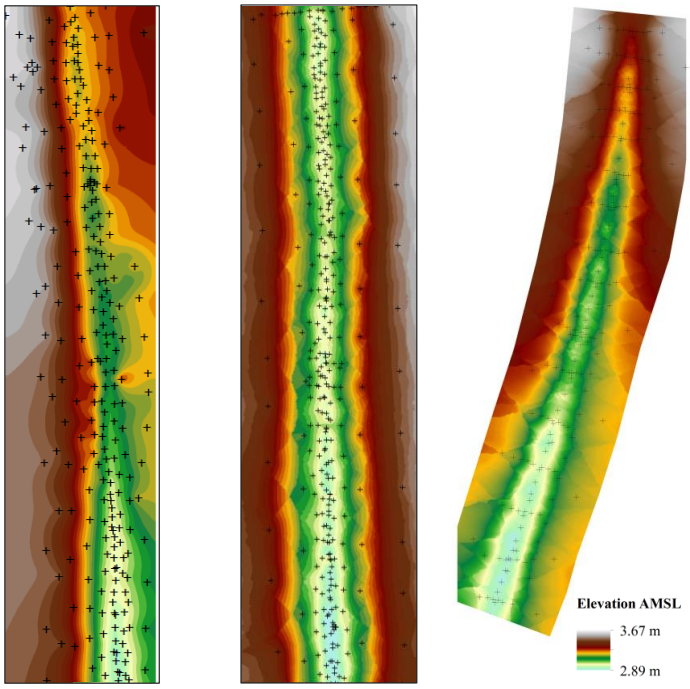

(a) Swale 1 Örnäset (b) Swale 2 Hertsön (c) Swale 3 Östermalm

Figure 19 a-c Illustration of different characteristics of swale topographies based on GPS-measured elevation points. The digital elevation models show the three test swale 30 m section, with upstream end starting at the top.

4.1.3 Discharge hydrographs and water balances

For the irrigation runs in the tested swales it was intended to control inflow rate and the time of inflow aiming for similar mean initial soil water contents, in order to produce three replicas for each of the four different inflow conditions. However, due to the variability of soil and soil water properties and weather conditions this was not achieved, mainly in the case of low initial SWC. The measured inflow-outflow events, therefore, have to be treated as independent experimental runs. Flow measurements for Swale 3 are excluded from further analysis due to measurement errors. Some typical inflow and outflow hydrographs for Swale 1 and Swale 2 are presented in Fig. 20 a-h. Inflow rates could be kept fairly constant allowing for the generation of block-rain driven truncated hydrographs for the two inflow rates, which were fairly well controlled with Q_{in1} = 1.06 Ls^{-1} ±0.03 and Q_{in2} = 2.65 Ls^{-1} ±0.07. Outflow rates, and the measured inflow and outflow hydrographs have different centroid lag times and peak flow reductions depending on the initial SWC, inflow rate and swale topography.

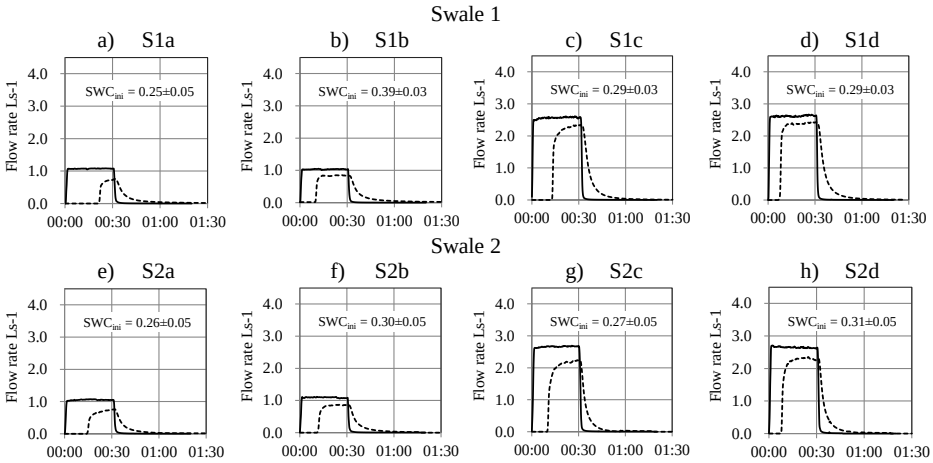

Figure 20 a-h. Example hydrographs derived from swale irrigation experiments in Luleå Örnäset, Hertsön (full line= block-rain mimicking inflow, dashed line =swale outlet discharge)

The water balances for Swales 1 and 2, are listed in Tab. 5, respectively (a detailed overview of the water balance data for Swale 1 and 2 are presented in Paper I). They are grouped according to the combinations of inflow rate and initial soil water content. It can be summarized that in the two Swales 1 and 2, 6-85% of the inflow infiltrated, and that the effect of the initial soil water content is significant regarding the volume and peak flow reductions. Detailed data are presented in Paper II.

Table 5 Initial swale channel SWC, average inflow rate Q_{in}; average flow volumes entering and leaving the swale, V_{in} and V_{out}, respectively; average infiltrated volume V_{inf}; and averages of the resulting relative swale flow volume reduction ΔV_{rel} of Swale 1- 2 (n= 3 for each averaged water balance parameter).

Swale	**SWC**	**SWC_{ini} (m^3m^{-3})**	**Q_{in} (Ls^{-1})**	**V_{in} (m^3)**	**V_{out} (m^3)**	**V_{inf} (m^3)**	**ΔV_{rel} (%)**	**$\Delta Q_{pk\ rel}$ (%)**	**T_{lag} (min)**
S1	SWC_{low}	0.24±0.03	1.07	1.99	0.52	1.47	0.74	0.40	15.10
	SWC_{high}	0.39±0.03	1.05	1.91	1.39	0.52	0.27	0.15	9.25
	SWC_{low}	0.28±0.03	2.64	4.96	2.85	2.11	0.42	0.12	9.40
	SWC_{high}	0.39±0.02	2.68	4.91	4.10	0.81	0.17	0.18	8.20
S2	SWC_{low}	0.26±0.05	1.04	1.95	0.84	1.12	0.57	0.32	10.85
	SWC_{high}	0.30±0.04	1.06	1.96	1.25	0.70	0.36	0.18	8.40
	SWC_{low}	0.27±0.05	2.62	4.84	3.10	1.74	0.36	0.12	6.48
	SWC_{high}	0.31±0.04	2.65	4.85	3.71	1.14	0.24	0.09	5.37
S3	SWC_{low}	0.19±0.05 0.18±0.06 0.21±0.04	Not calculated						
	SWC_{high}	0.32±0.04							

When plotting the relative volume reduction (see Fig. 21, panel (a)), the peak flow reduction (panel (b)), and the lag times (panel (c)) of each of the 24 events from Swales 1 and 2, decrease can be noted towards higher initial SWC. Especially for runoff volumes, the initial SWC is significant; as it can be observed for Swale 2 where even small differences between initial soil water content categories "low" and "high" (volumetric soil water content difference = 0.04 m^3m^{-3}) lead to a relative decrease by 44% for low inflow rates and 25% for high inflow rates.

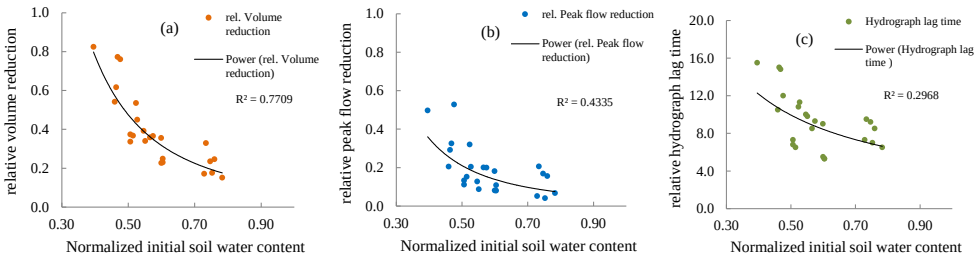

Figur 21 (a) Relative volume reductions, (b) relative peak flow reductions, and (c) hydrograph lag time (minutes) and the corresponding trend lines (power functions).

4.1.1 Soil water content (SWC) of grass swales

Soil water content is a function of the soil physical properties like porosity, compaction, water supply and the water already stored. SWC was measured with 15 Water Content Reflectometry probes (WCR-probes) as described in the methods section and in Paper II.

For each swale, one event with 1.06 or 2.65 L/s inflow rate, its duration and approximately identical initial SWC, has been selected to visualise the SWC progression over the course of four hours starting with the 30-min inflow event. The SWC readings are furthermore plotted separately for four sections of the swale, namely the swale channel (measured with five probes, denoted VWC1-VWC5), the irrigated side slope (four probes, denoted with VWCi 1 1-VWCi 4), the non-irrigated side slope (four probes, denoted with VWCni 1-VWCni 4) and at two depths below the swale channel bottom (at -0.3 m, VWC-0.3 and -0.6 m, VWC-0.6).

Based on the same inflow setting (inflow rate and inflow directions), the wetting of the swale channel represented by an immediate increase of the SWC in Fig. 22 a-c is proceeding until a maximum (the saturated state) SWC is reached, depending on the probe location. Note that VWC1, located close to the upstream inflow point, was the first to show elevated SWCs. The time lags between individual SWC readings in the three swales studied varied, because of the differences in swale topography, described by the longitudinal channel slope and channel depressions, which detain flow. The plots of the SWC of the swale channel also show the attainment of different SWC maxima, indicating variations in soil properties. The variations in soil properties, hydraulic conductivity and soil water retention, also impact the drying process at each location in the swale after the 30-min inflow stopped. While in Swale 1 the soil wetting and drying are more homogeneous, as confirmed by lower standard deviations (illustrated as a grey envelope of

plus/minus St.Dev. of the mean SWC), SWC progression in Swales 2 and 3 channels shows a larger spread.

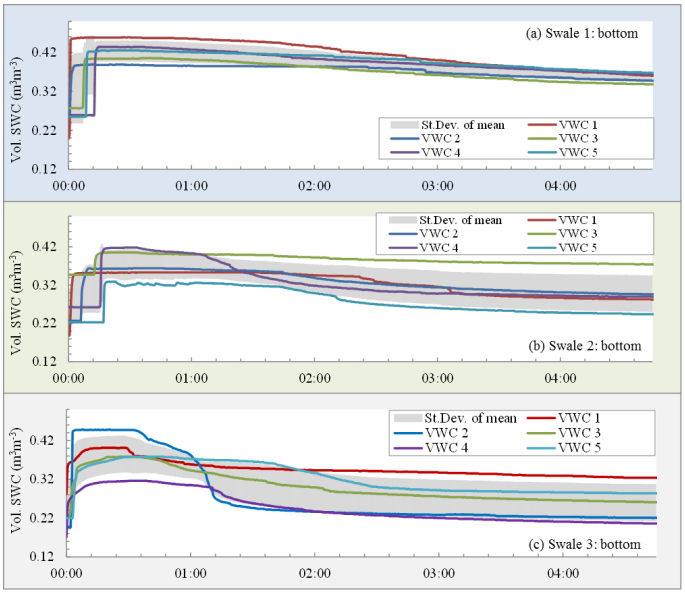

Figure 22 a-c Progression of the volumetric SWC of the five probes on the swale channel bottom of the three studied swales.

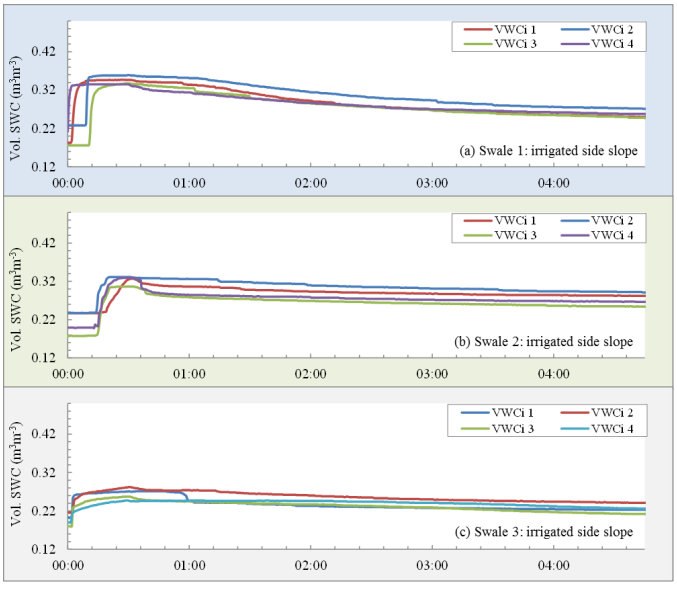

Figure 23 a-c: Progression of the soil water content measured by four WCR-probes on the irrigated side slopes in the three swales showing lower SWC variability than on the swale channel bottom.

The SWC progression at the four non-irrigated side slopes probes depends also on the side slope inclination and potential lateral infiltration of ponded water in the swale channel (Fig. 24 a-c). While Swale 1 (a) shows high SWC increases here (similar to the irrigated side slope), there is only a minor increase of SWC in Swale 2 (b) and almost no increase in Swale 3 (c), reflecting a delay of lateral infiltration over the measurement period.

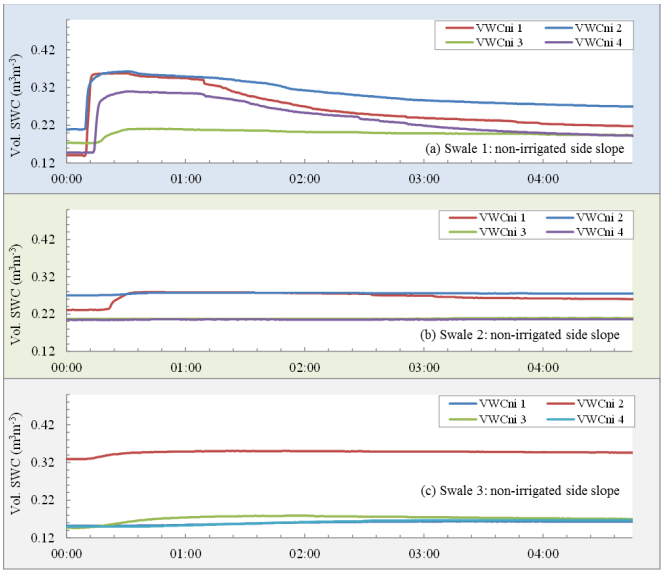

Figure 24 a-c: Progression of soil water content of 4 WCR-probes located at the non-irrigated side slope showing minor or no SWC progression.

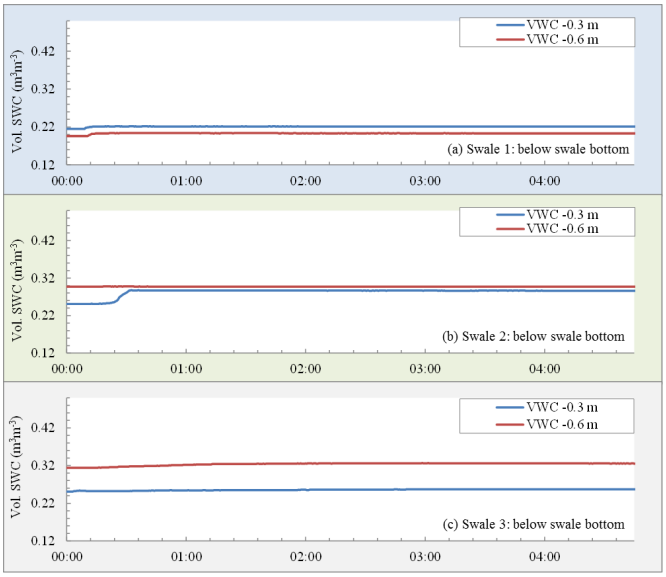

Figure 25a-c: Progression of soil water content of two WCR-probes below the swale channel bottom.

SWC readings displayed in Fig. 25 a-c, in the two measured depths (VWC-0.3 and VWC-0.6) make it evident that there was no significant percolation occurring in all the three swales for the various inflows and measurement periods. Just a minor increase in Swale 2 can be noted after the end of the inflow. In all swales assessed, SWC readings on the irrigated side slope did not reach values as high as on the swale bottom, which indicates, that due to the inclination, water is partly directly routed along the surface and partly drains through the upper soil layer of the side slopes towards the swale channel bottom. WCR-readings from non-submerged probes on the non-irrigated side slopes indicate that lateral infiltration occurred. With some delay the water content was raising, for example, by a maximum of 0.13 m^3m^{-3} (13 Vol.-%) in the Swale 1.

4.2 Comparison of observed and simulated hydrograph data

Results presented in this section are based on Paper III. The physically-based, distributed hydrological model Mike SHE was calibrated against the outflow hydrographs from irrigation experiments in Swale 1 and evaluated with respect to its capability of reproducing the observed hydrographs, for high spatial and temporal resolutions. After four parameter sets were found to represent well the four different inflow conditions in the field tests, eleven events were simulated with the calibrated model to assess the model performance. Examples of the simulated outflow hydrographs produced for the four parameter sets are displayed in Fig. 26 a-h and show a good fit between the observed calibration event and its simulation with the calibrated model, and samples of the best and worst fit hydrograph agreements between the measured hydrographs and simulations with the calibrated model, for the four parameter sets.

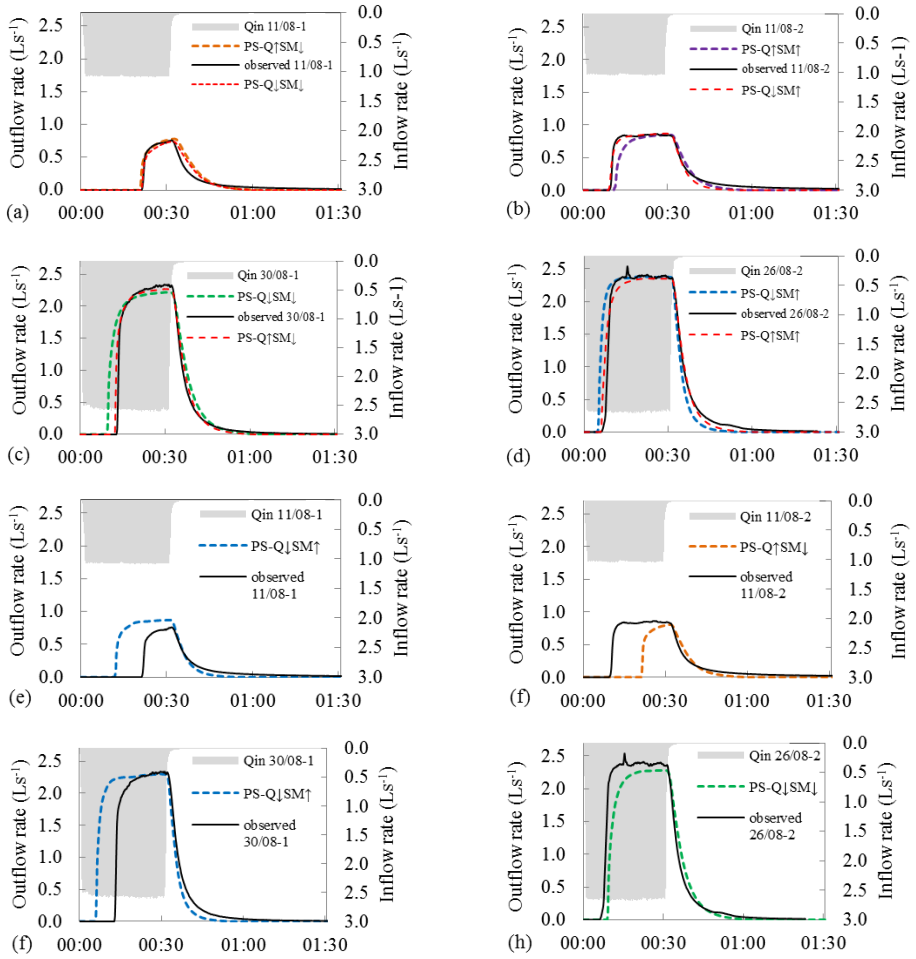

Figure 26 a-h: Measured and simulated hydrographs and hydrographs for irrigation experiments. Plots (a) - (d) show the observed hydrographs and those produced with the model calibrated for that event; Plots (e) - (h) show the worst agreements between the hydrographs produced with the calibrate model applied to other (verification) events.

The quantitative analysis of the performance criteria can be done with support of a plot of the normalized volumetric residual (NVr) and the normalized peak flow residual (NPFr) displayed in Fig. 27. Peak flow residuals between the observed and simulated hydrographs are generally small and insignificant. The volumetric residuals occur for all the derived parameter sets due to differences in the hydrograph shapes and the models insensitivity to the soil water content. Highest volumetric

residuals (>50%) can be found for calibration against high inflow and low initial SWC irrigation runs.

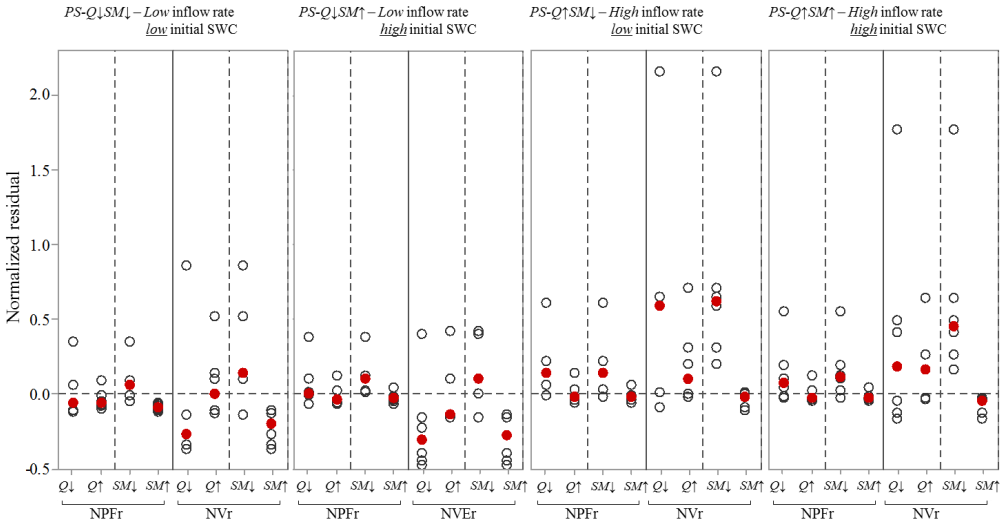

Figure 27: Dot plots of individual values of normalized peak flow residuals and normalized volumetric residuals for each parameter set (separated by boxes) and arranged according to the inflow rates and initial SWC (in subs-divisions). Sample size N=5-6 (results from calibration runs are excluded). Full red dots represent the medians.

5. Discussion

The results presented in the preceding chapter are discussed herein with respect to the effects of hydraulic/hydrological parameters on the grass swale hydrology and the significance of those parameters in swale design. More specifically, the discussion focuses on inflow rates/hydraulic loadings, the inflow direction, swale slope, antecedent soil moisture and the spatial variability of the swale channel characteristics. Furthermore, the use of field parameters determined in the conducted studies for distributed modelling of swale hydrology will be also discussed, and a summary of implications for swale planning and design will be given.

5.1 Effect of the inflow rate on swale hydrological performance

For the two inflows tested in the field, it was noted that less water infiltrated, relative to the applied volumes, for the increased inflow rate. This can be explained by the extended time of concentration and the corresponding increased time of hydraulic residence of water along the swale channel. Generally, higher inflows will cause an infiltration excess flow more rapidly, while smaller inflows are more likely to generate surface runoff only when the soil saturation capacity is exceeded. The final state swale flow reached after 5-15 minutes, during which the 30-m grass swale section was supplied with a steady inflow, can be described as mainly the flow conveyance, with only minor flow attenuation. Davis et al. (2012) defined three "treatment zones" for the various flow conditions during a range of actual storm event depths. The smallest storms were completely infiltrated; volumes and peak flows were attenuated for moderate storms, and the swale operated as a flow conveyance structure with, some flow smoothening, for the largest events. In this regard, our irrigation experiments mimicked moderate and severe storms. An increased inflow rate over the side slope would increase the surface area covered with runoff as shown by Garcia-Serrana et al. (2017a).

Mike SHE model simulations of the two mentioned flow regimes tested in Swale 1 suffered from the discovered lack of sensitivity of soil infiltration capacity in the model. The parameter sets studied resulted from calibrations, in which the parameters controlling the channel hydraulics (i.e., by increasing the hydraulic conductivity, depression storage and Manning n) were adjusted independently of soil parameters. This confirms that swales exposed to high inflows function as conveyance channels, with only minimal peak flow and volume reductions.

5.2 Effect of inflow direction and slopes on swale outflows

Inflow into swales can occur, at some points, in three directions: longitudinal inflow from upstream, longitudinal and lateral flows over the side slopes, or just the lateral flow over the side slopes. For all three cases the wetted areas, and the corresponding infiltration areas, with potentially different soil properties, would be of different sizes. In the tested swales, the channel bottom and one side slope contributed to flow reductions (by infiltration), but it can be speculated that the irrigation arrangement caused reduced hydrograph lag times, because of the pre-wetting of the channel by the concentrated longitudinal inflow. The swale side slope section received lateral inflows from the water supply system over 24 of the 30 m section length, and produced finger-flows of an increasing coverage, depending on the inflow rate. The instrumentation for the irrigation experiments did not

allow differentiating between the discharge from the swale channels and the side slopes. García-Serrana et al. (2017a) investigated the infiltration on side slopes and its control mechanisms, and found that runoff infiltration was larger than anticipated with increased infiltration on the longer side slope and higher saturated hydraulic conductivity. The side slopes of the swales tested in this thesis ranged from 1:2-2.5 (Swale 1) to 1:3-3.5 (Swale 2) and to 1:4.5-5 (Swale 3). Lateral flow over these side slopes was not measured but observed to partly infiltrate before it reached the swale bottom, especially at the beginning of each inflow event. Concerning the longitudinal slopes of the tested swales, effects on the hydraulic performance could not be detected as initial infiltration, swale channel irregularities and the mild slopes distort clear estimations. But it can be assumed that for lower slopes infiltration would be increased by decreased channel flow velocities. For Swale 2 with a longitudinal channel slope of 0.7% slope, it can be furthermore assumed that slower drainage involves also a prolonged periods of soil wetness, which would explain slow recovery of dry conditions and water ponded in swale depressions even after 3 hours. In a laboratory study of infiltration on grass slopes conducted by Morbidelli et al. (2016) they could show that grass reduces the effect of declining steady infiltration rates with an increasing slope gradient. They estimated that the K_{sat} was reduced by the factor of $\cos(\theta)$ (slope angle) and strictly depended on roughness of the sloped surface.

5.3 Effect of antecedent soil moisture on grass swale performance

The antecedent soil moisture in a grass swale depends on the antecedent rainfall and on swale soils. For the three studied swales, different final soil water contents were recorded after each irrigation event and after similar durations of dry periods, because of different soil characteristics. The initial soil water content had a significant effect on the swale hydrological/hydraulic response. The two groups of initial soil water content, defined as low SWC for dry conditions and high SWC for wet conditions, did not differ greatly in their magnitude. However, runoff retention by infiltration, flow attenuation and the outlet hydrograph was affected even by minor differences in soil moisture, especially for low initial soil water contents. In other studies the relevance of the soil water content was also reported. Garcia-Serrana et al. (2017a) quantified the impact of SWC on the infiltration capacity and volumes, and noted a sudden, linear increase in infiltration at low soil water contents.

In studies of runoff in swales by modelling soil with spatially heterogeneous SWC, Morbidelli et al. (2012) concluded that a spatially averaged SWC would be sufficient for the reproduction of hydrographs. In the presented study, using Mike SHE for simulating swale flows, the role of the magnitude of the initial SWC and spatial variability in the unsaturated zone, which were distributed in seven sections of the swale model, was found of minor importance. For all model settings tested in Paper III, the unsaturated zone reached the infiltration rates equal to the saturated hydraulic conductivity and saturated soil conditions almost equally rapidly for the two inflow rates tested, which agreed with the measured increases in the field. Uniform characteristics of the hydraulic conductivity, the saturated soil water content and soil parameters throughout the grass swale section simulated, overruled the initially inputted SWC variability, which confirms the findings of Morbidelli et al. (2012).

5.4 Effects of spatial variability of physical properties of grass swales

Elevation surveys of the three swales studied revealed swale bottom irregularities forming depressions 0.05-0.10 m deep. Like check dams, bottom depressions contribute to higher infiltration and retention of runoff and consequently greater lag times of the outflow hydrographs, as also reported by Davis et al. (2012) for check dams. Their observations showed significant volume attenuations and reductions for minor and intermediate storms in a swale with check dams. With a lower hydraulic loading to the swale, infiltration rates would increase because of extended detention of water in the depressions. Together with runoff storage in the upper layers of the soil matrix, it can be expected that they are beneficial for dissipating runoff small rainstorms and the early storm peaks. The effects of the topographical representation accuracy were addressed also by Helmers and Eisenhauer (2006) in simulations of flow over vegetative filters. Noting significant effects on the discharge hydrograph, their recommendation for considering high topographical detail in flow simulations can be confirmed by the results of the Mike SHE simulations for Swale 1. In fact, accurate, cell assigned elevation data contributed to a good reproduction of ponding areas in the swale channel and eventually to a better agreement between observed and simulated hydrographs. When pollutant removal efficiencies in grass swales are addressed in model simulations, such outcomes are highly useful.

5.5 Practical implication for swales in urban stormwater management

The test grass swales, located in Luleå, northern Sweden, were studied below their actual capacity limits, but nevertheless for fairly large flows, for which a steady discharge would be developed early and flow attenuation and hydrograph lag times would soon reach their minima. However, for low intensity storms, grass swales flow attenuation is increasingly sensitive to soil moisture and the soils used for the construction of swales can influence the soil water retention to allow for good drainage of the soil layer after rain events. The faster the soil infiltration capacity is re-established after the rainfall, the more robust the swale will be in attenuating the first runoff peaks. Where the native soils do not have a sufficient infiltration capacity and cannot be replaced, the swale channel dimensions have to compensate for reduced storage volume in the top soil and a low percolation rate into subsoils. An easy measure for enhancing flow attenuation in grass swales by creating depressions in the bottom or by properly designed check dams. Note however that such measures reduce the swale channel flow capacity. In spite of local restrictions on swale construction, swale features should be designed on the basis of design storm calculations for specific geographical regions, and on determined storm depths, soil texture and swale dimensions, including the swale lengths, depths, and side slopes, and further adjusted as needed. For detailed swale design considering the swale and its contributing area, the analysis of local rainfall records would be furthermore useful to analyse the antecedent moisture conditions (antecedent dry days). Such data could also serve for the calibration of continuous rainfall-runoff models considering the antecedent moisture conditions of the urban catchment. In swale design and planning a distributed model Mike SHE would have a limited practical use, because of the lack of detailed input data, including the initial soil moisture. However, often in design of such drainage facilities like grass swales, operational requirements limit the use of optimal longitudinal and side slopes. However, as numerous sources recommend, some of which are

listed in Chapter 2.2, longitudinal slopes should be in the range of 1- 5%, in order to provide positive drainage and prevent erosion (Schueler, 1987).

6. Conclusions

Based on the study findings included in this thesis the following conclusions can be drawn:

The transition between two main swale functions of runoff conveyance and control was reproduced in field irrigation experiments; starting with runoff dissipation under low initial soil water contents and changing to full runoff conveyance with high hydraulic loads, but with minor peak flow and runoff volume reductions. Hydraulic loading, initial soil water content and the saturated hydraulic conductivities were identified as influential factors determining the speed of the transition between the swale functions. The distributed model Mike SHE was found to have a good potential for process oriented simulations of small scale green infrastructure like grass swales.

Swale volume reductions for two of the swales tested were 36%-73% for dry antecedent conditions and 17-36% for initially saturated conditions, and hydrograph lag times for the 30-m sections varied between 5-15 minutes depending on the hydraulic loading and the initial soil water content. Highest flow attenuations were noted for the driest conditions, illustrating the significance of initial soil water content for the formation of swale hydrograph. Volume reductions, peak flow reductions and hydrograph lag times indicate a trend towards an asymptotic minimum under increasingly wet conditions.

Soil water content measurements at multiple points, starting at low SWC and up to saturated conditions and, indicate the range of runoff volumes abstracted in the swale top soil and together with temporary water storage in the swale channel depressions, small rains and storm peaks are retained without generating swale discharge prior any percolation of runoff into deeper zones.

The soil water content showed significant spatial variability with regard to the initial conditions and saturated conditions for all locations in the top soil layer, illustrating the spatial variability of soil properties within each swale. The increase of soil water content in the non-submerged side slope indicated lateral infiltration and the contribution of the side slope to flow attenuation. However, an effect of spatial variability on swale outflow was not observed.

The saturated hydraulic conductivity measured with double-ring infiltrometers (N=9/swale) varied among all tested swales and also varied spatially within each swale significantly (the coefficient of variation: 0.39-0.55, St.Dev. 1.0-4-2 cm/hr). However, the effect of spatial variability of infiltration on the discharge hydrograph could not be shown. Quasi-steady infiltration rates calculated from inflow and outflow hydrographs for Swales 1 and 2 provide hydraulic conductivities differing from DRI measurements, indicating both, the uncertainty associated with point measurements and probable contributions of other swale sections, besides the bottom, to the overall swale infiltration (including lateral infiltration through side slopes).

The swale channel bottom topography, containing numerous depressions and creating bottom surface storage, increased flow attenuation for runoff from storms with small to intermediate intensities (0.09-0.61m^3 = 5-32% of the 2-month storm inflow volume).

In distributed modelling with Mike SHE, the effect of spatial variation of swale characteristics could only be confirmed for swale topography, which impacted the initial retention of irrigation runoff. When dealing with the modelling of sedimentation and pollutant removal performance (outside of the thesis topic), such a feature is presumably relevant.

In simulations with the grass swale model, calibrated for each of the two selected discrete inflow events, the swale functioned mainly as a conveyance channel. Simulation results showed a good agreement with the observed outflow hydrographs. However, the unsaturated zone was of secondary importance in model calibration and adjustments of the soil parameters influencing the relative hydraulic conductivity and thus the soil water content, were dominating.

The calibrated Mike SHE model was furthermore hardly sensitive to the initial soil water content, which resulted in larger residuals (i.e. differences between the measured and simulated values) for runoff volumes and peak flows especially for low initial soil water contents. The best predictive accuracy, indicated by the Nash-Sutcliffe model efficiency was achieved with a calibration parameter set reflecting high inflow and high initial soil water content values.

7. References

Ackerman, D., & Stein, E. D. (2008). Evaluating the effectiveness of best management practices using dynamic modeling. Journal of Environmental Engineering, 134(8), 628-639.

Ahiablame L. M., Engel B. A. and Chaubey I. (2012). Effectiveness of low impact development practices: Literature review and suggestions for future research. Water Air Soil Pollut. 223(7), 4253-4273.

Abida, H., & Sabourin, J. F. (2006). Grass swale-perforated pipe systems for stormwater management. Journal of irrigation and drainage engineering, 132(1), 55-63.

Abu-Zreig, M., Rudra, R. P., & Whiteley, H. R. (2001). Validation of a vegetated filter strip model (VFSMOD). Hydrological processes, 15(5), 729-742.

Bäckström, M., (2002). Sediment transport in grassed swales during simulated runoff events. Water Sci. Technol. 45 (7), 41-49.

Barrett M., Walsh P., Jr. J. and Charbeneau R. (1998). Performance of Vegetative Controls for Treating Highway Runoff. J Environ Eng. 124(11), 1121-1128.

Bertrand-Krajewski, J. L., Barraud, S., & Chocat, B. (2000). Need for improved methodologies and measurements for sustainable management of urban water systems. Environmental Impact Assessment Review, 20(3), 323-331.

Beven K.J. (2012) Rainfall–runoff modelling-The Primer.2nd Edition. Chichester: JohnWiley & Sons Ltd.

Caraco, D. and Claytor, R. (1997). Stormwater BMP design supplement for cold climates. Center for Watershed Protection, Ellicot City, MD.

Chalmers, L., & Gray, S. (2004). Stormwater Management Manual for Western Australia". Department of Environment Consultation and guidance from the Stormwater Working Team.

Coffman, L. S. (2002). Low-impact development: an alternative stormwater management technology. In R. L. France (Ed.), Handbook of water sensitive planning and design (pp. 97–124). Washington, D.C.: Lewis.

Dahlström, B. (2010). Regnintensitet–en molnfysikalisk betraktelse. [Rain Intensity – a cloud physical contemplation] (in Swedish). Report 2010-05, Swedish Water and Wastewater Association, Svenskt Vatten AB, Stockholm.

Davis, A. P., Stagge, J. H., Jamil, E., & Kim, H. (2012). Hydraulic performance of grass swales for managing highway runoff. Water Research, 46(20), 6775-6786.

Deletic, A. (2001) Modelling of water and sediment transport over grass areas, Journal of Hydrology, 248(1-4), 168-182.

Deletic A., Fletcher T.D. (2006). Performance of grass filters used for stormwater treatment - A field and modelling study. Journal of Hydrology 317 : 261-75. DOI: 10.1016/j.jhydrol.2005.05.021.

D.L.Howell & Associates, Inc. (2017): Stormwater Management Best Practices. [swale picture] (Available online: https://www.dlhowell.com/blog/stormwater-management-best-practices/ , accessed on Oct 4, 2017)

DHI (Danish Hydraulic Institute) (2017). MIKE SHE User Manual. Hørsholm, Denmark: Danish Hydraulic Institute.

Dietz, M. E. (2007). Low impact development practices: A review of current research and recommendations for future directions. Water, Air, and Soil Pollution, 186(1-4), 351-363.

Duchene, M. L. (1991). Design of infiltration trenches using perforated pipe. MASc thesis, Univ. of Waterloo, Waterloo, Ontario, Canada.

FAO (Food and Agriculture Organization of the United Nations) (2014). World reference base for soil resources 2014. International soil classification system for naming soils and creating legends for soil maps. Update 2015. World soil resources reports 106. Rome, Italy.

Farahi, G., Khodashenas, S. R., Alizadeh, A., & Ziaei, A. N. (2017). New Model for Simulating Hydraulic Performance of an Infiltration Trench with Finite-Volume One-Dimensional Richards' Equation. Journal of Irrigation and Drainage Engineering, 143(8), 04017025.

Flanagan, K., Branchu, P., Ramier, D., & Gromaire, M. C. (2017). Evaluation of the relative roles of a vegetative filter strip and a biofiltration swale in a treatment train for road runoff. Water Science and Technology, 75(4), 987-997.

Fletcher, T. D., Andrieu, H., & Hamel, P. (2013). Understanding, management and modelling of urban hydrology and its consequences for receiving waters: A state of the art. Advances in Water Resources, 51, 261-279.

Fletcher T.D., Shuster W., Hunt W.F., Ashley R., Butler D., Arthur S., Trowsdale S., Barraud S., Semadeni-Davies A., Bertrand-Krajewski J., Mikkelsen P.S., Rivard G., Uhl M., Dagenais D., Viklander M. (2015). SUDS, LID, BMPs, WSUD and more – The evolution and application of terminology surrounding urban drainage. Urban Water Journal 12 : 525-42. DOI: 10.1080/1573062X.2014.916314.

García-Serrana, M., Gulliver, J. S., & Nieber, J. L. (2017a). Infiltration capacity of roadside filter strips with non-uniform overland flow. *Journal of Hydrology, 545*, 451-462.

García-Serrana, M., Gulliver, J. S., & Nieber, J. L. (2017b). Non-uniform overland flow-infiltration model for roadside swales. *Journal of Hydrology*, 552, 586-599.

Geerling, H. R. (2014). Infiltration Swales: Quantitative Performance on an Urban Catchment Scale". (M.Sc.) Delft University of Technology. Retrieved October 1, 2016, from http://www.tudelft.nl

Graham, E. I. (1990). An urban runoff infiltration basin model. MASc thesis, Univ. of Waterloo, Waterloo, Ontario, Canada.

Helmers, M. J., & Eisenhauer, D. E. (2006). Overland flow modeling in a vegetative filter considering non-planar topography and spatial variability of soil hydraulic properties and vegetation density. Journal of hydrology, 328(1), 267-282.

Kluge, B., Kaiser, M., Sommer, H., Markert, A., Pallasch, M. and M. Facklam (2016). Performance and current state of long-term-operating stormwater infiltration systems with bioretention. [Leistungsfähigkeit und Zustand langjährig betriebener dezentraler Regenwasserversickerungsanlagen] (in German). Fachberichte Regenwasserversickerung. In: gwf Wasser + Abwasser Vol. 157, 06/2016. 628-636.

Lucke, T., Mohamed, M. A. K.. Tindale, N. (2014). Pollutant Removal and Hydraulic Reduction Performance of Field Grassed Swales during Runoff Simulation Experiments. *Water*, 6: 1887-1904.

Marsalek, J. (2006). Overview of urban drainage impacts on aquatic habitat. Integrated urban water resources management, 181-190.

Morbidelli, R., Saltalippi, C., Flammini, A., Cifrodelli, M., Picciafuoco, T., Corradini, C., & Govindaraju, R. S. (2016). Laboratory investigation on the role of slope on infiltration over grassy soils. *Journal of Hydrology*, 543, Part B, 542-547.

Morbidelli, R., Corradini, C., Saltalippi, C., & Brocca, L. (2012). Initial soil water content as input to field-scale infiltration and surface runoff models. *Water Resources Management, 26*(7), 1793-1807.

Mualem, Y., 1976. A new model for predicting the hydraulic conductivity of unsaturated storm-water infiltration. J. Irrig. Drain Eng. 134(5): 652 – 658.

Nash, J. E.; Sutcliffe, J. V. (1970). "River flow forecasting through conceptual models part I — A discussion of principles". Journal of Hydrology. 10 (3): 282–290. doi:10.1016/0022-1694(70)90255-6

Niazi, M., Nietch, C., Maghrebi, M., Jackson, N., Bennett, B. R., Tryby, M., & Massoudieh, A. (2017). Storm water management model: performance review and gap analysis. Journal of Sustainable Water in the Built Environment, 3(2), 04017002.

Nishat, S., Guo, Y., & Baetz, B. (2010). Antecedent soil moisture conditions of different soil types in south-western ontario, canada. Hydrological Processes, 24(17), 2417-2424.

Pitt, R., and McLean, J. (1986). Toronto Area Watershed Management Strategy Study: Humber River Pilot Watershed Project. Ontario Ministry of the Environment, Toronto, Ontario, 486.

Prince Georg´s County (2014). Stormwater Management Design Manual. Department of Permitting, Inspection and Enforcement. ML, USA.

Qin, H., Li, Z., Fu, G. (2013). The Effects of Low Impact Development on Urban Flooding Under Different Rainfall Characteristics. J. Environ. Manage., 129(0), 577-585.

Richards, L.A., 1931. Capillary conduction of liquids through porous mediums. J. Appl. Phys. 1 (5), 318‑333.

Ruelle, P. and J.P. Laurent (2008). CS616 (CS615) water content reflectometers. In: S.R. Evett, L.K. Heng, P. Moutonnet, M.L. Nguyen (Eds.), Field Estimation of Soil Water Content: A Practical Guide to Methods, Instrumentation, and Sensor Technology. IAEA-TCS-30, International Atomic Energy Agency, Vienna, Austria (2008) ISSN 1018-5518

Schueler, T. (1987). Controling urban runoff: A practical manual for planning and designing urban BMPs. Washington Metropolitan Water Resources Planning Board, Washington, D.C., USA.

Shen, J. (1981). Discharge characteristics of triangular-notch thin-plate weirs: Studies of flow to water over weirs and dams. Water supply paper No.1617, U.S. Geological Survey.

Semadeni-Davies, C. Hernebring, G. Svensson, and L.-G. Gustafsson (2008).The impacts of climate change and urbanisation on drainage in helsingborg, sweden: Combined sewer system, Journal of Hydrology 350, 100.

SvenskVatten (Swedish Water and Wastewater Association) (2011). P105 Hållbar dag-och dränvattenhantering-råd vid planering och utförande. (In Swedish) [Sustainable stormwater and drainage management – Guidelines for planning and construction]. Svensk Vatten, Stockholm. ISSN 1651-4947

UDFCD (Urban Drainage and Flood Control District) (2010). Urban storm drainage criteria manual, Vol. 3. UDFC, Denver, CO, USA.

U.S. EPA (1983). NURP Priority pollutant monitoring project – summary of findings. EPA report 831204. U.S. Environmental Protection Agency, Washington, DC. USA.

U.S. EPA (1999). Storm Water Technology Fact Sheet Vegetated Swales. U.S. Environmental Protection Agency. Office of Water, Washington, DC, USA.

U.S. EPA (2000). Low impact development (LID). A literature review. Washington, D.C: Office of Water. U.S. Environmental Protection Agency. EPA-841-B-00-005. Washington, DC, USA.

U.S. EPA (2014). Enhancing sustainable communities with Green Infrastructure. Washington, D.C: Office of Sustainable Communities. U.S. Environmental Protection Agency. EPA 100-R-14-006. Washington, DC, USA.

Wanielista, M. P., Yousef, Y. A., & Avellaneda, E. (1988). Infiltration Capacity of Roadside Swales. FL-ER-38-88. Florida Department of Transportation, Tallahassee, FL.

Wanielista, M.P., Yousef, A.Y. (1992). Stormwater management. John Wiley & Sons, Inc., New York, N.Y., USA.

Van Genuchten, M. T. (1980). A Closed-Form Equation for Predicting the Hydraulic Conductivity of Unsaturated Soils. *Soil Science Society of America Journal*, 44(5), 892-898.

Viklander, M., Marsalek, J., Malmquist, P. & Watt, W. E. (2003). Urban drainage and highway runoff in cold climates: Conference overview. Water Science and Technology, 48(9), 1-10.

Paper I

Rujner, H. Leonhardt, G., Perttu, A-M., Marsalek, J. and M. Viklander (2016)

Advancing green infrastructure design: Field evaluation of grassed urban drainage swales.

In: Novatech 2016: 9th International Conference on planning and technologies for sustainable management of Water in the City. Lyon, France.

Rujner, H. Leonhardt, G., Perttu, A-M., Marsalek, J. and M. Viklander (2016). Advancing green infrastructure design: Field evaluation of grassed urban drainage swales. In: Novatech 2016: 9th International Conference on planning and technologies for sustainable management of Water in the City. Lyon, France.

Advancing green infrastructure design: Field evaluation of grassed urban drainage swales

Améliorer la conception des infrastructures vertes: évaluation sur site de rigoles de drainage gazonnées en milieu urbain

Hendrik Rujner*, Günther Leonhardt*, Anna-Maria Perttu*, Jiri Marsalek*, Maria Viklander*

* Urban Water Engineering, Department of Civil, Environmental and Natural Resources Engineering. SE-971 87 Luleå, Sweden,
E-mail: hendrik.rujner@ltu.se

ABSTRACT

Grassed drainage swales, which represent common elements of urban green infrastructures, are designed for different soils, flow capacities, dimensions, slopes and vegetation. Their design is often based on local experience rather than technical guidelines, and consequently, the design and performance of grassed swales, with respect to flow capacity and stormwater management objectives may significantly vary from one jurisdiction to another. To improve this situation and reduce design uncertainties, a field study of grassed swales was conducted by assessing their hydrologic performance. A 30-m section of an urban grassed swale in sandy soils, located in the City of Luleå (Northern Sweden), was equipped with a mobile water supply system and instrumented for measuring swale flow characteristics. The water supply system comprised five containers (~ 1 m^3 each) providing controlled longitudinal and lateral inflows into the tested swale section. These inflows were selected to mimic stormwater runoff from a typical drainage area. At the first test site, 14 rainfall events of 30-minute duration were simulated and the resulting swale flows and soil moisture conditions were measured. The experimental variables addressed included wet and dry antecedent conditions, and three inflow rates. The preliminary results indicate that the degree of swale inflow attenuation depended on the magnitude of runoff inflow, on the initial soil moisture conditions and that significant volumes of water can be stored and transmitted during the stormwater drainage process.

KEYWORDS

Vegetated swale, hydrologic performance, soil moisture, urban green infrastructure design

1 INTRODUCTION

Grassed drainage swales generally perform three tasks in stormwater management: convey urban runoff, reduce runoff volumes and discharges by infiltration, and enhance runoff quality by filtration and settling (US EPA 1997, Barrett et al. 1998, Dietz 2007, Ahiablame et al. 2012). In regions with seasonal snow covers, they also provide space for snow storage and melting (Pitt et al. 1986). The design of such common elements of green infrastructure varies among jurisdictions and more or less follows local experience reflecting physical conditions. As a consequence, the environmental performance of swales varies from case to case, and is subject to significant uncertainty.

To date, a number of different hydraulic/hydrological parameters were used to assess the performance of swales, primarily with respect to runoff delay and volume reduction. Factors influencing these performance criteria were investigated by a number of researchers and found to vary in the context of different geographic and climatic conditions and local swale designs. Yousef et al. (1987) found that the swale flow reduction depended on the inflow rate and flow velocity; inflows of less than 0.1 L/s were fully dissipated in the swale, but an inflow of 1.3 L/s was reduced only by about 10%. Using simulated inflows, Bäckström (2002) demonstrated for 30-minute runoff events, with flow rates from 0.32 to 0.77 L/s, that one to two thirds of the runoff volume infiltrated into the surrounding soils. With respect to antecedent soil conditions, Barrett (2008) reported that in 14 swales 30-147 m long, 50% of the runoff volumes were dissipated in the case of low initial soil moisture. Deletic and Fletcher (2006) developed a swale infiltration model and verified it on grassed filter strips 65 m long, for steady inflows. The measured runoff volume reductions ranged from 33 to 87% for inflow rates of 2-15 L/s. Furthermore, they observed an increase in the overland flow during the experiment, because of the clogging of soil pores by sediment, and concluded that the hydraulic conductivity was the most important model calibration parameter. Davis et al. (2012) analysed responses of highway swales of various designs to dynamic inflows during 52 storm events. Due to estimated low storage capacity, a direct transition from attenuation to conveyance was documented, but a continuing reduction of flow rates was independent of the swale design.

In spite of the fact that the swale hydrology is mainly controlled by the soil conditions, only a few studies addressed soil moisture processes and the spatial variability of the factors determining runoff and flow characteristics. The non-uniform nature of runoff infiltration was demonstrated by Jensen (2004), who used a dye to track the subsurface flow pattern at a highway swale in Denmark. After a uniform flow abstraction in the first few centimetres of the turf, preferential flow occurred due to inhomogeneity of the subsoil, thus emphasizing the role of spatial and temporal dynamics of rainfall excess. Lucke et al. (2014) used field simulations of runoff from a one-year storm in 30-35 m long swales, and also demonstrated that with lower initial soil moisture content, the flow reduction increased greatly. Detailed infiltration measurements designed to quantify the spatial variability of the saturated hydraulic conductivity by Ahmed et al. (2015) showed that the hydraulic conductivity varied by up to two orders of magnitude, within the same test section, and highlighted the need of further research at these small scales.

The literature survey summarized above concluded that field experiments with simulated runoff represent a preferred approach to investigating swale flow processes and the overall hydrological performance of vegetated swales. To advance the understanding of such processes, a field study of swales was initiated with the overall objective of determining swale water balance for various events and different soil moisture conditions, and the impact of antecedent soil moisture on the test section outflows. Recognizing that actual storm events would introduce another variable into the experiments, in the form of varying hydraulic loads, and also slow study progress because of waiting for rainfall events, it was decided to supply the swales with sub-potable water mimicking runoff from selected block rainfalls. To elucidate the evolution of flow in the swale, the inflow was controlled at a constant flow rate. This experimental arrangement was independent of the weather and the catchment size, and allowed simulation of runoff from different hydraulic loads to various swales. As street and road drainage swales typically develop longitudinal flow with lateral runoff inflows, the same inflow arrangement was created in the field experimental set up. The study was conducted in the City of Luleå, Sweden, where swales are used for conveyance and pre-treatment of runoff, before it enters storm sewers, and also for snow storage in winter. The paper that follows presents descriptions of the experimental setup and methods, and the results obtained for the swale tested in the first experimental series completed in 2015; extension of field monitoring to other sites is planned in 2016.

2 MATERIAL AND METHODS

2.1 Study site

A 30-metre section of a grassed swale, 3.1 m wide, was selected for study as a representative type of urban swales that can be found close to the centre of the city of Luleå. The swale is located between a gravel surface parking area on one side and a well-frequented bicycle path on the other side; these two adjacent areas drain into the swale. At the upstream end, the swale starts at a small asphalt road and at the downstream end it drains into a drop shaft connected to the storm sewer system. The swale channel appears to be compacted, likely due to maintenance practices over the years, and minor sediment deposits suggest ongoing sedimentation in the swale. Both these features would then contribute to reduced infiltration rates in the swale. The vegetation cover is provided by a dense grass turf with grass blade lengths of 5-10 cm. The infiltration capacity of the swale bottom section was investigated using the double-ring infiltrometer measurements, which were conducted along the swale longitudinal axis at every 4 m (see Table 1). The side slopes were accurately determined with a RTK-GPS survey (real time kinematic–GPS) and the subsequent GIS processing of the data. For determination of the soil texture, soil samples were collected along the swale bottom at points 7.5 m apart, after flooding experiments. The grain size distributions were analysed in the laboratory by wet sieving and indicated a gradual change in the texture from slightly-silty sand, in the upstream swale section, to intermediate-silty sand in the downstream sections.

Table 1: Swale characteristics.

Swale section [m]	Mean width [m]	Mean slope [%]	Infiltration capacity [mm/h]
0-3	3.8	1.33	220
3-6	3.4	2.0	220
6-9	3.3	1.0	450
9-12	3.0	2.67	180
12-15	2.8	-0.67	480
15-18	2.9	-0.67	
18-21	2.9	4.33	300
21-24	2.9	0.67	288
24-27	3.1	0.33	678
27-30	3.2	1.33	450
Mean	3.1 ±0.3	1.24 ±1.52	393 ±154

2.2 Simulation of runoff events by swale irrigation

For simulating runoff flows in the swale, a mobile water supply system consisting of five IBC water containers (1 m^3 each) was used and the swale inflow was distributed in such a way that one part entered as a longitudinal flow at the upstream end and the rest entered on one side only as a lateral inflow, which was quasi-uniformly distributed over the length of 24 m (see Figs. 1 and 2). The lateral flow distribution was achieved by laying two sections of a 160 mm PVC half-pipe, with closely spaced small V-notch overflow weirs (a labyrinth weir), along the swale and feeding the flow through this structure, whose slope could be manually adjusted to achieve a relatively uniform flow distribution. A nearby canal served as a source of water, which was pumped into the IBC containers. The container discharge was controlled using tap valves and control marks at the measuring weirs.

As shown in Fig. 1, four stainless steel flow measuring weirs were used to measure swale inflow at the upstream end, two sections of the lateral inflow, and the swale outflow. By maintaining constant heads in all the IBC-containers during their discharge, it was possible to simulate preselected and repeatable block-rainfall events of preselected rainfall intensities. Another critical requirement was maintaining fairly well synchronized inflows, especially from the lateral inflow distributors, to allow for uniform wetting of the swale sloping side.

The magnitudes of the simulated inflow volumes and design flow rates were derived from the rational method, by considering a contributing drainage area of 560 m^2 and a runoff coefficient of 0.8 for the combined impervious and unpaved subareas. The design storm intensity for different return periods was calculated from an IDF (intensity-duration-frequency) equation recommended for drainage design in Sweden (Dahlström 2010):

$$i = 190\sqrt[3]{T}\,\frac{\ln(D)}{D^{0.98}} + 2$$

Where i = rain intensity [litres/s/ha], D = duration [minutes], and T= return period [months]. The flow rates and volumes selected for swale experiments are listed in Table 2 for the duration of 30 minutes.

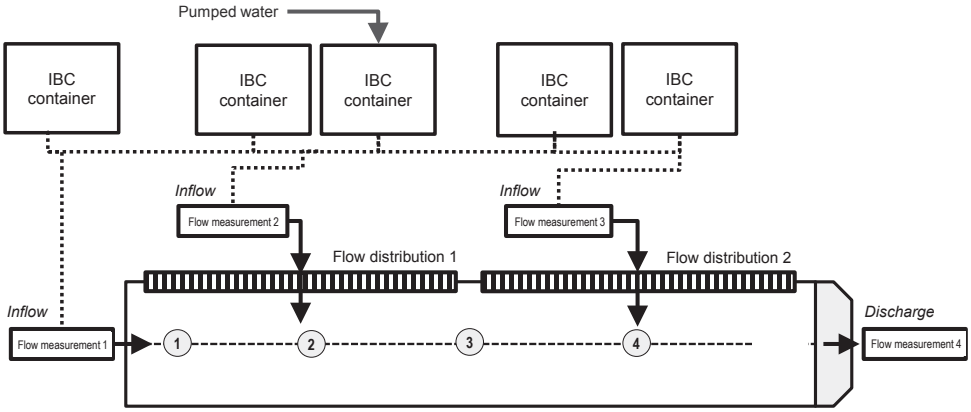

Figure 1: Schematic overview of the swale, the water supply system, and measuring weirs. Numbered circles (1-4) indicate locations of the soil moisture probes.

Table 2: Simulated rainfall intensities and drainage flows for the swale tested.

Design storm return period	Rain intensity [mm/h]	Calculated inflow rates for A = 0.056 ha	Calculated inflow volumes (m^3)
0.5-year storm	13.5	2.1	3.8
1-year storm	17.6	2.7	4.9
2-year storm	30.3	4.7	8.5

A further requirement of the swale assessment was consideration of design flows on dry or wet soils. In view of high infiltration rates measured in the swale, the antecedent conditions were considered as dry, when there was no rainfall or swale irrigation for an antecedent period of at least 16 hours, otherwise the conditions were assumed to be wet.

2.2.1 Flow measurements

Flow measurements were performed in constructed channels equipped with outflow weirs and ISCO 2150 flow meters (using their depth measurement feature only). Since the inflow was divided into three components, individual measurements required good precision, which was achievable by measuring heads over the custom made measuring weirs. Heads were measured with pressure transducers characterized by an accuracy of ±0.003 m. The longitudinal inflow (Fig.1) entered the swale via a 250 mm pipe with a downstream 90° V-notch weir. The two lateral inflow distributors were fed with water (Fig. 1) via 160 mm pipes with 45° V-notch outflow weirs. The swale outflow was measured in a 2.5 m long rectangular channel fitted with a compound constriction flow meter combining an orifice and a rectangular weir with the crest above the orifice opening (Fig. 3). All measuring devices were sharp-crested and made of 1 mm stainless steel. The slope of the measurement channels was adjusted to 0.01 to minimize the occurrence of supercritical flows. To minimise losses of swale water by seepage around the flow measurement structure, a 2.5 m long plastic sheet was placed in the swale just upstream of the measurement channel, and the upstream end of the sheet was inserted 15 cm below the turf ground. Flow measurements were initiated when water started to flow into the swale section tested, and in data analysis, the three inflow components were integrated to produce the total inflow, which was then compared to the swale outflow. In the initial analysis of data, the end of runoff events was set equal to the time when the flow rate at the outlet fell below 0.05 L/s; such trickle flows were observed even 45 min after the simulated inflow stopped.

2.2.2 Soil moisture measurements

Soil moisture measurements were collected by the water content reflectometer probes (CS 616 WTR-probes, by Campbell Scientific) at four points distributed along the 30 m grassed swale at 7.5 m apart (Fig. 1, Points 1-4). These sensors measure the relative average soil volumetric water content (VWC) in m^3 of water per m^3 of soil (hence dimensionless), over the entire length of the sensor rod. VWC in the soil volume of about 0.56 L is measured with an accuracy of ±0.025. The measurements were made using the factory calibration; soil specific calibrations are recommended for clayey soils, or soils with high organic content or large porosity (Jones et al. 2002, Chow et al. 2009), which were not encountered in this study. The 30 cm probe rods were inserted into the undisturbed top soil layer at a 45° angle close to the swale bottom centreline, to minimise flow obstructions by the probe head especially during small flows. The soil water content was logged at 30 s intervals, and the logging started just before the runoff event.

Figure 2. Swale water supply system comprising IBC tanks, longitudinal inflow pipe, and two lateral inflow distributors.

Figure 3: Outlet measurement channel with a compound constriction flow meter (an orifice and a rectangular weir).

3 RESULTS

The presentation of results focuses on two aspects of swale flow: (a) Runoff response described by the time lag of runoff with respect to rainfall, and (b) water infiltration into, and storage in, underlying soils.

3.1 Swale runoff response

Parameters describing the hydrological performance of the tested swale were monitored during 14 runoff simulations mimicking longitudinal, concentrated inflow into the swale and lateral inflow in the form of side slope sheet flow. As soon as the inflow started, surface runoff developed in the upstream swale section, where concentrated flow was released. The irrigated swale side initially abstracted the water trickling in from the flow distributors, but contributed to the swale flow in the form of Hortonian runoff, when rain excess exceeded infiltration rates. Because of breaks in the swale longitudinal slope (see Table 1), water started to pond in small depressions, especially near the half-point of the swale section, but this state was quickly overcome and water started to flow downstream. When the surface runoff reached the outlet weir, some ponding developed and backwater extended upstream to the plastic sheet laid on the swale bottom.

The intended design storm inflow rates and volumes could not be achieved because of difficulties in operating flow controls; namely, the pumped feed serving to compensate outflow from the water containers and the container discharge controlled by four valves required simultaneous adjustments. In spite of these challenges, three sets of design flow rate replicas of 0.9, 2.0 and 3.1 L/s were achieved, with some uncertainties (see Table 3). The flow rates set in the experiments corresponded to rainfall depths of approximately 2.9 mm, 6.7 mm (≈0.5-year storm) and 10.0 mm (1.5-year storm), over the duration of 30 minutes.

Table 3: Inflow rates, the corresponding rainfall intensities and water content of the control soil volume serving to measure soil moisture below the swale bottom (V = wetted perimeter x probe depth x length of swale section) for wet and dry antecedent conditions.

Run No.	1	2	3	4	5	6	7	8	9	10	11	12	13	14
Inflow rate (L/s)	0.9	2.5	1.8	3.4	3.1	3.0	3.0	2.0	2.1	2.1	3.2	3.2	3.1	1.2
Inflow volume (m^3)	1.6	4.49	3.17	6.08	5.54	5.45	5.41	3.63	3.78	3.86	5.71	5.76	5.62	2.19
Corresponding rainfall intensity (mm/ 30 min)	2.9	8.0	5.7	10.9	9.9	9.7	9.7	6.5	6.8	6.9	10.2	10.3	10.0	3.9
Δ Soil water content (%)	20.5	6.7	22.6	8.7	8.4	2.5	4.1	16.5	12.1	3.3	14.2	9.7	3.3	17.5
Control soil volume (m^3)	3.35	3.75	3.35	4.19	4.00	4.00	3.87	4.32	4.26	4.06	4.45	4.32	4.26	3.03
Total stored water (m^3)	0.69	0.25	0.76	0.36	0.33	0.10	0.16	0.71	0.52	0.13	0.63	0.42	0.14	0.53

Two out of the 14 runs did not fit into groups of replicas, but nevertheless could be included in the analysis. Swale hydrographs of two simulation runs are displayed in Figs. 4 and 5, for dry and wet antecedent conditions, respectively. The hydrographs show that using the study setup, well-defined events could be established in the swale tested. Elevated inflows in the beginning of the event were mainly caused by storage tank valve adjustments, but a quasi-uniform feed flow was quickly achieved and sustained for the rest of the run. Comparison of the inflow and outflow hydrographs shows the delay of outflow in relation to the inflow, and this delay is referred to as lag time, which can be determined as the time difference between the centroids of both hydrographs (Viessman et al. 1989). It was further observed in the field that the swale discharge durations were similar for all the runs, regardless of the inflow volumes applied. The shapes of outflow hydrographs in Figs. 4 and 5 differed; the relatively small rate of 1.2 L/s (Run #14) produced a slow build-up of flow in the swale and an immediate flow recession after the inflow ended. For this rate, the run duration of 30 min was not sufficient to generate a constant swale discharge. Furthermore, the outflow hydrograph suggests that flow was attenuated by continuing constant infiltration over the 30 m swale section. The resulting inflow rate reduction was 40% (12%-62%) and the volumetric reduction was 55% (27-73%). For a large event on an initially wet soil (not shown here), the increase of the outflow rate was strong and resulted in flow rates larger than the inflow of 3.1 L/s. After 9-10 minutes of flow build-up, a relatively constant swale discharge was established and lasted over the rest of the inflow duration, until a rapid recession after the inflow ceased. There was no observable attenuation of the swale flow rate or event volume for such events.

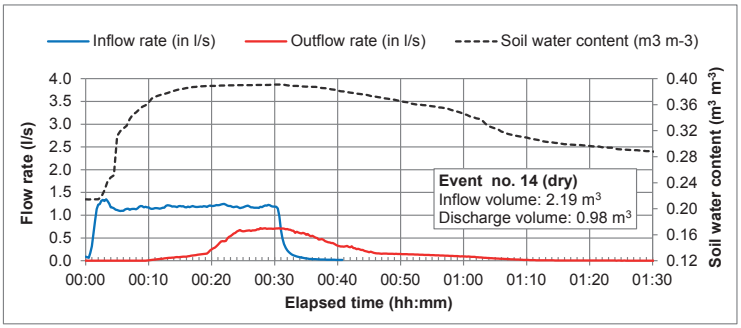

Figure 4: Inflow and outflow hydrographs of a small event on initially dry soil and evolution of soil water content.

The response lag for Run #14 shown in Fig. 4 is 18 min. For Run #7, with higher inflow rates and wet swale ground, the lag was 10 min. Lag times were determined for all the experimental runs and are plotted in Fig. 6. The plot indicates that lags varied from 7 to 19 minutes and declined with increasing inflow rates (i.e., simulated rainfall intensities), especially for runs in dry conditions, which is in agreement with lag time formulas in the literature (Viessman et al. 1989). Higher inflow rates on wet antecedent conditions tend to show similar lag times.

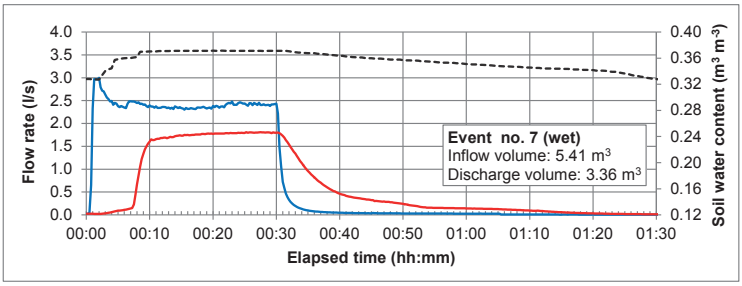

Figure 5: Inflow and outflow hydrographs of a relative large event on initially wet soil and evolution of soil water content.

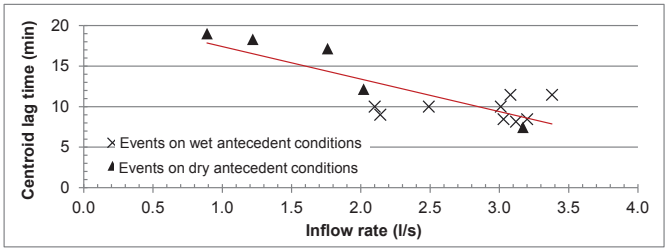

Figure 6: Plot of lag times vs. inflow rates for 14 experimental runs.

For Runs 1-2, 4-7, and 14, the outflow volume was smaller than the inflow volume; for the remaining runs, the outflow exceeded inflow. Potential reasons for this condition are given in the discussion section.

3.2 Swale soil moisture storage

In the preliminary analysis of soil moisture storage, the readings from the four moisture sensors were averaged and used for soil moisture storage calculations. Individual sensor readings varied depending on soil conditions adjacent to the sensors and the propagation of inflow waves in the swale.

Runoff generation and flow propagation were faster for higher inflow rates and wet turf, and such conditions also affected the outflow volumes, as shown in Figs. 4 and 5. For a low initial soil water content of 0.21 m^3m^{-3}, the available soil water storage capacity allowed for infiltration and filling of soil pores towards reaching saturation. For the small event simulated, a maximum soil water content of 0.39 was reached.

The filling of soil moisture storage in individual runs differed from run to run, as shown in Figs. 8 and 9 for all 14 runs (wet initial conditions: Runs Nos. 2, 4, 6, 7, 9, 10, 12, and 13; dry initial conditions: Runs Nos. 1, 3, 8, 11 and 14). The process of filling starts with a rapid increase in water content during the first 5 and 12 minutes, for wet and dry conditions, respectively. After this sharp increase of soil water content, further uptake is rather slow and more or less stops after 10-15 minutes. Regardless of the initial soil moisture and inflow rate, the soil water content reaches comparable maximum values in the range from 0.36 to 0.39. In dry soils, the water content appeared to be slightly rising even at the end of experimental runs (30 min), when it reached values in the range from 0.37 to 0.39.

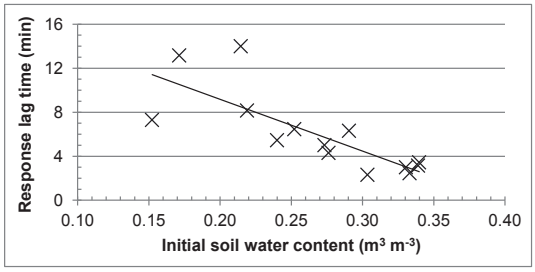

Figure 7: Swale response lag time vs. the initial soil water content.

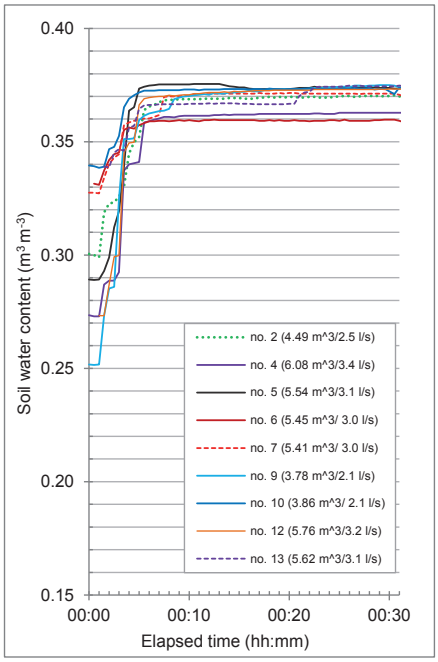

Figure 8: Temporal evolution of the average soil water content calculated from four moisture sensors placed along the swale bottom for 9 runs and wet antecedent conditions.

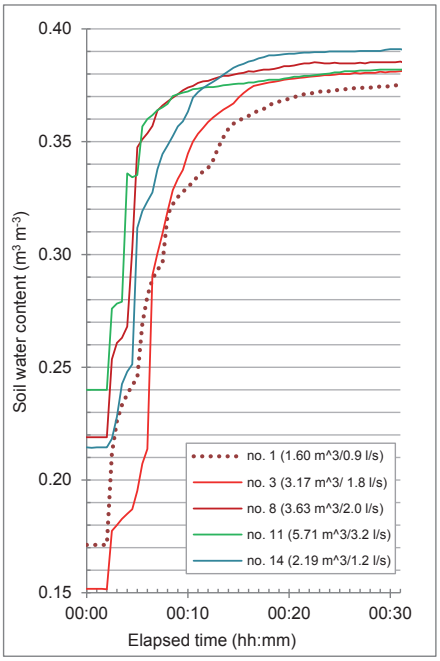

Figure 9: Temporal evolution of the average soil water content calculated for four moisture sensors placed along the swale bottom for 5 runs and dry antecedent contitions.

It was further noted that even for replica runs with similar inflow rates, the soil moisture volume filling curves differed for each run, particularly where the development of soil moisture started at low values.

Preliminary estimates of water storage in the soil matrix for all experimental runs were produced and listed in Table 3. Of the applied volumes of water between 1.60 to 6.08 m^3, the soil matrix absorbed from 0.10 to 0.76 m^3 of water. In these calculations, soil moisture storage further away from the swale was not taken into account.

4 DISCUSSION

Field scale evaluations of actual green infrastructure facilities are subject to multiple challenges arising from the complexity of rainfall/runoff processes and limitations of experimental techniques. The experimental approach applied here relied on simulation of rainfall events by swale irrigation, which allowed application of simulated rainfalls of known depths and constant rainfall intensities. While this arrangement allowed running swale flow experiments independently of the occurrence of rain events, the flow distribution system required frequent adjustments and the flow measurement system was sensitive to such changes. Three main sources of flow measurement uncertainty can be noted: (a) adjustments of the measurement channels housing the weirs, (b) head measurements, and (c) the adoption of standard weir or orifice equations for converting heads into flow rates. For all the four constriction flow meters used, namely two 45° V-notch, one 90° V-notch and an orifice-weir structure, volumetric measurements of flow rates showed a fair fit to the standard rating curves, within the range of measurement uncertainty. For the initial analysis this was deemed to be adequate, but the occurrence of systematic under or over estimation cannot be excluded.

The accuracy of the sensor used for head measurements is ±0.003 m which is typical for field meters, but leads to higher relative errors in flow measurements by the constriction meters used. Although the pipes used for the inflow monitoring were carefully levelled prior to each run, their initial vertical alignment could not be guaranteed during experimental runs. The weight of water passing through the pipes during experimental runs may have changed the pipe alignment. The combined effects of the aforementioned issues may provide an explanation of erroneous water budgets of some events,

especially in the case of higher inflow rates providing more outflow than inflow. By minimising the above mentioned uncertainties in the next stage, other conceivable sources could be excluded. There are also natural sources of sub-surface runoff, which might contribute to higher outflows than inflows, as suggested e.g. by Kirkby (1988) and Shuster et al. (2008). The former author noted that the possibility of return flows, where subsurface flow is constrained by underlying impermeable layers and may exfiltrate due to additional water infiltrating into such a system. The latter authors referred to the possible occurrence of a saturated layer developed during a previous inflow event and its activation during the subsequent event. However, especially for dry antecedent soil conditions the mass balance calculations for the 30-m swale section generally confirmed the findings of previous studies with respect to significant flow reductions and flow delay for smaller flows. Reductions of flow volumes by 55% and peak flows by 40% were observed.

Inclusion of continuous soil water content measurements (below the swale bottom) in the study provided important information on moisture storage in the unsaturated zone and served to estimate thresholds for generating infiltration as well as saturation excess flows. The moisture sensors were inserted at different points along the swale bottom and reflected soil permeability at a relatively small sector. The initial analysis, therefore, used just averages of the four point readings. As the probes send electrical impulses to measure the water content in the adjacent soil pores, such measurements may be influenced by differing temperatures and the movement of water in the soil matrix, as the viscosity changes (Emerson and Traver 2008). Nevertheless, the spatial heterogeneity and temporal variations at the plot scale can be described sufficiently accurately and moreover allow for volumetric estimations of stored runoff and swale storage capacity that will complement the swale water balance estimations during further analysis.

The ratio of overlapping infiltration and saturation excess flow is mainly controlled by the inflow rates, soil texture and antecedent soil conditions (Zhao et al. 2014). With respect to the simulated inflow rates, higher flow rates passing through the studied drainage swale seem to reduce the infiltration rates due to smaller residence times, and therefore increase the infiltration excess flow and generate surface runoff more rapidly, which is supported by the measured shorter lag times. This assumption coupled with the available storage capacity was also reported by Davis et al. (2012).

Deletic & Fletcher (2006) assumed that the infiltration was also related to the length of the antecedent dry period, but independent of the inflow magnitude. In our study, dryer antecedent conditions not only allowed for good infiltration efficiency, but also an increased storage capacity, as the systematically higher soil water contents suggested for fully saturated conditions after 30 min of inflow The increased water storage volume is up to 3% higher than under wet antecedent conditions. Possible explanations could be the changes in the soil matrix during the drying process.

In continuation of this study, it is envisaged extending the soil water content measurements to more locations in the swale and at different depths, in order to further elucidate the processes of soil moisture storage. Also, more efforts will be devoted to improving the data acquisition system. The work performed so far confirmed that the experimental approach used provided good swale flow data, whose usefulness will further increase with improved measurement systems.

5 CONCLUSIONS

A 30-m section of an urban drainage swale, located in sandy soils in Luleå (Northern Sweden), was investigated with respect to swale flow characteristics. For this purpose, the swale was irrigated by flows corresponding to three simulated rainfall intensities over the duration of 30 min, applied for either dry or wet antecedent conditions. In the first experimental series, the analysis focused on swale flow and soil water content measurements. For some events, e.g., a 30 min event with an inflow of 1.2 L/s, the swale peak flow and runoff volume was reduced by 40 and 55%, respectively. For a number of events, outflow volumes exceeded the inflow volumes, as a result of flow measurement uncertainties. The soil water content measurements at multiple points indicated that considerable volumes of water can be stored, or transmitted to deeper layers, in a relatively small drainage facility. A maximum increase of volumetric water content of 0.225 m^3m^{-3} was observed and indicated the total water storage soil in the control soil layer below the swale bottom as 0.760 m^3, over the whole swale length. Conveyance of irrigation water was promoted by wetter antecedent soil conditions, but in dryer initial conditions, swale flows were greatly attenuated. The experimental approach employed was found feasible to pursue the study objectives, with some improvements of the water supply system and flow measurements.

ACKNOWLEDGEMENTS

This study was conducted under the research cluster Dag&Nät and supported by the Swedish Water and Wastewater Association (Svenskt Vatten), and within the research project GrönNano funded by VINNOVA and Formas. The authors would like to thank the colleagues from the Urban Water Engineering group at the LTU as well as staff of the Luleå municipality for their support.

LIST OF REFERENCES

Ahiablame L. M., Engel B. A. and Chaubey I. (2012). *Effectiveness of low impact development practices: Literature review and suggestions for future* research. Water Air Soil Pollut. 223(7), 4253-4273.

Ahmed F., Gulliver J. S. and Nieber J. L. (2015). *Field infiltration measurements in grassed roadside drainage ditches: Spatial and temporal variability.* Journal of Hydrology. 530, 604-611.

Bäckström, M., (2002). *Sediment transport in grassed swales during simulated runoff events*. Water Sci. Technol. 45 (7), 41-49.

Barrett M., Walsh P., Jr. J. and Charbeneau R. (1998). *Performance of Vegetative Controls for Treating Highway Runoff.* J Environ Eng. 124(11), 1121-1128.

Barrett, M.E. (2008). *Comparison of BMP performance using the international BMP database*. J. Irrig.Drain. Eng., 134, 556–561.

Chow, L., Xing, Z., Rees, HW., Meng, F., Monteith, J. and Stevens, L. (2009). *Field Performance of nine Soil Water Sensors on Sandy Loam Soil in Brunswick, Maritime Region, Canada.* Sensors 2009, (9) 9398-9413.

Dahlström B. (2010). *Regnintensitet - en molnfysikalisk betraktelse. (Rain Intensity–a cloud physical contemplation)*, Svenskt Vatten Utveckling, rapport 2010-05.

Davis A. P., Stagge J. H., Jamil E. and Kim H. (2012). *Hydraulic performance of grass swales for managing highway runoff.* Water Res. 46(20), 6775-6786.

Deletic A., Fletcher T. D. (2006). *Performance of grass filters used for stormwater treatment - A field and modelling study*. J Hydrol. 317(3-4), 261-275.

Dietz M. E. (2007). *Low impact development practices: A review of current research and recommendations for future directions*. Water Air Soil Pollut. 186(1-4), 351-363.

Emerson, C. and Traver, R.G. (2008). *Multiyear and seasonal variation of infiltration from storm-water best management practices*. J. Irrig. Drain., 10.1061/(ASCE)0733-9437(2008)134:5(598), 598–605.

Jensen, M. B. (2004). *Hydrological Conditions for Contaminant Leaching through Highway Swales.* Water Air Soil Pollut., 158(1), 169-180.

Kirkby, M. (1988). *Hillslope Runoff Processes and Models*. Journal of Hydrology, 100(1), 315-339.

Lucke, T., Mohamed, M. A. K., Tindale, N. (2014). *Pollutant Removal and Hydraulic Reduction Performance of Field Grassed Swales during Runoff Simulation Experiments*. Water (Switzerland), 6(7), 1887-1904.

Jones, SB., Wraith, JM. and Or, D. (2002). *Time domain reflectometry measurement principles and applications*. Hydrol. Process. 16, 141–153 (2002).

Pitt, R., and McLean, J. (1986). *Toronto Area Watershed Management Strategy Study: Humber River Pilot Watershed Project*. Ontario Ministry of the Environment, Toronto, Ontario, 486.

Shuster, W., Pappas, E., Zhang, Y. (2008*). Laboratory-Scale Simulation of Runoff Response from Pervious-Impervious Systems.* J. Hydrol. Eng., 13(9), 886-893.

USEPA (US Environmental Protection Agency) (1997*). Stormwater BMP Design Supplement for Cold Climates*. US EPA Office of Wetlands, Oceans and Watersheds and US EPA Region 5. Washington, D.C: Office of Water.

Viessman, W., Lewis, G.L. and Knapp J.W. (1989*). Introduction to Hydrology*. 3rd edition. Harper&Row, New York, N.Y.

Yousef, Y. A., Hvitved-Jacobsen, T., Wanielista, M. P., Harper, H. H. (1987). *Removal of Contaminants in Highway Runoff Flowing through Swales.* Sci. Total Environ., 59(0), 391-399.

Paper II

Rujner, H., Leonhardt, G., Marsalek, J., & M. Viklander (in press)

The effects of initial soil moisture conditions on swale flow hydrographs.

(article in press, Hydrological Processes).

Rujner, H., Leonhardt, G., Marsalek, J., & Viklander, M. (2018). The effects of initial soil moisture conditions on swale flow hydrographs. Hydrological Processes DOI 10.1002/ hyp.11446 (article in press)

The effects of initial soil moisture conditions on swale flow hydrographs

Hendrik Rujner[1]*, Günther Leonhardt[1], Jiri Marsalek[1], Anna-Maria Perttu[2], Maria Viklander[1]

[1] Department of Civil, Environmental and Natural Resources Engineering, Luleå University of Technology, Luleå 97187 Sweden
[2] SENS Sustainable Energy Solutions, Nacka 12154, Sweden

*****Correspondence to**:** Department of Civil, Environmental and Natural Resources Engineering, Luleå University of Technology, 97187 Luleå, Sweden.

E-Mail of authors: hendrik.rujner@ltu.se*, guenther.leonhardt@ltu.se, jiri.marsalek@ltu.se, anna-maria.perttu@sens.se, maria.viklander@ltu.se

Abstract

The effects of soil water content (SWC) on the formation of runoff in grass swales draining into a storm sewer system were studied in two 30-m test swales with trapezoidal cross-sections. Swale 1 was built in a loamy fine-sand soil, on a slope of 1.5% and Swale 2 was built in a sandy loam soil, on a slope of 0.7%. In experimental runs, the swales were irrigated with two flow rates reproducing runoff from block rainfalls with intensities approximately corresponding to two-month and three-year events. Runoff experiments were conducted for SWC_{ini} (initial SWC) ranging from 0.18 to 0.43 m^3m^{-3}. For low SWC_{ini}, the runoff volume was greatly reduced by up to 82%, but at high SWC_{ini}, the volume reduction was as low as 15%. The relative swale flow volume reductions decreased with increasing SWC_{ini} and, for the conditions studied, indicated a transition of the dominating swale functions from runoff dissipation to conveyance. Runoff flow peaks were reduced proportionally to the flow volume reductions, in the range from 4-55%. The swale outflow hydrograph lag-times varied from 5 to 15 minutes, with the high values corresponding to low SWC_{ini}. Analysis of swale inflow/outflow hydrographs for high SWC_{ini} allowed estimations of the saturated hydraulic conductivities as 3.27 and 4.84 cm/h, in Swales 1 and 2, respectively. Such estimates differed from averages (N=9) of double-ring infiltrometer measurements (9.41 and 1.78 cm/h, respectively). Irregularities in swale bottom slopes created bottom surface depression storage of 0.35 and 0.61 m^3, for Swales 1 and 2, respectively, and functioned similarly as check-berms contributing to runoff attenuation. The experimental findings offer implications for drainage swale planning and design: (i) SWC_{ini} strongly affect swale functioning in runoff dissipation and conveyance during the early phase of runoff, which is particularly important for design storms and their antecedent moisture conditions, and (ii) concerning the longevity of swale operation, Swale 1 remains fully functional even after almost 60 years of operation.

Key words: grass swales, Green Infrastructure, field study, water balance, soil moisture, flow attenuation and conveyance

1. Introduction

Grass swales are traditional drainage elements typically designed to convey, attenuate, and treat stormwater runoff from roads and other surfaces (Barrett et al., 1998; Dietz, 2007; Mohamed et al. 2013). In regions with seasonal snowpacks, they also serve for snow storage (Viklander et al., 2003). As an inexpensive and environmentally friendly alternative to the conventional concrete drainage elements, swales attracted renewed attention during the emergence of Low Impact Development (LID) and Green Infrastructure (GI) approaches to mitigation of the impacts of urbanization on catchment hydrology (Dietz & Clausen, 2008; Houle et al., 2013; Valinski & Chandler, 2015). Grass swales are designed to collect urban runoff in upstream reaches of the drainage area and discharge it into downstream drainage elements, such as stormwater management facilities or storm sewers inlets (Li & Hogenbirk, 1998; Zimmerman et al., 2010).

Common experience of urban drainage professionals in Sweden shows that swales are mostly designed on the basis of local experience and built with roadwork residual soils, which results in some uncertainties in the estimated swale capacities and discharges into the downstream drainage facilities. Hence, swale operation is of interest for the assessment of the drainage system performance, particularly in a changing climate, and tangible benefits can be gained by advancing the knowledge of the functioning and maintenance needs of swales.

Focusing the discussion herein on runoff flow rates and volumes only, hydrological and hydraulic processes are of particular interest when examining the role of swales in stormwater management (Yousef et al., 1987; Wanielista and Yousef, 1992; Ahiablame et al., 2012). The hydrology/hydraulics of swales is rather complex and described by three regimes, depending on the severity of the rainstorms (Davis et al., 2012): (i) for minor rainfalls, all rainwater infiltrates into swale soils and there is no runoff, (ii) for intermediate rainfalls, hydrologic abstractions (particularly infiltration) substantially reduce excess water and the conveyed runoff, and this effect can be further increased by using check berms; and, (iii) for severe rainfalls, swales function primarily as conveyance channels with relatively small reductions of flow peaks and volumes. In terms of water balance, the major components include the longitudinal inflow into the swale at the upstream end, lateral inflows along the swale channel, direct input of rainwater over the swale footprint area; and, outflows in the form of hydrologic abstractions including infiltration in the swale channel, and the downstream outflow. Depending on the magnitude of these components, different flow conditions from infiltration to saturation excess flows occur in swales (Dunne & Leopold, 1978). Besides rainfall characteristics, the swale hydrology is affected by the channel geometry, vegetation and depressions (or check dams) (Davis et al., 2012), the saturated hydraulic conductivity K_s of swale soils (Ahmed et al. 2015), and by the antecedent wetness (Nishat et al., 2010).

A plethora of data on runoff volume reductions in swales was published by researchers studying swales exposed to actual rainfall, or applied irrigation. Generally, the reported reductions of swale inflow volumes broadly varied: 9-100% (Yousef et al. 1987), 33-66% (Bäckström, 2002),

12-89% (Lucke et al. 2014), and 41% (a median value; Geerling, 2014). In this connection, Davis et al. (2012) reported some events with outflow volumes exceeding those of inflows, resulting from "otherwise unconnected drainage areas contributing to the swale drainage during peak flows", and concluded that the swale flow attenuation cannot be adequately described by a "percent reduction". Swale longitudinal slopes were noted in the studies listed above, but not addressed as an influential variable; however, minimum slopes for positive drainage (≥2%) (UDFCD, 2010) and maximum permissible slopes (≤ 5%), or flow velocities (≤ 0.91 m/s) were suggested to maintain swale performance in stormwater control and prevent erosion (Schueler, 1987).

The dissipation of swale flow volumes is strongly affected by infiltration into soils, which is commonly described by the saturated hydraulic conductivity, K_s, and estimated from the literature data for soils of various textures (Lee et al., 2016), field measurements with infiltrometers (NTCD, 2014; Ahmed et al., 2015; Fatehnia et al. 2016), or from water balance considerations (Wanielista and Yousef, 1992). Applications of these methods are exposed to high uncertainties resulting from great variability of infiltration rates (Ahmed et al., 2015).

Little has been published on the effects of antecedent moisture conditions (AMC) on swale flows and their attenuation. The knowledge of AMC is required when dealing with discrete storms (Watt & Marsalek, 2013), either in field experiments with irrigated swales, or in applications of design storms to swales. Estimates of average AMC can be obtained from continuous simulations of soil moisture for local rainfall data and the known soil characteristics (porosity and the saturated hydraulic conductivity), as reported by Nishat et al. (2010).

The objectives of the study presented herein were to: (i) assess the swale channel water balance for two hydraulic loadings and varying initial soil water content (SWC_{ini}), (ii) demonstrate the transition of swale operation from runoff flow attenuation to flow conveyance, depending on swale channel SWC_{ini}, and (iii) collect data for future swale flow modelling.

2. Methods

Study sites

Two grass swales in residential suburbs of Luleå, northern Sweden (65°35'03"N, 22°09'17"E), were selected as study sites. Swale 1, built in 1956, drains a two-lane road and has a small pine stand on the opposite side. Swale 2, built in 2006, drains an asphalted bus lane and is located next to an open meadow. For the purpose of this study, in each swale, a 30-metre downstream section, with an appearance of homogeneous surface topography and vegetative cover, was selected as a test site. Dimensions of both swales are shown in Fig.1.

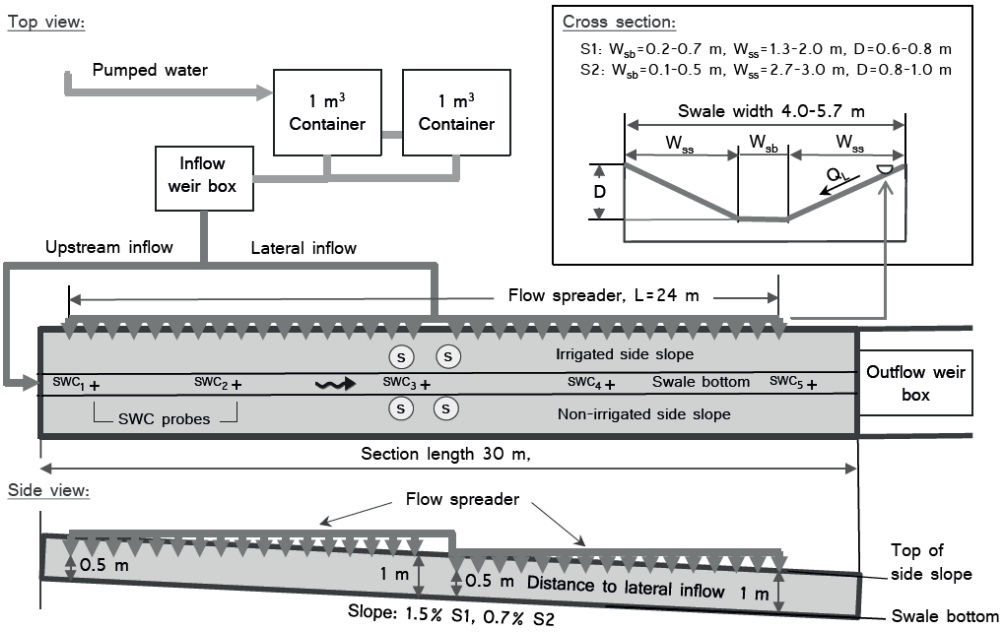

Figure 1 Schematics of the experimental water supply system, dimensions of Swale 1 (S1) and Swale 2 (S2) and measurement locations for inflow, outflow and soil water content. SWC1-5 indicate the locations of SWC measurements, s-symbols indicate additional soil sampling points at the side slopes.

Detailed topographical information was collected by a RTK-GPS (Real Time kinematic GPS, with 20-25 mm horizontal and 30-35 mm vertical accuracy; Swedish National Land Survey, 2017). The main advantage of using this method was the ease of making a high number of measurements, which indicate a number of breaks and depressions in the swale longitudinal profiles. The volumes of such depressions were estimated with the 3D Analyst in Esri´s ArcGIS® as 0.35 and 0.61 m^3 for Swales 1 and 2, respectively. The overall slopes between the inlet and outlet were calculated by linear regression as 1.5% for Swale 1 and 0.7% for Swale 2.

Swale structure and soils

Both swales were designed without a particular arrangement of soil layers, addition of soil amendments, or underdrains. Starting from the top, the swale horizons consisted of a 0.05-0.15 m turf layer, with a visibly higher organic content, a 0.15-0.50 m layer of homogeneous sandy material, and an underlying mixed bed of sand and boulders. Due to relatively high local water tables, some seasonal interference of shallow groundwater with swale drainage can be expected. In Swale 2, periodical groundwater emergence was observed by local residents. The runoff contributing areas of both swales were estimated as 450 m^2 each.

Soil samples were collected along the swale bottom at the points, where soil moisture probes were located and on the side slopes; for detailed positions, see Fig. 1. The grain size distribution of the top 0.3 m layer was determined in the laboratory according to ISO 11277 (ISO, 2009) and used to classify the soil texture at each sampling point: Swale 1, clay 0.3-3.1%, silt 6.6-32.4%, and sand 60.8-93.1%; Swale 2, clay 1.7%, silt 10.9-50.8%, and sand 41.2-87.4%. The soil textures within each swale varied noticeably. Soil porosity was derived after determining the soil bulk density according to ASTM-D7263 (ASTM, 2009), using quasi-undisturbed soil samples collected by coring. Prior to collecting soil samples, a double-ring infiltrometer was used to measure infiltration rates at nine points along the swale bottom, at intervals of about 3 m (one measurement every 3.3 m), to determine the saturated hydraulic conductivities (K_s). The soil characteristics, including the texture, porosity and measured K_s, are summarized in Tab. 1 for both study sites.

Table 1 Locations of soil water content probes, texture classes, porosities and saturated hydraulic conductivities in Swales 1 and 2.

		Swale 1			Swale 2		
Distance to outlet (m)	SWC-probe	Soil texture WRB[2]	Measured ϕ[4]	Measured[5] K_s (cm/hr)	Soil texture WRB	Measured ϕ	Measured K_s (cm/hr)
1.5	SWC_5[3]	loamy fine sand	0.56	7.40	silt loam	0.57	2.20
4.5				4.80			4.00
7.5	SWC_4	fine sand	0.57	5.60	fine sand	0.50	1.90
10.8				14.40			1.10
14.0	SWC_3	sandy loam	0.54	4.40	sandy loam	0.45	2.10
17.5				10.30			0.49
21.0	SWC_2	sandy loam	0.42	15.40	loamy fine sand	0.43	1.58
24.5				7.50			2.00
28.0	SWC_1	sandy loam	0.49	14.85	loamy fine sand	0.52	0.68
Average value / condition		Loamy fine sand	0.52 ±0.06[6]	9.41 ± 4.21	Sandy loam	0.50 ±0.05	1.78 ± 0.98

[1] Soil textures for the side slopes were determined based on four soil samples (2 each side) close to SWC_3: For Swale 1 roadside slope: fine sand-loamy fine sand, opposite slope: loamy fine sand; for Swale 2 roadside slope: sandy loam, opposite slope: loamy fine sand-sandy loam, [2] World Reference Base (FAO), [3] soil water content, [4] soil porosity, [5]measured with a double-ring infiltrometer, [6]standard deviation

Neither swale showed any signs of soil compaction, which could be caused by pedestrian or vehicular traffic, and their bottoms appeared to have an intact, soft turf. Prior to any runoff simulation tests, vegetation in the test swales was mowed to a height of about 0.05 m and any debris was cleaned out.

Stormwater runoff simulation by irrigation

A portable swale irrigation system (Fig. 1) was designed to mimic two main equal water inflows into the swales – a longitudinal inflow at the upstream end and a distributed lateral inflow in the form of an overland flow along the swale side slope next to the road shoulder. The lateral flow was spread over the width of 24 m on the swale side slope by means of two half-pipes with labyrinth weirs. The length of the lateral feed (overland) flow was 0.5-1.0 m, measured from the overflow edge of the feed half-pipes to the swale bottom edge. Shorter lengths corresponded to the upstream end of the feed half-pipe and the longer ones to the downstream ends.

Routine stormwater runoff simulation runs were performed for two constant inflow rates of 1.06 and 2.65 L/s (providing specific lateral inflows of $1.77 \cdot 10^{-5}$ and $4.42 \cdot 10^{-5}$ m^2/s, respectively, over the section length of 30 m), applied over a duration of 30 minutes, and for two classes of the initial swale soil water content (SWC), operationally referred to as 'low' and 'high' (hereafter abbreviated as SWC_{low} and SWC_{high}). Furthermore, to obtain some understanding of the variability of swale responses in such runs, similar runoff conditions (i.e. similar inflow and initial SWC) were reproduced in sets of three runs. Thus, for each swale, 12 runs were performed (2x2x3).

To assess the significance of generated runoff flows, the corresponding rainfall intensities were estimated for a steady state runoff, assuming the runoff contributing area of 450 m^2 and the composite volumetric runoff coefficient of 0.75 (C_{vol} = 0.5 for the pervious half of the area, C_{vol} = 1.0 for the asphalted half). For the computed intensities (i = 11.3 and 28.3 mm/h) and the duration of 30 minutes, one can estimate the corresponding storm event average return periods on the basis of the statistical relationships published in the Swedish national guide to rain intensity-duration-frequency curves (Dahlström, 2010), as 2 months and 3 years, respectively.

Swale flow measurements

Swale inflow and outflow were measured using compact weir boxes, with sharp-crested V-notch weirs manufactured according to the standard ASTM-D5242 (ASTM, 2013) and stilling wells, in which ISCO depth sensors were used to record weir heads (ISCO, 2009) at 15 s intervals. Two weir angles were used, 45° for Q=1.06 L/s and 90° for Q=2.65 L/s. The weir heads were converted into flow rates using the Kindsvater-Shen equation for V-notch weirs (Shen, 1981). For the representative ranges of the measured weir heads and the accuracy of the head sensor (±3 mm), the overall accuracies of such measurements were estimated as 6-10% for the 45° V-notch and 9-14% for the 90° V-notch.

Swale flow depths and widths were manually measured at cross-sections located every 3 m along the test swale section, at 5 min intervals, while the swale was irrigated and discontinued 5 min after the irrigation stopped. The measurements focused on the submerged part of the swale channel; no hydraulic or hydrological data were collected for the side slopes.

Soil water content measurements

The test swale sections were instrumented with five Water Content Reflectometer (WCR) probes (Type CS516, Campbell Scientific, Inc., accuracy ±0.025 m^3m^{-3} (Evett et al., 2008)). The WCRs located along the swale bottom (Fig. 1) were used to measure the volumetric soil water content θ over the depth of 0-0.21 m and such readings were logged by a multiplexer data logger (Campbell Scientific Inc.) every 30 s. The probes were inclined at a 45° angle to the swale bottom in the flow direction to minimize their interference with flow during the initial phase of runoff. They were installed at least one week before the experiments, in order to allow the natural setting of soil particles around the probe supporting rods and thereby reduce any preferential flows along the rods.
The observed SWC were normalized according to Van Genuchten (1980):

$$\theta^* = \frac{\theta - \theta r}{\phi - \theta r}$$

Where θ^* is the normalized soil water content (hereafter refered to as SWC_{norm}), or effective saturation, ϕ is the soil porosity (assumed equal to the saturated soil water content θ_s), and θ_r is the soil specific residual water content. Residual water content θ_r of the soils studied was adopted from Rawls et al. (1982) as θ_r=0.035 and 0.041 m^3m^{-3}, for loamy sand and sandy loam, respectively.

Selection of the initial SWC conditions tested
The selection of the initial soil moisture conditions in field experiments was used to decide when to start irrigation experiments, depending on the antecedent moisture conditions (AMC) resulting either from a rain event, or a previous irrigation experiment. In this context, two categories of AMC were described by the antecedent dry weather period (ADWP), shown in Table 2, and average SWC. Recognizing that the tested swales were built in different soils with different drainage (see Tab. 1), the ADWPs of the individual swales differed.

Table 2 Dry and wet antecedent moisture conditions defined for Swales 1 and 2, and the corresponding antecedent dry weather periods.

AMC	Swale 1	Swale 2
Dry	1 d ≤ ADWP	2 d ≤ ADWP
Wet	ADWP ~ 1 h	ADWP ~ 3 h

The SWC_{ini} was set equal to the mean of the last SWCs recorded just before the experimental run. The time required by soils to drain and reach dry AMC in Swale 1 was just one day, in Swale 2 it was two days. For both swales, wet AMC conditions were set equal to the state

attained immediately after the water ponded on the swale bottom disappeared, which was approximately one hour for Swale 1 and three hours for Swale 2, after the irrigation ceased.

Data processing and analysis

The measured flow hydrographs were plotted for all runs for visual checking of data quality. Based on the flow rate time series, the total flow volumes and the mean lag times were calculated, as well as the swale flow volume and peak flow reductions (see Fig. 2).

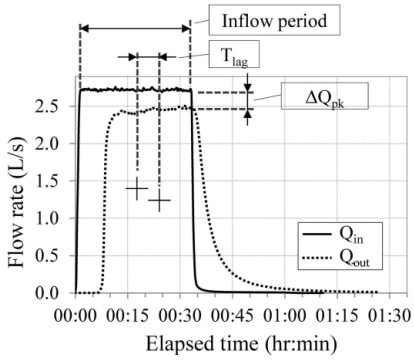

Figure 2 Characteristic inflow and outflow hydrographs observed in the field and the notation used.

As expected for a controlled quasi-constant inflow rate, the swale outflow hydrographs had relatively flat peaks, and the highest outflow rate before stopping the site irrigation was adopted for calculations of peak flow reductions. The peak flow reduction (ΔQ_{pk}) was defined as the difference between the inflow and outflow hydrograph peaks, and was further used to estimate spatially averaged values of K_s. When the inflow and outflow hydrographs reach a quasi-equilibrium, ΔQ_{pk} represents the abstraction due to infiltration, and K_s can be expressed as $(\Delta Q_{pk}) / A_{inf}$, where A_{inf} represents the infiltration area estimated over the test swale length, for the initially high SWC and the two inflows tested.

For experimental swale runs of limited duration (30 min.), the water budget of the swale channel can be described as $V_{in} = V_{out} + V_{inf}$, recognizing the dominating nature of infiltration into swale soils. All the three components can be evaluated from the measured data and are presented in the Results, together with the initial soil water content readings (SWC_{ini}), inflow rates (Q_{in}), and three calculated parameters explained below.

The actual inflow rates Q_{in} were fairly constant, with average variations among the runs of about 6%. The inflow and outflow volumes (V_{in}, V_{out}) were calculated by integration of the respective hydrographs; for the outflow hydrograph, the cut-off flow rate, at which the integration was stopped, was 0.05 L/s. The difference between both volumes was then taken as the infiltrated volume, $V_{inf} = V_{in} - V_{out}$, and the relative swale flow volume reduction was calculated as

$\Delta V_{rel} = (V_{in} - V_{out}) / V_{in}$. Furthermore, the relative swale flow peak reduction was defined, for the flat part of hydrographs, as $\Delta Q_{pk\ rel} = (Q_{in} - Q_{pk\ out}) / Q_{in}$. Finally, the outflow hydrograph lag time, T_{lag}, which was defined as the difference between the centroid times of the inflow and outflow hydrographs, was calculated.

3. Results

After introducing the irrigation flow into the swale channel, an infiltration excess flow developed and reached the test section outlet in 7-22 minutes. In general, shorter travel times to the outlet applied to Swale 2, with less permeable soils. Examples of observed inflow and outflow hydrographs in Swales 1 and 2 are shown in Fig. 3 for two inflow rates and two sets of initial soil moisture conditions (SWC_{low} and SWC_{high}). For individual combinations of the inflow rate and the initial SWC, the hydrologic response of the swales varied as discussed below.

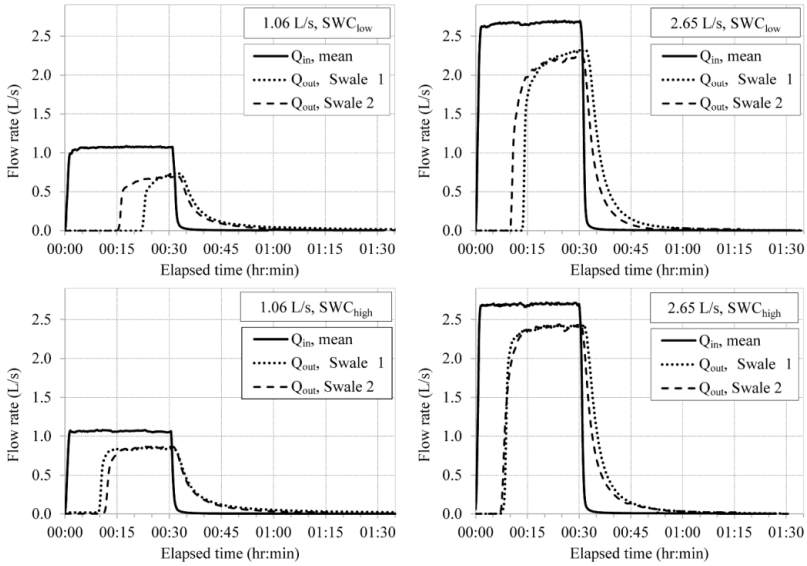

Figure 3. Examples of inflow and outflow hydrographs in Swales 1 (dotted line) and 2 (dashed line) for 1.06±0.02 L/s inflow at low SWC_{ini} (top left), 1.06 ±0.02 L/s inflow at high SWC_{ini} (bottom left), 2.65 ±0.05 L/s at low SWC_{ini} (top right) and 2.65 ±0.05 L/s at high SWC_{ini} (bottom right).

Initial soil water content for swale runs

Operational definitions of dry and wet AMC were supported by measurements of the soil water contents by five probes, whose averaged readings, both as measured or normalized, are listed in Table 3 for 24 experimental runs. In Swale 1, the average initial SWCs equaled 0.262 (coefficient of variation $C_v = 0.14$) and 0.391 ($C_v = 0.09$), for dry and wet AMC, and both low

and high inflows combined; in Swale 2, the corresponding values were 0.265 (C_v = 0.19) and 0.304 (C_v = 0.14). Even though the differences between both states (dry and wet) are relatively small (in Swale 1, 0.13, or 0.27 for normalized values, and 0.04, or 0.08 for normalized values, in Swale 2), as discussed later, these differences affected the swale hydrological response.

Swale channel water balance

The main components of the water balance of the trapezoidal swale channel, V_{in} , V_{inf} , and V_{out} , were listed in Table 3, together with the initial soil water content readings (SWC_{ini}), inflow rates (Q_{in}), and calculated ΔV_{rel} , $\Delta Q_{pk\ rel}$ and T_{lag} for the 24 runs conducted.

Table 3 Initial top layer SWC and SWC_{norm}; inflow rate Q_{in}; flow volumes entering and leaving the swale, V_{in} and V_{out}, respectively; infiltrated volume V_{inf}; relative swale flow volume reduction ΔV_{rel}; relative swale flow peak reduction $\Delta Q_{pk\ rel}$; outflow hydrograph lag time T_{lag} (min.).

	Scenario	SWC_{ini} (m^3m^{-3})	Mean $SWC_{norm\ ini}$	Q_{in} (L/s)	V_{in} (m^3)	V_{out} (m^3)	V_{inf} (m^3)	ΔV_{rel}	$\Delta Q_{pk\ rel}$	T_{lag} (min)
S1	SWC_{low}	0.25±.02[1]	0.46	1.07	1.97	0.76	1.22	0.62	0.29	15.0
		0.22±.02	0.40	1.06	1.93	0.34	1.59	0.82	0.50	15.5
		0.25±.03	0.47	1.09	2.06	0.47	1.59	0.77	0. 32	14.8
	SWC_{high}	0.39±.03	0.75	1.04	1.90	1.45	0.45	0.23	0.16	9.2
		0.40±.03	0.76	1.04	1.90	1.43	0.47	0.25	0.15	8.5
		0.38±.03	0.73	1.06	1.94	1.30	0.64	0.33	0.21	9.5
	SWC_{low}	0.29±.03	0.55	2.56	4.87	3.22	1.65	0.34	0.09	9.8
		0.29±.03	0.55	2.67	4.97	3.02	1.95	0.39	0.13	10.0
		0.25±.03	0.46	2.70	5.04	2.31	2.73	0.54	0.20	10.5
	SWC_{high}	0.38±.02	0.73	2.76	4.98	4.13	0.85	0.17	0.05	7.3
		0.39±.02	0.75	2.65	4.90	4.04	0.86	0.18	0.04	7.0
		0.40±.01	0.78	2.62	4.85	4.12	0.73	0.15	0.07	6.5
S2	SWC_{low}	0.25±.05	0.48	1.04	1.95	0.52	1.43	0.73	0.55	12.0
		0.27±.05	0.53	1.03	1.96	1.08	0.88	0.45	0.20	11.3
		0.27±.05	0.52	1.05	1.95	0.91	1.04	0.53	0.31	10.8
	SWC_{high}	0.30±.04	0.57	1.05	1.94	1.23	0.71	0.37	0.20	9.3
		0.31±.04	0.60	1.04	1.92	1.24	0.68	0.35	0.18	9.0
		0.29±.04	0.57	1.09	2.01	1.29	0.72	0.36	0.20	8.5
	SWC_{low}	0.26±.05	0.51	2.63	4.87	3.05	1.82	0.37	0.13	6.8
		0.27±.05	0.51	2.65	4.87	3.08	1.79	0.37	0.15	6.5
		0.27±.05	0.51	2.59	4.79	3.18	1.61	0.34	0.11	7.3
	SWC_{high}	0.31±.04	0.60	2.65	4.84	3.73	1.11	0.23	0.08	5.3
		0.31±.04	0.60	2.65	4.84	3.74	1.10	0.23	0.08	5.5
		0.31±.04	0.60	2.64	4.88	3.67	1.21	0.25	0.11	5.3

[1] standard deviation

Data in Table 3 indicate that swale channel infiltration represented between 15 and 82% of the flow volume entering the swale. The low values were observed for wet AMC in Swale 1 (SWC_{ini} = 0.40) and the high inflow rate, the high values corresponded to dry AMC (SWC_{ini} = 0.22) and the low inflow rate, also in Swale 1.

Swale channel infiltration rates over steadily wetted areas during the established swale flows are presented in Table 4. The infiltration values obtained for SWC_{high} were assumed to correspond to the saturated conditions and were taken as spatially integrated estimates of K_s.

Table 4 Hydraulic conductivities calculated from quasi-constant differences in peak flow reductions (due to infiltration) and the infiltration areas in the swale channel, for SWC_{high}.

	Irrigation event	Q_{in} (L/s)	ΔV_{rel}	Average steadily submerged area area (m^2)	Quasi-constant peak flow reduction (Ls^{-1})	Spatially integrated K_s (cm/h)
Swale 1	11/08-2	1.04	0.23	21.29	0.20	3.38
	11/08-3	1.04	0.25	20.93	0.23	3.96
	15/08-2	1.06	0.33	20.45	0.20	3.52
	24/08-2	2.76	0.17	24.25	0.19	2.78
	26/08-2	2.65	0.18	23.07	0.23	3.59
	30/08-2	2.62	0.15	22.65	0.15	2.38
Swale 2	13/09-2	1.05	0.37	17.90	0.23	4.63
	16/09-2	1.04	0.35	18.34	0.20	3.93
	27/09-2	1.09	0.36	18.82	0.23	4.40
	18/09-2	2.65	0.23	19.17	0.25	4.60
	22/09-2	2.65	0.23	18.39	0.25	4.84
	24/09-2	2.64	0.25	18.47	0.34	6.63

Finally, estimates of K_s from double-ring infiltrometer (DRI) measurements, swale inflow and outflow hydrographs, and reference values for the swale soil texture are summarized in Table 5.

Table 5. Estimates of K_s (cm/h) for the swales studied by various methods, with standard deviations and 95% confidence interval (CI).

	Swale 1			Swale 2		
	K_s (cm/h)	SD[1]	95% CI[2]	K_s (cm/h)	SD[1]	95% CI[2]
DRI Measurements	9.41	4.21	6.17 – 12.65	1.78	0.98	1.03 – 2.53
Swale flow hydrographs (SWC_{high})	3.27	0.58	2.66 – 3.88	4.84	0.93	3.86 – 5.82
Reference data (soil texture)	6.3 (loamy sand)	-	-	2.8 (sandy loam)	-	-

[1] Standard deviation
[2] 95% confidence intervals calculated from Student´s t

Attenuation of swale flows

For a simulated 30-min. block rain event with a 2-month return period and under dry AMC conditions, on average, 74% of the inflow volume infiltrated in Swale 1. For wet AMC (SWC_{high}), this effect was reduced to 27%. For a 3-year event and dry AMC (SWC_{low}), 42% of the inflow infiltrated, while at wet AMC just 17% infiltrated. Flow volume attenuations in Swale 2 with less permeable soils showed smaller variations for different experiments; for the 2-month event and dry and wet AMC indicating an average attenuation of 57 and 36%, respectively, and smaller attenuations (36 and 24%) for the high inflow (3-year event) and dry and wet AMC, respectively. Thus, in both swales, the relative swale flow volume attenuation decreased with increasing initial soil moisture and the inflow magnitude. For a direct comparison of Swales 1 and 2, with different soils, the SWC data were normalized and the relative volume reduction ΔV_{rel} vs. SWC_{norm} was plotted in Fig.4.

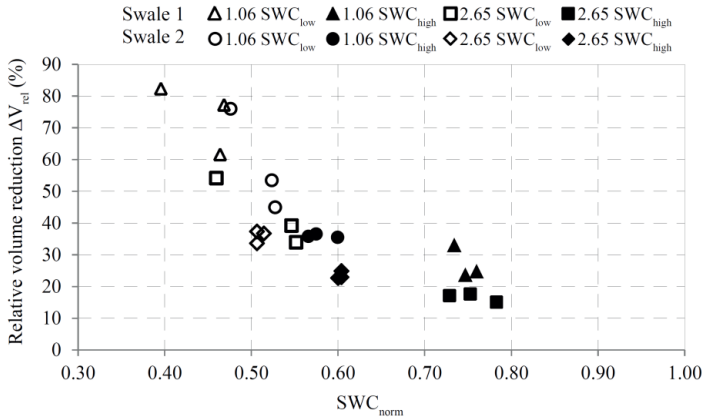

Figure 4 Relative swale flow volume reduction vs. the normalized soil water content, SWC_{norm}, for Swales 1 and 2.

The use of SWC_{norm} as an independent variable produced a consistent decline in the relative swale flow volume reduction, with the increasing SWC_{norm}, and, for the conditions studied, demonstrates the functioning of swales in stormwater management: for low soil moisture, the swale functioned predominantly as a runoff volume control measure (with additional water quality benefits), but for high soil moistures, it transitioned to a conveyance element with small effects on flow rates and volumes.

Swale flow peak attenuation was comparable in both swales, and to a large extent followed variations in flow volume reductions. The highest peak attenuation was noted for dry AMC and the 2-month event (on average 37 and 35% in Swales 1 and 2, respectively) and the lowest attenuation was noted for the 3-year event and wet AMC (on average 5 and 9% for Swales 1 and

2, respectively). A plot of relative peak flow reductions vs. relative volume reductions, for all 24 runs, is presented in Fig. 5.

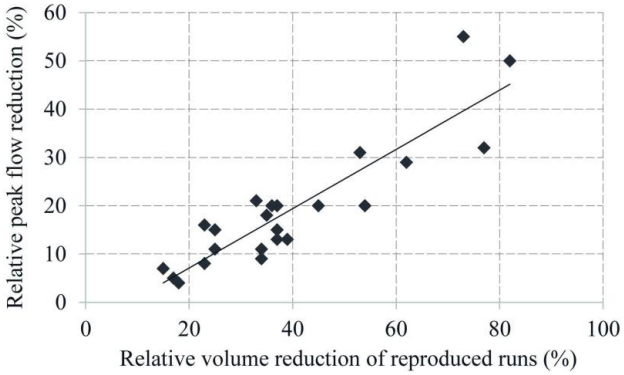

Figure 5 Relative peak flow reduction vs. relative volume reduction (for all 24 runs) and the fitted linear regression line (the coefficient of determination $R^2 = 0.81$).

Lag Time (T_{lag}) of swale outflow

The last swale flow hydrograph attribute examined was the outflow hydrograph lag time (T_{lag}), with respect to the inflow hydrograph, also listed in Table 3. This parameter bears significance for determining the time of concentration of runoff from the swale contributing area (i.e., a part of roadway and the swale footprint) for design purposes. The observed lag times in the 30-m swales studied varied between 5 and 15 minutes; the highest lag times (15 min) were noted for the 2-month event in Swale 1 and dry AMC. Lag times for individual runs varied in a similar way as flow volume reductions; the longest times were noted for the highest reductions and the shortest for the smallest volume reductions. The lag times were shorter in Swale 2 especially for dry AMC.

Lag times in Swales 1 and 2 were plotted as T_{lag} vs. SWC_{norm} in Fig. 6. The plot shows that the lag time decreases with the increasing SWC_{norm}, and the transition of the swale operation from a runoff volume control measures towards a stormwater conveyance element.

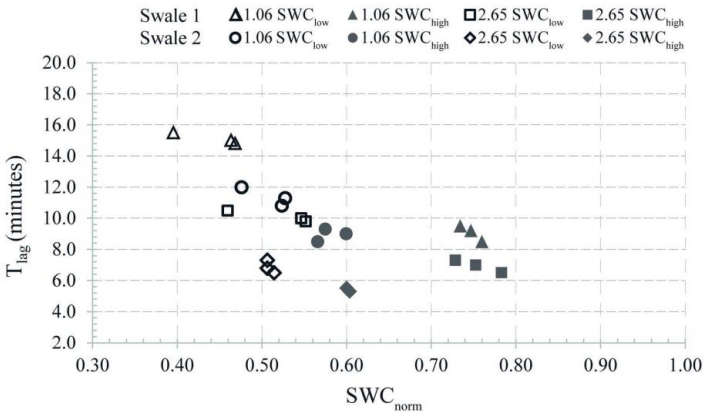

Figure 6 Outflow hydrograph lag time vs. normalized initial SWC for Swales 1 and 2.

Swale bottom slope and surface depressions

Swale channel may temporarily store water in bottom surface depressions. Based on the generated elevation models, the total depression volumes in the studied swales were estimated as 0.35 and 0.61 m^3 for Swales 1 and 2, respectively. Such volumes represented 7-18% and 12-31% of the inflow volume for Swales 1 and 2, respectively. These depressions function in a similar way as storage created by check berms used in some swale designs and are recognized for increasing flow attenuation (Davis et al., 2012).

4. Discussion

The discussion presented below focuses on swale general design and dimensions, soil characteristics, water balance, flow attenuation and lag time, experimental limitations of the collected data, and implications for swale design and research.

In Swedish practice, grass road swales are typically designed to convey runoff from design storms with return periods 5 to 10 years and a 10-minute duration (Swedish Transportation Administration, 2003). Such designs should provide acceptably low risks of erosion or flooding of the downstream areas. In the conditions tested, characterized by relatively short return periods (≤ 3 years) mimicked in field runs and short swale sections (30 m), there were no signs of swale flow approaching channel capacity, or the occurrence of erosion. It was noted that for a uniform flow in Swales 1 and 2, the flows calculated from Manning equation for a depth of 0.4 m were about an order of magnitude higher (0.127 and 0.129 m^3/s, respectively) than applied in the irrigation tests. The corresponding flow velocities (0.179 and 0.119 m/s, respectively) were safely below the limit of ≤ 0.915 m/s recommended by Schueler (1987) for the prevention of erosion. For high hydraulic loadings, the swale outflow would be controlled by the hydraulics characteristics of the inlet to the storm sewer system. In the case of

swale channel or sewer inlet blockage, the excess flow would spill onto the green areas on the swale side opposite to the roadways.

Runoff infiltration into swale soils is a highly influential process with respect to swale hydrology. Note however that in practical swale design, the options for selecting infiltration rates are limited – essentially to reference values of soils in the design area (notwithstanding disturbances of soils during construction, or additions of soil amendments). Additional options are available in field experiments, where the observations of swale flows can be supported by estimates of the saturated hydraulic conductivity K_s from field measurements with infiltrometers (NTCD , 2014; Ahmed et al., 2015; Fatehnia et al. 2016), or from analysis of flow hydrographs (Wanielista and Yousef, 1992).

Recent developments of the methods for K_s estimation based on discrete, point measurements of infiltration addressed the site-specific minimum numbers of measurements required to attain certain levels of uncertainty (Ahmed et al., 2015) and the development of faster ways of collecting infiltration data, compared to the commonly used double-ring infiltrometers. Working with a swale 350 m long, Ahmed et al. (2015) recommended 20 measurements for obtaining "a good estimation" of K_s; however, this number is likely affected by the variability of data in the specific dataset and the size of the area studied. Occurrences of physical soil structures (e.g., clay lenses, compacted soils, or macropores) may also provide some explanations of great variations in K_s data. A greater efficiency of collecting soil infiltration data was achieved by the development of the Modified Philip-Dunne (MPD) infiltrometer (Ahmed et al. 2015), which is a falling-head device allowing to conduct simultaneous infiltration measurements. Infiltration measurements obtained with the MPD and double-ring infiltrometers were found comparable, within an order of magnitude, by NTCD (2014).

For estimating K_s in the study reported herein, the preference was given to swale hydrographs (in and out) analysis, supplemented by cursory checks provided by double-ring infiltrometer (DRI) measurements and the texture-based reference data. Wanielista and Yousef (1992) calculated infiltration rates from the measured swale hydrographs at a site in Florida as 8.8 cm/h, which was significantly smaller than 12.7 cm/h measured by the DRI. The findings in this study also indicated differences between the infiltrometer measurements and flow hydrograph derived data for the whole test section (see Table 5). While in Swale 1 DRI data exceeded the hydrograph derived data, the opposite was true for Swale 2. A closer scrutiny of DRI data showed that they varied with the distance from the swale outlet; in Swale 1, the smaller K_s were measured near the outlet (where the flow depth and concentration is the greatest), and in Swale 2, the higher K_s were observed by the outlet. Thus, in Swale 1, the mean DRI K_s is likely to overestimate space-averaged K_s value, and in Swale 2, the mean DRI K_s is likely to underestimate the space averaged K_s. Assuming that the observed gradients in K_s were valid and caused by gradients in soil properties, the observed disagreement between the spatially integrated data (i.e., from flow hydrographs) and the DRI measurements would not improve even with higher numbers of K_s measurements with infiltrometer devices, without accounting for the above noted spatial

variations. However, infiltrometer data might be more meaningful for describing flow attenuation during real events, as suggested by Erickson et al. (2010).

During the experiments, some stretches of the swale bottom drained much faster, particularly at the upstream end exposed to the longitudinal inflow only. Slow drainage was observed where runoff clearly exceeded the infiltration capacity, e.g., at the downstream end. This would explain differences in saturation levels at the measurement locations and the fact that considerable flow abstractions occurred in the less saturated areas, which may have had a lower density of SWC probes.

Two additional factors may influence swale flow – the bottom slope and the related surface depressions on the bottom. The bottom slope influences the grass channel flow velocity and possibly the rate of infiltration. Morbidelli et al. (2016) tested infiltration rates on inclined planes and noted that the increased plane slope reduced infiltration, because water particles had less time to infiltrate. However, in drainage design, the choice of grass swale slopes is controlled by operational requirements. The literature lists numerous sources specifying the ranges of swale slopes facilitating positive drainage and/or preventing channel erosion. For example, The Urban Drainage and Flood Control District (2010) recommends the minimum longitudinal slope of 2%; for milder slopes, the swale may have to be fitted with an underdrain, and the maximum slope was recommended by Schueler (1987) as 5%. Both swales studied had milder slopes than the recommended minimum (Swale 1 -1.5% and Swale 2 - 0.7%), which may have contributed to the observed slow drainage of Swale 2 with prolonged durations of elevated soil wetness.

Depressions along the swale bottom were noted in detailed elevation surveys of both swales. Deviations of 0.05-0.10 m from the uniform slope line were common and created depression storage on the swale bottom, with estimated volumes of 0.35 and 0.61 m^3 in Swale 1 and 2, respectively. Such storage acts similarly as that in swales with check dams, generally contributing to higher runoff infiltration volumes and greater delays of outflow hydrographs, as e.g. reported by Davis et al. (2012). The role of temporary water storage in surface depressions and in the top soil layer bears more importance for buffering runoff from small rainstorms.

As reported by others (Pitt et al., 2008; Lee et al., 2016), the soil texture may not characterize well the actual infiltration in swales, because of variations in individual textural classes and spatial variability of soil characteristics within the studied facilities. In our study K_s estimated from the soil texture were about twice as large as those estimated from swale hydrographs in Swale 1, but smaller (by a factor of 0.6) in Swale 2, when compared to averages of the corresponding soil texture class (Nishat et al., 2010). Such discrepancies can be explained by the presence of thawing-freezing cycles (contributing to enhanced infiltration), macropores resulting from biological activity, or maintenance, as also suggested by other authors (Ahmed et al., 2015; García-Serrana et al., 2017). The measured SWC time series, together with the known effective saturation, therefore indicated that during the experimental runs with high inflows and 30 min. of

continuous swale bottom inundation, the available soil pore volume has never been saturated completely (as indicated by the SWC_{norm} data), which might be explained by the high flow velocities during swale irrigation.

Although the lateral overland flow on side slopes (sloping 1:2-2.5 in Swale 1 and 1:3-3.5 in Swale 2) was not measured in this study, it was observed that it may have partly infiltrated into the soil, even though the infiltration rates would be reduced on steep slopes (Morbidelli et al., 2016), but the infiltrated water may reappear on the surface in the lower part of the slope. The lateral inflow introduced by the water supply system over 24 m of the 30 m swale length generated finger-flow type of runoff with increasing coverage at higher inflows, as also reported by García-Serrana et al. (2017). When sheet flow was observed during irrigation runs, its width was less than 1 m. The nature of the swale instrumentation system did not allow differentiation between flows in the swale channel and down the side slope, which contributed to experimental uncertainties.

The relevance of knowledge of the SWC and its impact on runoff generation on plot-scale grass areas was also reported by García-Serrana et al. (2017), who quantified the influence of soil moisture (i.e., the difference between porosity and initial SWC) on the actual infiltration capacity and infiltrated volumes, and found that the infiltration rapidly rose at higher soil moisture deficits. Regarding the spatial heterogeneity of SWC, Morbidelli et al. (2012) concluded in a study of runoff hydrographs for a range of initial SWC values that a spatially averaged value of SWC was sufficient to reproducing hydrographs, but SWC became more relevant if the spatial variability of saturated hydraulic conductivity was considered. They hypothesized that spatially variable K_s masked the effect of different initial SWC on surface runoff.

Although the SWC for the operationally defined SWC_{low} (dry AMC) and SWC_{high} (wet AMC) conditions did not greatly differ, such differences affected outflow hydrographs, runoff retention and flow delay significantly. Particularly the small differences in SWC under dry conditions indicated potentially significant reductions in swale infiltration volume. The pattern of flow volume attenuation in our study follows that described by Davis et al. (2012) for swale drainage during intermediate-to-severe rainfalls. The relative swale volume reductions decreased with increasing inflows, i.e., for rain storms with longer return periods, as the infiltration capacity of swale soils was quickly reached and exceeded. Generally, the swale flow volume reductions from 15 to 82% found in this study for a set of 24 experiments agree with the results of grass swale investigations with comparable simulated constant inflow rates, as reported by Bäckström (2002) - 33-66% for 5-10 m swales with 0.5-7% slopes over 0.5 hours, Lucke et al. (2014) - 12-89%, in 30-35 m swales with ≤1% slope and concentrated inflow of 0.5 hours, or Yousef et al. (1987) - 9-100% in 53 and 170 m swales with 0.1-3.0% slopes and concentrated inflow of durations of 3-5.5 hours.

Limitations of the field experiments conducted need to be recognized with respect to the selected sites, their physical characteristics, including the soils, introduction of irrigation flows, and measurements of hydrological data focusing on the swale channel flow (no measurements done over the irrigated side slope). The test sections of the swales were limited to 30 m, in order to

achieve a well-defined flow distribution with the equipment available. However, even over these relatively short lengths, the swale characteristics were not perfectly uniform, but varied as should be expected for earthen structures in real life. Swale bottom longitudinal profiles indicated irregular slopes with local depressions functioning in a similar way as check-berms creating bottom surface storage. As pointed out e.g. by Davis et al. (2012) such storage increases flow attenuation in swales, for storms with small-to-intermediate rainfalls. Thus, in the experiments reported here infiltration was likely enhanced in both swales, to a various extent, with higher infiltration rates in the case of the lower hydraulic loading (corresponding to a 2-month event), and the milder slope (0.007, for Swale 2) contributing to greater surface depression storage (0.61 m^3 for Swale 2, compared to 0.35 m^3 for Swale 1). Considering the mild swale slopes and a fair magnitude of swale flows, clear differences of lag times in Swale 1 and Swale 2, due to infiltration, could not be detected.

The duration of controlled irrigation runs was limited to 30 minutes, as this was a practical limit of the irrigation water supply system and its controls. As noted for outflow hydrographs in Fig 4, longer inflows would have allowed fully reaching the equilibrium conditions for outflow from both swales, particularly in the case of dry AMC. However, the selected inflow duration was considered acceptable in relation to the estimated time of concentration of the runoff contributing area. Further uncertainties were introduced by splitting the inflow into longitudinal and lateral components, which was deemed necessary to mimic operation of actual swales. While an assumption has been made that flow over a short band of the irrigated side slope (0.5 – 1.0 m wide) would reach the swale channel flow, either above or below the ground surface, because of the steep slope, no experimental proof can be offered. Even though the SWC probes were placed in the same pattern and proximities with respect to the dual irrigation flow inlets, they were exposed to ponded water to different degrees, which may have affected the measurements due to different hydraulic heads and residence times of water adjacent to the measuring probes, contributing to increased SWC readings.

Implications of study results for swale design and future research

The study findings indicate the importance of the initial soil moisture conditions for the formation of the swale channel flow, depending on soils K_s. In sandy loams studied, the reestablishment of dry conditions would take at least two days, and in loamy sand, at least one day. Analysis of rainfall data for the antecedent dry days (ADDs) would serve to select and test the appropriate AMC. The collected data can be used to calibrate a rainfall/runoff model for a typical catchment comprising a swale section, with the associated runoff contributing area formed by a road, road shoulder and the swale. This model can then be used to examine various design scenarios. Additional practical findings include the need to check DRI measurements for spatial tendencies, which may skew estimates of K_s in specific cases. The experimental findings will be also of use to study the stormwater quality enhancement in grass swales during various stages of the development of swale channel flow. Finally, Swale 1 with loamy sand soil exhibits

high infiltration rates even after almost 60 years of operation. This follows from high storage capacity of the swale soil and adequate infiltration rates.

5. Conclusions

The primary motivation of the conducted swale experiments was to advance the knowledge of the influence of the initial soil moisture conditions on swale channel hydrographs. Within the limitations of the experimental program, the following conclusions can be drawn:

- The presentation of the relative swale flow reduction vs. the normalized soil water content illustrated, for the conditions studied, the principal grass swale functions in runoff control and conveyance; the transition between these two functions evolved from full runoff dissipation for low SWC and hydraulic loads to runoff conveyance at high SWC, with minimal runoff abstractions. The speed of this transition accelerated with increasing hydraulic loading and reduced K_s of swale soils. The variation of swale flow volume reduction for two sets of initial AMC (wet and dry) was in this study 36-73% and 17-36%, for swales 1 and 2, respectively.
- Swale outflow hydrograph lag times varied between 5 and 15 minutes and decreased with an increasing SWC_{norm}. Such information is of interest when estimating the time of concentration of the swale-road catchment.
- Comparisons of the swale inflow and outflow hydrographs for wet initial AMC indicated quasi-steady infiltration rates of 3.27 and 4.84 cm/h, in Swales 1 and 2, while the DRI data produced the corresponding average values of 9.41 and 1.78 cm/h, respectively. DRI data may have been affected by their spatial gradients specific to the study sites.

Acknowledgement

This study was conducted under the research cluster Stormwater & Sewers, supported by the Swedish Water and Wastewater Association (Svenskt Vatten), and was funded by the Swedish Research Council FORMAS, project 2015-121. The authors would also like to acknowledge support of the Technical and Urban Planning Departments of the Luleå municipality.

6. References

Ahiablame, L. M., Engel, B. A., & Chaubey, I. (2012). Effectiveness of low impact development practices: Literature review and suggestions for future research. *Water, Air, and Soil Pollution, 223*(7), 4253-4273.

Ahmed, F., Gulliver, J. S., & Nieber, J. L. (2015). Field infiltration measurements in grassed roadside drainage ditches: Spatial and temporal variability. *Journal of Hydrology, 530*, 604-611.

ASTM (2013). D5242, Standard Method for Open-Channel Flow Measurement of Water With Thin-Plate Weirs. *American Society of Testing and Materials, West Conshohocken, PA.*

ASTM (2009). D 7263, Standard test methods for laboratory determination of density (unit weight) of soil specimens. *American Society of Testing and Materials, West Conshohocken, PA.*

Bäckström, M. (2002). Sediment transport in grassed swales during simulated runoff events. Water Science and Technology, 45(7), 41-49.Barrett, M., Walsh, P., Jr., J., & Charbeneau, R. (1998). Performance of vegetative controls for treating highway runoff. *Journal of Environmental Engineering, 124*(11), 1121-1128.

Barrett M., Walsh P., Jr. J., Charbeneau R. (1998). Performance of Vegetative Controls for Treating Highway Runoff. *Journal of Environmental Engineering* 124 : 1121-8. DOI: 11(1121).

Dahlström, B. (2010). Regnintensitet–en molnfysikalisk betraktelse. [Rain Intensity – a cloud physical contemplation] (in Swedish). Report 2010-05, Swedish Water and Wastewater Association, Svenskt Vatten AB, Stockholm.

Davis, A. P., Stagge, J. H., Jamil, E., & Kim, H. (2012). Hydraulic performance of grass swales for managing highway runoff. *Water Research, 46*(20), 6775-6786.

Dietz, M. E. (2007). Low impact development practices: A review of current research and recommendations for future directions. *Water, Air, and Soil Pollution, 186*(1-4), 351-363.

Dietz, M. E., & Clausen, J. C. (2008). Stormwater runoff and export changes with development in a traditional and low impact subdivision. *Journal of Environmental Management, 87*(4), 560-566.

Dunne, T., & Leopold, L. B. (1978). *Water in environmental planning.* San Francisco, CA: W.H. Freeman and Company.

Erickson, A. J., Weiss, P. T., & Gulliver, J. S. (2010). *Stormwater treatment: Assessment and maintenance*. St. Anthony Falls Laboratory. Retrieved from the University of Minnesota Digital Conservancy, Minneapolis, Minnesota.

Evett, S., Heng, L., Moutonnet, P., & Nguyen, M. (2008). Field estimation of soil water content. *A Practical Guide to Methods, Instrumentation and Sensor Technology. International Atomic Energy Agency. Vienna, Austria,* , 131.

Fatehnia, M., Tawfiq, K., Ye, M. (2016). Estimation of saturated hydraulic conductivity from double-ring infiltrometer measurements. *European Journal of Soil Science*, 67, 135-147.

García-Serrana, M., Gulliver, J. S., & Nieber, J. L. (2017). Infiltration capacity of roadside filter strips with non-uniform overland flow. *Journal of Hydrology, 545*, 451-462.

Geerling, H. R. (2014). Infiltration Swales: Quantitative Performance on an Urban Catchment Scale". (M.Sc.) Delft University of Technology. Retrieved October 1, 2016, from http://www.tudelft.nl

Houle, J. J., Roseen, R. M., Ballestero, T. P., Puls, T. A., & Sherrard, J. (2013). Comparison of maintenance cost, labor demands, and system performance for LID and conventional stormwater management. *Journal of Environmental Engineering, 139*(7), 932-938.

ISCO, Teledyne (2009). 2150 Area Velocity Flow Module and Sensor Installation and Operation Guide. Lincoln, NE: ISCO Teledyne.

International Organization for Standardization (2009). ISO 11277: Soil quality-Determination of Particle Size Distribution on Mineral Soil Material - Method by Sieving and Sedimentation. *Beuth, Berlin.*

Lee, R. S., Traver, R. G., & Welker, A. L. (2016). Evaluation of soil class proxies for hydrologic performance of in situ bioinfiltration systems. *Journal of Sustainable Water in the Built Environment, 2*(4), 04016003.

Li, J., Orland, R., & Hogenbirk, T. (1998). Environmental road and lot drainage designs: Alternatives to the curb-gutter-sewer system. *Canadian Journal of Civil Engineering, 25*(1), 26-39.

Mohamed, M. A. K., Lucke, T., & Boogaard, F. (2013). Using swales to pre-treat stormwater runoff and prolong the effective life of permeable pavement systems. In *Proceedings of the 8th International Conference NOVATECH* (pp. 1-10). Novatech Graie.

Lucke, T., Mohamed, M. A. K.. Tindale, N. (2014). Pollutant Removal and Hydraulic Reduction Performance of Field Grassed Swales during Runoff Simulation Experiments. *Water*, 6: 1887-1904.

Morbidelli, R., Saltalippi, C., Flammini, A., Cifrodelli, M., Picciafuoco, T., Corradini, C., & Govindaraju, R. S. (2016). Laboratory investigation on the role of slope on infiltration over grassy soils. *Journal of Hydrology*, 543, Part B, 542-547.

Morbidelli, R., Corradini, C., Saltalippi, C., & Brocca, L. (2012). Initial soil water content as input to field-scale infiltration and surface runoff models. *Water Resources Management, 26*(7), 1793-1807.

Nevada Tahoe Conservation District (NTCD) (2014). Modified Philip-Dunne infiltrometer testing. NTCD, Zephyr Cove, NV, USA (available on line: http://lands.nv.gov/mwg-internal/de5fs23hu73ds/progress?id=xaWpBySHXXSs9DnMgq6VLba7WIEU7bYLTE0B6zqVyGE,&dl; accessed on Aug. 15, 2017).

Nishat, S., Guo, Y., & Baetz, B. (2010). Antecedent soil moisture conditions of different soil types in south-western ontario, canada. *Hydrological Processes, 24*(17), 2417-2424.

Pitt, R., Chen, S., Clark, S. E., Swenson, J., & Ong, C. K. (2008). Compaction's impacts on urban storm-water infiltration. *Journal of Irrigation and Drainage Engineering, 134*(5), 652-658.

Rawls, W., Brakensiek, D., & Saxtonn, K. (1982). Estimation of soil water properties. *Transactions of the ASAE, 25*(5), 1316-1320.

Schueler, T. (1987). Controling urban runoff: A practical manual for planning and designing urban BMPs. Washington Metropolitan Water Resources Planning Board, Washington, D.C., USA.

Shen, J. (1981). *Discharge characteristics of triangular-notch thin-plate weirs: Studies of flow to water over weirs and dams.* Water supply paper No.1617, U.S. Geological Survey.

Swedish National Land Survey (Landmäteriet) (2017). SWEPOS - Network-RTK-service, expected uncertainty. URL: https://swepos.lantmateriet.se/tjanster/realtid/natverksrtk/matosakerhet.aspx

Swedish Transport Administration (Trafikverket) (2003). *Vägdikens funktion och utforming-En beskrivning av multifunktionella diken*. [Road ditch function and design - A description of multifunctional ditches] (in Swedish). Publikation 2003:103. Borlänge: Trafikverket. Retrieved from: https://trafikverket.ineko.se/se/tv11607

UDFCD (Urban Drainage and Flood Control District) (2010). Urban storm drainage criteria manual, Vol. 3. UDFC, Denver, CO, USA.

Valinski, N. A., & Chandler, D. G. (2015). Infiltration performance of engineered surfaces commonly used for distributed stormwater management. *Journal of Environmental Management, 160*, 297-305.

Van Genuchten, M. T. (1980). A Closed-Form Equation for Predicting the Hydraulic Conductivity of Unsaturated Soils. *Soil Science Society of America Journal*, 44(5), 892-898.

Viklander, M., Marsalek, J., Malmquist, P. & Watt, W. E. (2003). Urban drainage and highway runoff in cold climates: Conference overview. *Water Science and Technology, 48*(9), 1-10.

Wanielista, M.P., Yousef, A.Y. (1992). Stormwater management. John Wiley & Sons, Inc., New York, N.Y., USA.

Watt, E., & Marsalek, J. (2013). Critical review of the evolution of the design storm event concept. *Canadian Journal of Civil Engineering, 40*(2), 105-113.

Yousef Y.A., Hvitved-Jacobsen T., Wanielista M.P., Harper H.H. (1987). Removal of contaminants in highway runoff flowing through swales. *Science of The Total Environment,* 59: 391-9. DOI: //dx.doi.org/10.1016/0048-9697(87)90462-1.

Zimmerman, M.J., Waldron, M.C., Barbaro, J.R., Sorenson, J.R., 2010. Effects of Low-impact-development (LID) Practices on Streamflow, Runoff Quality, and Runoff Quality in the Ipswich River Basin, Massachusetts: A Summary of Field and Modeling Studies, US Department of the Interior, US Geological Survey.

Paper III

Rujner, H., Leonhardt, G., Marsalek, J., & M. Viklander (submitted)

High-resolution modelling of the grass swale response to runoff inflows with Mike SHE.

(submitted to Journal of Hydrology, January 2018).

Rujner, H., Leonhardt, G., Marsalek, J., & M. Viklander (submitted). High-resolution modelling of the grass swale response to runoff inflows with Mike SHE. (submitted to Journal of Hydrology, January 2018).

High-resolution modelling of the grass swale response to runoff inflows with Mike SHE

Hendrik Rujner*, Günther Leonhardt, Jiri Marsalek, Maria Viklander

Department of Civil, Environmental and Natural Resources Engineering, Luleå University of Technology, Luleå 97187 Sweden

*Correspondence to: Department of Civil, Environmental and Natural Resources Engineering, Luleå University of Technology, 97187 Luleå, Sweden. E-mail: hendrik.rujner@ltu.se

Abstract

The feasibility of simulating the hydrological response of a grass swale to runoff inflows was examined using the hydrological model Mike SHE and the available input data from 12 irrigation events mimicking runoff from block rainfalls. The test swale channel had a trapezoidal cross-section, bottom slope of 1.5%, length of 30 m, and was built in loamy fine sand. The irrigation events consisted in releasing two equal constant inflows to the swale: a concentrated longitudinal flow at the upstream end and a distributed lateral inflow along the swale side slope adjacent to the contributing drainage area. The total inflows approximated runoff from two events with return periods of 2 months and 3 years, respectively, for durations of 30 minutes. Irrigation experiments were done for two states of the initial soil moisture, dry and wet antecedent moisture conditions (AMC). Mike SHE has been extensively used on catchments of various sizes, but rarely for small stormwater management facilities and their detailed topography investigated in this study. The latter application required high spatial and temporal resolutions, with computational cells of 0.2 x 0.2 m and time steps of 15 s. For dominant hydrological processes, the following computational options in Mike SHE were chosen: Soil infiltration - the Van Genuchten equation, unsaturated zone flow - the one-dimensional Richards equation, and overland flow – the diffusive wave approximation of the St. Venant equations. For study purposes, the model was calibrated for single events representing one of four combinations of low and high inflows, and dry and wet AMC, and then applied to the remaining 11 events. The goodness of fit was statistically assessed for observed and simulated peak flows, hydrograph volumes, Nash-Sutcliffe model efficiencies (NSE), and soil water content (SWC) in swale soil layers. The best fit (NSE > 0.8) was obtained for high inflows and wet AMC (i.e., when the primary swale function is flow conveyance); the least fit was noted for low inflows and dry AMC, when the primary swale function is flow attenuation. Furthermore, this observation indicates the overall importance of correct modelling of the soil infiltration. The effects of spatial variation of SWC on the swale discharge hydrograph could not be confirmed from simulation results, but high topographical accuracy was beneficial for reproducing well the locations of the observed water ponding. No significant increases in simulated SWC at 0.3 m or greater depths were noted, which agreed with field observations. Overall, the results indicated that Mike SHE was effective in process-oriented small-scale modelling of grass swale flow hydrographs.

Key words: Grass swale, distributed modelling, Mike SHE, soil water content, LID modelling

1. Introduction

The aging urban drainage infrastructure and anticipated upscaling of design rainfalls by climate change pose risks to urban populations and their environment. In search for risk mitigation measures, the decentralisation of stormwater drainage has been promoted together with practices helping restore natural hydrological functions of urban catchments. Such functions include storage, infiltration, and evapotranspiration of stormwater and can be substantially achieved by implementing urban Green Infrastructure (GI). However, the incorporation of GI measures into urban drainage challenges stormwater management, because of an increased heterogeneity of drainage processes and uncertain drainage capacities and operability (Dietz and Clausen 2008, etc.). This observation may help explain why local authorities are often hesitant to incorporate GI and low impact development (LID) measures in urban drainage systems.

Among the GI measures, relatively simple infiltration and conveyance structures, such as traditional grass drainage swales, represent low-cost, low-maintenance measures that can reduce the hydraulic and pollution loads to downstream drainage sections and receiving waters (Li & Hogenbirk, 1998; Zimmerman et al., 2010). Where space is available, grass swales are widely used as replacements of the conventional curb and gutter drainage (Dietz, 2007; Ahiablame et al., 2012) and serve to convey and attenuate stormwater runoff and improve its quality. The reduction of peak flow rates and runoff volumes is mainly achieved by infiltration of stormwater into the soils of the swale channel and by extending the time of concentration, which results in delayed discharges into downstream drainage facilities. Such benefits of swale operation vary with the rainstorm intensity: during intermediate and severe rainstorms, swales primarily act as runoff conveyance channels with minor flow reductions (Davis et al. 2012) that vary depending on the antecedent moisture conditions (AMC) and the saturated hydraulic conductivity (K_{sat}) of the swale soil (Pitt et al., 2008).

For implementing grass swales in the current drainage practice, mathematical models of swale flows are needed for designing such facilities and assessing their vulnerabilities in a changing climate. Even though some existing urban runoff models can be, and have been, applied in swale design, their applications may be subject to limitations arising from the fact that those models were principally built for other purposes (Elliot and Trowsdale, 2007). Consequently, other models dedicated to understanding swale operation also appeared in the literature.

Deletic (2002) developed the 1-D physically-based model TRAVA for runoff and sediment transport in grass swales. The model was further verified by Deletic and Fletcher (2005) and produced acceptably accurate predictions of swale outflows, but less satisfactory predictions of transport of total suspended solids (TSS). The conceptual model MUSIC was applied for Low Impact Development (LID) planning and simulations of flow and TSS transport in swales (Wong et al, 2006, Deletic and Fletcher, 2004). However, more recent attempts by Imteaz et al. (2013) to reproduce experimental observations in swales with the MUSIC were unsuccessful, raising the issue of general applicability of this model. Most recently, García-Serrana et al. (2017) published a "swale calculator" (Minnesota dry swale calculator) developed to simulate swale infiltration and flows, from the side slopes and in the swale channel, for varying soil moisture contents.

Besides the above research-oriented models, the feasibility of applying the leading hydrological modelling packages, including HSPF (Bicknell et al., 1997), Mike SHE (DHI, 2017), Mike Urban (DHI, 2016), and the SWMM (Rossmann, 2010) to modelling swales, has been also investigated. Helmers et al. (2006) applied uncalibrated Mike SHE to analyse the effects of spatial variability of hydraulic properties of a vegetative filter on outflow hydrographs generated by irrigation experiments. They used 26 samples of saturated hydraulic conductivity ranging from 0.36-13.30 cm/h, over an area of 13x15 m, selected the model spatial resolution of 0.76 m, and compared the results to simulations with spatially uniform soil

hydraulic properties, but found no significant differences. They noted that the simulation of higher inflow rates produced better agreements for overland flow (OL) travel times to the outlets. Ackerman and Stein (2008) used the continuous simulation model HSPF (The Hydrologic Simulation Program-FORTRAN) to study the sensitivity of swale drainage to model parameters over a range of storms and concluded that the swale effectiveness in improving stormwater quality increased with increasing infiltration rates of the underlying soils. Flanagan et al. (2017) used SWMM to simulate the treatment performance of a road-vegetative filter/swale system over a period of several years. They identified the saturated hydraulic conductivity of swale soils as the most sensitive model parameter, whose correct estimation reduced uncertainties in modelling results. Niazi et al. (2017) reviewed SWMM performance concerning calibration and verification, water-quality simulations and GI/LID design. They concluded that the model is well suited for large and medium scale applications, but may require coupling to other algorithms or models for simulating GI/LID implementation scenarios at small scales.

A recent field study of the hydrology of grass swales, focusing on generation of swale inflow and outflow hydrographs by irrigation, and measurements of swale soil water content (SWC) (Rujner et al. 2017; under review), offered an opportunity to examine the intricacies of applying Mike SHE to simulation of flows in grass swale channels. Consequently, such a study was undertaken with the following objectives: (i) Demonstrate whether swale inflow and outflow hydrographs, and the associated SWC changes, observed in field irrigation experiments, can be reproduced with the Mike SHE model, (ii) Calibrate Mike SHE for different calibration event characteristics and high temporal and spatial resolutions, and (iii) Identify the implications of Mike SHE calibration/verification simulations for model parameter selection and the predictive performance.

2. Methods

2.1 Study site and field data

Physical characteristics of the test site

The study site is a 30-m grass swale section located in the residential suburb of the City of Luleå, northern Sweden (65°35'03"N, 22°09'17"E), draining a two-lane road. The swale has a trapezoidal cross-section, with the bottom width varying from 0.2-0.7 m, the channel depths from 0.6 to 0.8 m, and relatively steep side slopes 1:2 to 1:2.5. Topographical information was collected at 486 elevation points with a RTK-GPS device and served to estimate the bottom slope as 1.5%. The swale design did not include any particular arrangement of soil layers, or the use of soil amendments, or an underdrain. The soil horizons consisted of ca. 0.1 m turf layer with organic material and loamy sandy soil, of which soil texture varied noticeably within the 30 m test section. A 0.1-0.5 m layer of homogeneous loamy sand and an underlying bed of sand and boulders followed. Double-ring infiltrometer (DRI) measurements at nine locations in the test section produced an average saturated hydraulic conductivity K_{sat}= 94.1 mm/hr (St. dev. 42.1 mm/hr).

Stormwater runoff simulation by irrigation

Twelve irrigation runs, with inflows of 1.06 or 2.65 L/s, were performed to mimic runoff corresponding to that generated by block rainfalls with the return periods of 2 month and 3 years, as estimated from the Swedish national IDF curves (Dahlström, 2010) and the Rational method. Two equal irrigation water inflows were introduced into the swale: a concentrated longitudinal inflow at the upstream end and a laterally distributed inflow (over 24 m, through 220 openings of a labyrinth weir) on the swale side slope next to the roadway. Each irrigation event with a low variability of the flow rate (see Fig. 1) lasted 0.5 h.

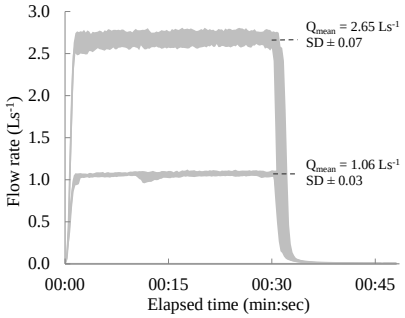

Figure 1: Two irrigation inflow rates measured during the field experiments in intervals of 15 s. Grey areas represent flow rate variations of the respective inflow rates for all the 12 experimental runs combined.

Beside the inflow and outflow, the SWC at 15 points, were measured continuously. Five SWC probes were located on the swale bottom, inserted at a 45°-angle up to a depth of 0.21 m, four probes each at irrigated and non-irrigated side slopes, inserted vertically and the remaining two were buried horizontally at swale channel depths of -0.3 and -0.6 m, approximately 1.5 m upstream of the outlet (see Fig.2). The experimental runs were initiated when the soil moisture reached a preselected state, which was affected by the antecedent rain events, or the earlier irrigation runs. The ranges of the corresponding measured soil water contents (SWC_{av}) are summarized in Table 1 for different locations in the swale as well as for two depths below the swale bottom. In the subsequent description of the experimental and simulation conditions, low soil moisture and high soil moisture are designated by symbols "*SM*↓" and "*SM*↑", respectively.

Table 1: Mean initial soil water contents at different sections and in two depths of -0.3 and -0.6 m of the study swale described as SM↓- and SM↑-conditions.

	Swale bottom (n=5)	**Non-irrigated side slope (n=4)**	**Irrigated side slope (n=4)**	**- 0.3 m below ground (n=1)**	**- 0.6 m below ground (n=1)**
SM↓ (as SWC_{av})	0.262, C_v = 0.14[1]	0.176, C_v = 0.08	0.209, C_v = 0.10	0.213, C_v = 0.04	0.197, C_v = 0.01
SM↑ (as SWC_{av})	0.391, C_v = 0.09	0.268, C_v = 0.06	0.295, C_v = 0.05	0.213, C_v = 0.02	0.200, C_v = 0.01

[1]Coefficient of variation

In each run, measurements were recorded for a total duration of 1:30 h. Inflow and outflow hydrograph data were used to calculate swale channel water balance for individual events. Table 2 summarizes the following experimental data: the inflow rate (Q_{in}), total inflow volume (V_{in}), total outflow volume (V_{out}), volume reduction (ΔV_{rel}), peak flow reduction ($\Delta Q_{pk\ rel}$) and the centroid lag time between the inflow and outflow hydrograph (T_{lag}).

Table 2 Water balance data from experimental runs used for model calibration and evaluation. Dates of experimental runs are used as identifiers with indicators of low and high initial SWC (SM↓, SM↑)

Event date	Q_{in} (L/s)	V_{in} (m^3)	V_{out} (m^3)	V_{inf} (m^3)	ΔV_{rel}	$\Delta Q_{pk\ rel}$	T_{lag} (min)
11/08-*SM*↓	1.07	1.97	0.76	1.22	0.62	0.29	15.0
15/08-*SM*↓	1.06	1.93	0.34	1.59	0.82	0.50	15.5
05/09-*SM*↓	1.09	2.06	0.47	1.59	0.77	0. 32	14.8
11/08-*SM*↑	1.04	1.90	1.45	0.45	0.23	0.16	9.2
11/08-*SM*↑	1.04	1.90	1.43	0.47	0.25	0.15	8.5
15/08-*SM*↑	1.06	1.94	1.30	0.64	0.33	0.21	9.5
30/08-*SM*↓	2.56	4.87	3.22	1.65	0.34	0.09	9.8
31/08-*SM*↓	2.67	4.97	3.02	1.95	0.39	0.13	10.0
03/09-*SM*↓	2.70	5.04	2.31	2.73	0.54	0.20	10.5
24/08-*SM*↑	2.76	4.98	4.13	0.85	0.17	0.05	7.3
26/08-*SM*↑	2.65	4.90	4.04	0.86	0.18	0.04	7.0
30/08-*SM*↑	2.62	4.85	4.12	0.73	0.15	0.07	6.5

2.2 Mike SHE

Mike SHE is a comprehensive hydrological model capable of simulating the main terrestrial water cycle and hydrological processes (Refsgaard and Storm, 1995; Sahoo et al. 2006). It was selected for this study, because it couples the overland flow (OL) processes with the unsaturated zone (UZ) flows by explicit simulation and the generation of high-resolution time series including the soil water content. As a raster-based model, its advantages include the capability to operate in various spatial (grid-) and temporal scales and account for different spatial and temporal variabilities of the catchment characteristics, with respect to the study objectives. In our study, the Mike SHE ver. 2017 application focused on simulating two components of the swale water balance: overland flow and infiltration into the UZ, but neglecting any feedback from the saturated zone (SZ). The model was set up and calibrated using the parameter values, initial conditions and input data from field measurements (saturated hydraulic conductivity K_{sat}, initial soil water content SWC_{ini}, saturated water content θ_{sat} as well as Q_{in}, Q_{out} and topography)(Rujner et al., 2017; under review), and supplementing such information by model default and literature values.

2.2.1 Model set up and simulation settings

Mike SHE was set up to represent the studied grass swale and to simulate the overland flow and processes in the unsaturated zone. The basic conceptual and computational settings of the model are listed in Tab. 3 for both the OL- and UZ-modules. To calculate OL, the diffusive wave approximation of the Saint-Venant equations was used, whereas the one-dimensional Richards equation (Richards, 1931) was solved for soil water movement in the UZ (DHI, 2017). The time step was selected with respect to the experimental runoff duration and the catchment size, and to match the time resolution of field measurements of 15 s. The numerical solver type for OL was selected as an explicit scheme (instead of the implicit iteration), which in Mike SHE generates more accurate results and is often used to calculate surface water flows during flooding. The model domain area covering the tested swale is 307.2 m^2 with a grid cell size of 0.04 m^2, which was considered reasonable with respect to the computational times required during the manual parameter estimation.

Table 3: Mike SHE Simulation specification for high-resolution swale modelling.

Simulation specification		Setting/value
Water Movement	Overland flow	Diffusive Wave, Finite difference solver
	Unsaturated flow	Richards equation
	Evapotranspiration	2.5 mm/day
	Time step control	
	Initial time step	15 sec
	Max OL and UZ time step	15 sec
Model domain		
	Catchment size and orientation	40 x 192 cells
	Cell size	0.2 x 0.2 m^2

Essential inputs for the Mike SHE model set-up can be arranged in the following categories:

- Hydro-meteorological inputs: rainfall (here replaced by near-surface irrigation, inflow), reference evapotranspiration
- Land use: vegetation (the leaf area index (LAI), root depth)
- OL: Manning M (equals the reciprocal value of Manning n, used hereafter), detention storage
- UZ: Soil profile definitions, initial water content

Although the simulation period is short, reference evapotranspiration was applied (2.5 mm/day; Eriksson, 1981), because the implementation of the Richards-equation in Mike SHE requires the definition of a sink term. Standard values for LAI and root depth were adopted for developed grass layers.

Inputs relevant for overland flow

Swale channel elevation points were used to generate a 0.1x 0.1-m grid digital elevation model (DEM) in ArcGIS. A higher resolution for the topography than in the model domain was used to allow the application of the multi-cell method in Mike SHE, which mitigates the loss of topographic detail relevant to detention storage and OL. Manning n and detention storage were considered as calibration parameters subject to adjustments and were set spatially uniform in the whole modelling domain.

Accounting for near-surface irrigation in the model

The Mike SHE´s model structure does not directly allow for a near-surface irrigation or an external inflow into the domain in a specific location. In order to reproduce the experimental inflow conditions in the model, the irrigated grid cells were assigned the inflow rate time series, which corresponded to their actual locations in the field (Fig. 2, depicted as arrows). Furthermore the cells upstream the inflow cells were assigned a hydraulic conductivity allowing no significant infiltration (with K_{sat} as low as $1*10^{-20}$ m/s). This arrangement allowed for controlled inflow, and in order to ensure that the directly introduced inflows from cells are routed towards the swale bottom, the model topography was modified upstream of the inflow points by means of steep slopes. For each of the near-surface irrigation events a spatial time series file was generated (=12).

Initial soil water content

The soil water content measured at 15 points was an important input to the model. Typically such measurements are considered valid for a 1-litre volume surrounding the sensor. However, to introduce some spatial variability of the initial SWC into the model, seven sub-sections were defined, five within the swale bottom and two on each of the irrigated and non-irrigated side slopes (Fig. 2). These subsections

were then assigned the SWC_{ini} values from the corresponding measurement probes. Initial SWC for each simulation represented the conditions measured in the field.

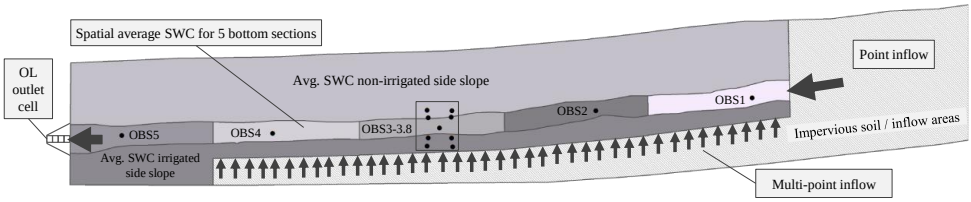

Figure 2: A plan view of the model domain of the studied swale composed of five sub-sections along the swale bottom, the irrigated and non-irrigated side slopes and the inflow sections (assigned minimum K_s and modified slopes to direct inflow). Inflow points and outflow directions are marked with arrows.

Soil profile definitions

Soils were represented uniformly along the swale modelled (except for the inflow areas) and defined in layers with uniform properties; those layers were further subdivided into computational layers. A model cross-section is presented in Fig. 3 showing the vertical discretization. State variables that affect vertical flow processes are calculated by the van Genuchten formula (Van Genuchten, 1980) for fitting the soil water retention curve in combination with the Mualem function (Mualem, 1976) for the relative hydraulic conductivity. The measured average K_{sat} was used for the first (top) soil layer. The measured maximum SWC was assumed to correspond to the saturated SWC (θ_{sat}) and applied uniformly for the entire swale; the residual water content θ_r, adopted here from Rawls et al. (1982) as $\theta_r = 0.035$ for loamy sand, was treated the same way. The Van-Genuchten parameters for the soil water retention curve n_r, α_r and for the relative hydraulic conductivity, n_c, α_c, and the curve fitting shape factors, were subject to calibration.

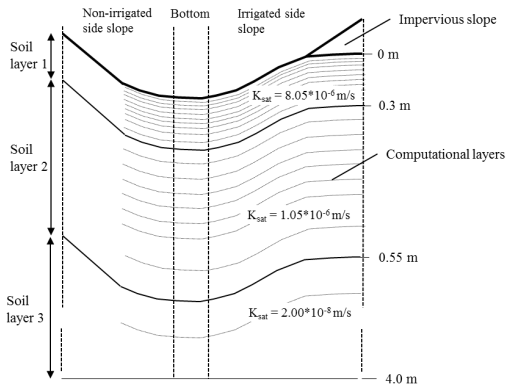

Figure 3: A schematic cross-section of the swale model in Mike SHE with three major soil layers and their subdivision into computational layers of various thicknesses.

2.4 Calibration parameters

Overland flow and infiltration into the unsaturated zone are the dominant processes in grass swales and the corresponding model parameters had to be calibrated. Consequently, Manning n and depression storage were calibrated for overland flow, and for the unsaturated zone, the Van-Genuchten parameters were calibrated. The model defaults or literature values were selected as starting values in the calibration process (see Tab. 4). The swale model comprised three major soil layers, whose layer-specific soil parameters could be adjusted. Soil parameters of the first layer were the most relevant calibration parameters, whereas the parameters of the lowest soil layer could be safely neglected.

Table 4: Initial parameterization of Mike SHE for adjusting the overland flow, and water infiltration and storage, in two soil layers (by Van-Genuchten parameters) and the corresponding initial values from the literature.

Module		Parameter	unit	Initial value	Reference
OL	Swale surface	Manning n[1]	$s/m^{1/3}$	0.1	Helmers et al. (2006)
		Detention storage	mm	1	default
UZ	Soil 1 VG Retention curve	n_{r1}[2]		3.85	Ghanbarjan-Alavijeh et al. (2016)
		α_{r1}	1/cm	0.007	Stephens et al. (1987)
	Soil 2 VG Retention curve	n_{r2}		3.85	Ghanbarjan-Alavijeh et al. (2016)
		α_{r2}	1/cm	0.007	Stephens et al. (1987)
	Soil 1 hydraulic conductivity	n_{c1}		3.85	Ghanbarjan-Alavijeh et al. (2016)
		α_{c1}	1/cm	0.007	Stephens et al. (1987)
		shape factor	(-)	0.001	default
	Soil 2 hydraulic conductivity	n_{c2}		3.85	Ghanbarjan-Alavijeh et al. (2016)
		α_{c2}	1/cm	0.007	Stephens et al. (1987)
		shape factor	(-)	0.001	default

[1] In Mike SHE Manning M is used; for clarity, we use the Manning coefficient n (=1/M) herein.

[2] the used reference provided values of m, which were converted to Van-Genuchten $n_{r/c}$ ($m=1-1/n_{r/c}$).

2.5 Manual calibration procedure

Four of the twelve events monitored in field experiments were selected for discrete-event model calibrations. These four events were characterized by different inflow conditions: low inflow rates (Q↓) + low soil moisture (SM↓) (event 11/08-SM↓), low inflow rate + high soil moisture (SM↑) (event 11/08-SM↑), high inflow rate (Q↑) + low soil moisture (event 30/08- SM↓) and high inflow rate + high soil moisture (event 26/08- SM↑). The reason for selecting these specific events was the fact that their initial SWC were close to the average initial SWC of the sets of three runs targeting the same values of initial SWC and inflows.

Manual parameter calibration was conducted by changing one parameter at a time, within the preselected individual intervals, while keeping the other parameters constant, and subsequently running the model. Visual comparisons of the outlet hydrographs, $Q_{out,\ obs}$ and $Q_{out,\ sim}$, formed the basis for deciding whether to continue or stop this iterative process. When assessing such an agreement, the emphasis was placed on similarities of the starting limbs, peak flows and the falling limb shapes. After acceptable agreement was noted, the Nash-Sutcliffe model efficiency coefficient (Nash and Sutcliffe, 1970) was calculated, and when it reached or exceeded the value of 0.95, the calibration process was stopped.

The manual calibration procedure followed a certain sequence for parameter adjustments to fit the simulated hydrograph (Fig. 4): 1. increasing α_{r1} and reducing n_{r1} to reach a reasonable hydraulic soil configuration, 2. Increasing α_{c1}, reducing n_{c1} to achieve an increase in OL generation, after that the detention storage and Manning n were adjusted to change the shape of the rising and falling limbs and the timing of the hydrograph on the time axis. The same procedure was applied for the second soil layer, but with insignificant effects on the simulated hydrographs. The resulting final four parameter sets (PS) are denoted with *PS-Q↓SM↓*, *PS-Q↓SM↑*, *PS-Q↑SM↓*, *PS-Q↑SM↑*.

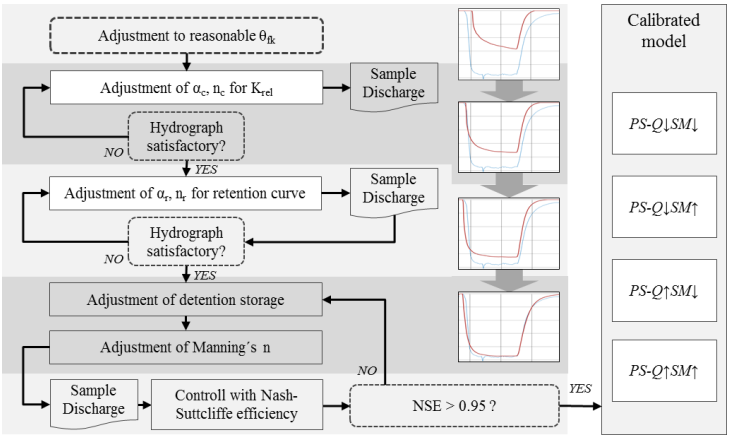

Figure 4: Manual calibration scheme for event-based calibration of the swale flow hydrographs.

2.6 Evaluation of the predictive power of the calibrated model

After the calibration of Mike SHE for each of the four calibration events was finalised, the calibrated model was evaluated against the remaining eleven events in the dataset, by comparing the measured and simulated V_{out}, Q_{out} and the average soil water content in the top 0.21 m layer of the UZ.

2.6.2 Statistical evaluation

To assess the performance of the individual calibration parameter sets, common statistical measures were used as listed below.

(i) Volumetric residual: $r_{vol} = V_{obs} - V_{sim}$

(ii) Normalised volumetric residual: $NVr = \frac{r_{vol}}{V_{obs}} - 1$

(iii) Peak flow residual: $E_{peak} = Q_{peak,\ sim} - Q_{peak,\ obs}$

(iv) Normalized peak flow residual: $NPFr = \frac{E_{peak}}{Q_{peak}}$ - 1

(v) Root mean squared error: RMSE = $\sqrt{\frac{1}{n}\sum_{i=1}^{n}(Q_{obs,i} - Q_{sim,i})^2}$

(vi) Nash-Sutcliffe model efficiency coefficient (Nash and Sutcliffe 1970):

$$E = 1 - \frac{\sum_{i=1}^{n}(Q_{obs,i} - Q_{sim,i})^2}{\sum_{i=1}^{n}(Q_{obs,i} - \overline{Q_{obs}})^2}$$

The last two statistics were calculated only for periods when either $Q_{sim} > 0$ or $Q_{obs} > 0$. The predictive performance for the SWC was measured only by the RMSE.

The calibrated parameter sets were analysed using the above criteria and the results for individual sets were mutually compared. Performance statistics were also applied to each inflow/SWC_{ini} condition, in order to identify for which the calibration produced satisfactory results. Those combinations were grouped and plotted by the following categories: 1. performance criteria – NVr, NPFr, NSE; 2. the inflow/SWC_{ini} conditions ($Q{\downarrow}SM{\downarrow}$, $Q{\downarrow}SM{\uparrow}$, $Q{\uparrow}SM{\downarrow}$, $Q{\uparrow}SM{\uparrow}$).

3. Results

The material presented in the results section is divided into the following subsections: (i) Manual model calibration, (ii) comparison of the observed and simulated swale discharge hydrographs, (iii) Predictive performance of the four calibration parameter sets, and (iv) agreement between the observed and simulated soil water contents.

3.1 Manual model calibration

Four individual event calibrations were performed to calibrate Mike SHE against the outflow hydrographs of four swale irrigation events, which resulted in four individual calibrated parameter sets, with the main calibration parameters limited to: two independent parameters of the Van-Genuchten (VG) soil water retention curve of the two top soil layers α_r n_r, two independent parameters of the VG relative hydraulic conductivity of the two top soil layers α_c n_c , and Manning n and depression storage values. An initial fitting of the VG retention curve by α_{r1} n_{r1} was done to achieve a reasonable specific yield and field capacity. Subsequently α_{c1} n_{c1} had to be adjusted to reduce the relative hydraulic conductivity to allow early excess flow and OL, as the initial parameter setting allowed complete abstraction of inflow. After that Manning n was increased to delay the outflow hydrograph and adjustments of the detention storage further increased the flow retardation and the flattening of the individual hydrograph limbs. In general, the parameters were adjusted in a way that the soil permeability was reduced in all PS. For SM↓ and SM↑, α_{c1} had to be increased (from 0.007 to at least 0.089) and n_{c1} reduced (from 3.85 to 1.28). It turned out that primarily n_c and secondarily α_c, had a strong influence on the magnitude of the resulting flow rate, and Manning n and detention storage exerted a strong influence on the timing and the duration of simulated discharges. For *Q*↓, Manning n had to be increased in order to delay outflow and to produce the typical "plateau" of the hydrographs visible in the measured data. Depression storage had to be increased significantly for low initial SWC in order to achieve meaningful results. The calibration process indicated that the soil parameters of the second soil layer, located at -0.3 to -0.55 m below the ground surface ($\alpha_{r2,}$ $n_{r2,}$ α_{c2} n_{r2}, shape factor) had negligible influence on the resulting hydrograph shape. The same finding also applied to the shape factor for both the water retention curve and relative hydraulic conductivity, which did not affect the tested hydrographs.

*Table 5: Final calibration results for two inflow rates (*Q↓, Q↑*) and two initial water contents (*SM↓, SM↑*)*

	Calibration parameter			*Q*↓	*Q*↑
SM↓	0-0.3 m	Retention curve	α_{r1} (1/cm)	0.02	0.01
			n_{r1}	3.0	4
		Hydraulic conductivity	α_{c1}	0.089	0.095
			n_{c1}	1.44	1.28
	Manning n ($s/m^{1/3}$)			0.26	0.2
	Depression storage (mm)			3.1	10
	0.3-0.55 m	Retention curve	α_{r2} (1/cm)	0.004	0.07
			n_{r2}	2.1	4.85
		Hydraulic conductivity	α_{c2}	0.009	0.09
			n_{c2}	1.5	1.7
SM↑	0-0.3 m	Retention curve	α_{r1} (1/cm)	0.007	0.018
			n_{r1}	4.55	3.2
		Hydraulic conductivity	α_{c1}	0.095	0.11
			n_{c1}	1.28	1.35
	Manning n ($s/m^{1/3}$)			0.11	0.18
	Depression storage			0.5	0.05
	0.3-0.55 m	Retention curve	α_{r2} (1/cm)	0.007	0.02
			n_{r2}	3.85	3.85
		Hydraulic conductivity	α_{c2}	0.007	0.01
			n_{c2}	3.85	3.85

3.2 Comparison of the observed and simulated swale outflow hydrographs

The final calibrated parameter sets for each of the four calibration events were used to simulate the remaining eleven evaluation events. The observed and simulated hydrographs of the calibration events are displayed in Fig 5 and indicate an excellent agreement, as also confirmed by high NSE values (see Tab. 6). The adjustments of calibration parameters allowed for an accurate alignment of the rising limbs and the hydrograph peak. Minor deviations occurred in the case of falling limbs and short duration disturbances of measured flows observed in Fig. 5d.

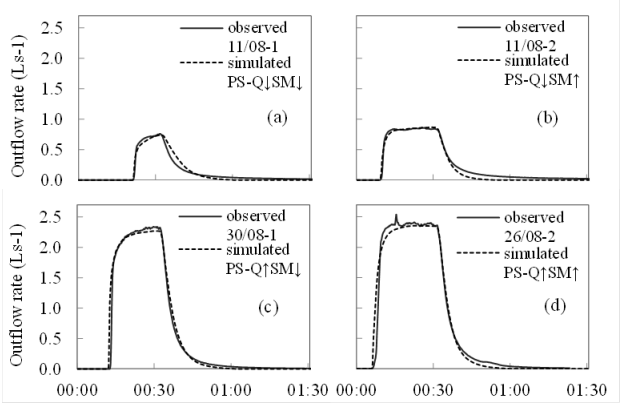

Figure 5 Observed and simulated hydrographs for a) PS-Q↓SM↓, b) PS-Q↓SM↑, c) PS-Q↑SM↓, d) PS-Q↑SM↑.

The plot of simulated hydrographs of the evaluation events (Fig. 6) indicates variations in the goodness of fit of the simulated to observed hydrographs, with main deviations in the simulated flow volumes and hydrograph lag times. It can be observed that the PS derived for low soil moisture underestimated the outflow from evaluation events with high soil moisture, and vice versa. Thus, the effects of changes in the initial SWC, as measured in the experiments, especially for events with low initial SWC, were not reproduced well. Such deviations were partially mitigated in the case of higher inflow rates, as seen in Fig. 6d. Peak flows were reproduced fairly well for various inflow conditions.

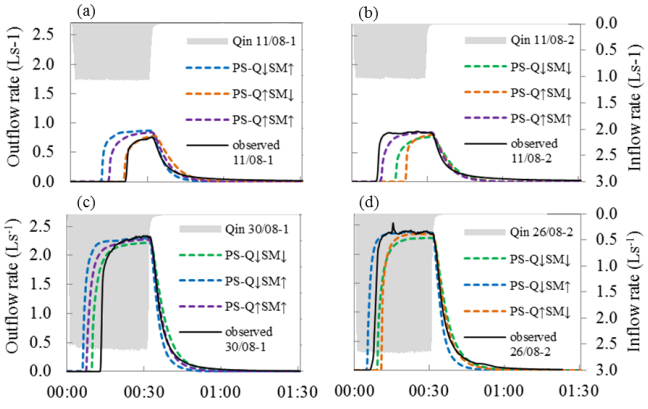

Figure 6 Goodness of fit of simulated evaluation event outflow hydrographs to the observed ones for the four parameter sets.

3.3 Predictive performance of the four calibration parameter sets

The calibration procedure indicated that the soil parameters that influence the hydraulic conductivity were critical parameters for generating surface runoff. The quantitative assessment of the performance criteria, including the volumetric residual and NSE for the calibration events as well as for all the (11) evaluation events, is summarized in Tab. 6 (peak flow residual and RMSE can be found in the supplementary material). In general, the smallest differences between the simulated and observed values and the lowest RMSEs were simulated with *PS-Q↓SM↓* and *PS-Q↑SM↓*. The RMSEs between these two PS as well as between *PS-Q↓SM↑* and *PS-Q↑SM↑* show similar patterns indicating a weak predictive performance for *Q↑* and *SM↓* events. Generally the model predictive efficiency is lower for PS derived for low initial soil moisture, compared to those for high initial soil moisture. The worst model performance was noted for *PS-Q↑SM↓* for *Q↓SM↑* events and for *PS-Q↓SM↑* and *PS-Q↑SM↑* for the 03/09-1 event. However, lower relative deviations from observations occurred with high flow rates.

Table 6: Statistics of simulated and observed hydrographs for the calibration events (first four) and the evaluation events.

		Event	*statistics*	*PS-* Q↓SM↓	*PS-* Q↓SM↑	*PS-* Q↑SM↓	*PS-* Q↑SM↑
*Calibration event I (*Q↓SM↓*)*		1108-1	r_{vol}	-9	-	-	-
			NSE	0.959	-	-	-
*Calibration event II (*Q↓SM↑*)*		1108-2	r_{vol}	-	-166	-	-
			NSE	-	0.982	-	-
*Calibration event III (*Q↑SM↓*)*		3008-1	r_{vol}	-	-	10	-
			NSE	-	-	0.980	-
*Calibration event IV (*Q↑SM↑*)*		26082	r_{vol}	-	-	-	-93
			NSE	-	-	-	0.982
Evaluation events	*Q↓SM↓*	1108-1	r_{vol}	-	436	-171	308
			NSE	-	0.402	0.659	0.616
		1508-1	r_{vol}	-301	-759	-141	-623
			NSE	0.638	0.083	0.776	0.242
		0509-1	r_{vol}	-107	500	-120	375
			NSE	0.913	0.323	0.855	0.525
	Q↓SM↑	1108-2	r_{vol}	-537	-	-694	-242
			NSE	0.194	-	-0.261	0.889
		1108-3	r_{vol}	-487	-123	-642	-194
			NSE	0.285	0.978	-0.141	0.923
		1508-2	r_{vol}	-360	15	-519	-61
			NSE	0.463	0.935	0.083	0.972
	Q↑SM↓	3008-1	r_{vol}	324	658	-	509
			NSE	0.886	0.674	-	0.791
		3108-1	r_{vol}	424	955	301	804
			NSE	0.892	0.619	0.937	0.736
		0309-1	r_{vol}	1198	1663	969	1490
			NSE	0.674	0.432	0.751	0.54
	Q↑SM↑	2408-2	r_{vol}	-465	-2	-600	-113
			NSE	0.936	0.87	0.878	0.952
		2608-2	r_{vol}	-442	14	-576	-
			NSE	0.915	0.915	0.848	-
		3008-2	r_{vol}	-520	-77	-657	-178
			NSE	0.895	0.913	0.824	0.978

Fig. 7 shows box plots of the normalized peak flow residuals, normalized volumetric residual as well as RMSE and NSE for each of the four PS (n=11). For all PS, peak flows were reproduced with minor residuals, while there was a large spread of the volumetric residuals, with an indication, that *PS-Q↓SM↓*and PS- Q↑SM↓ (parameter sets based on calibrations for low initial soil moisture) tended to underestimate volumes and *PS- Q↓SM↑* and PS- *Q↑SM↑* overestimated volumes as seen in the hydrograph plots. Event 03/09 with low initial soil moisture conditions (below the average) was the source of outliers

in the data sets. Concerning the box plot means, *PS- Q↓SM↓*and PS- *Q↑SM↑* achieved slighlty better results than the rest.

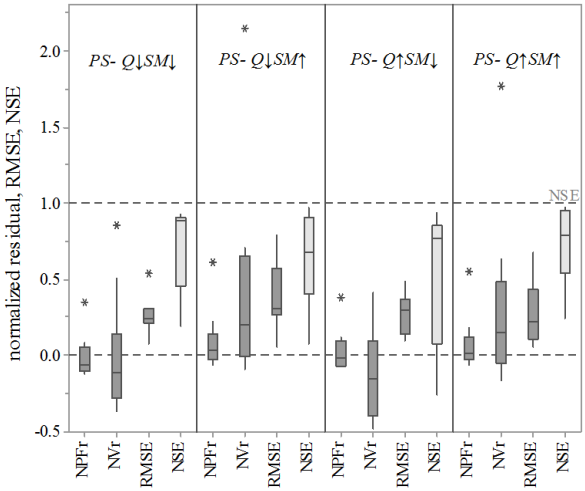

Figure 7: Overall predictive performance of the calibrated model: Normalized peak flow residual, normalized volumetric residual, RMSE and NSE (light grey) produced by PS-Q↓SM↓ *to* PS-Q↑SM↑ *(for each of n=11 samples). The top of the box is third quartile, the bottom the first quartile, the line in the box is the median and the whiskers show the lowest and highest values. Outliers are marked as asterisks.*

Independently of any specific parameter set, Figure 8a-c summarizes the performance of the model in reproducing various inflow conditions. It shows that independent of the parameter sets' specific setting , predictions are the worst for low inflow rates (*Q↓*) and low initial soil moisture (*SM↓*). The least residuals and the best model predictive efficiencies were noted for the event combination *PS-Q↑SM↑* indicating that the model calibrated with that specific parameter set is most robust.

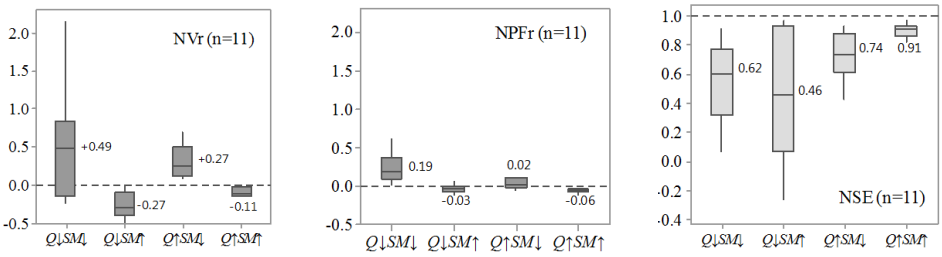

Figure 8: Box and whisker plots of the normalized volumetric residual, normalized peak flow residual and NSE for different inflow conditions and all parameter sets combined.

3.4 Agreement between the observed and simulated soil water contents

Soil water content measurements at the study site in the top 0.3 m soil layer indicated only minor water movement (Rujner et al. 2017, under review), which agrees well with the simulation results for the UZ.

While in the first computational layer (0.0-0.05 m) the maximum saturation was reached quickly, below 0.175 m, no significant increase in water content occurs within the 1.5 h simulation period. However, the SWC referred to represented SWC averaged over a 0.21 m soil layer and showed immediate and large changes, which only applied to SWC changes in the modelled UZ for the first two computational layers (see Fig. 9). Thus, to achieve an equivalency between the field and simulated measurements, SWC of the depth-weighted average of the computational layers 1-8 (which is equivalent to 0 - 0.20 m of soil depth) was calculated, compared to the observed values, and the RMSE was calculated.

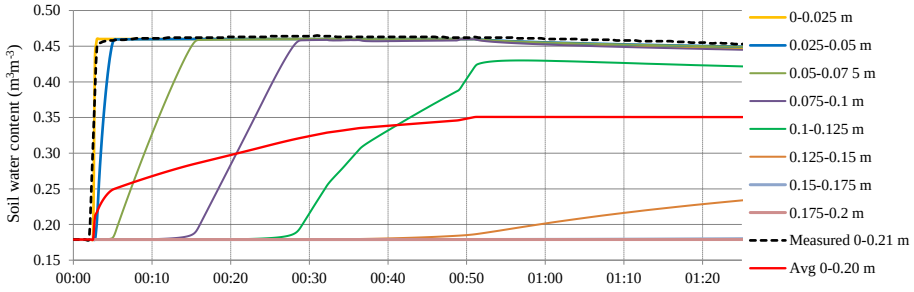

Figure 9: Progression of soil wetting in the vertical direction at a selected point in the model over eight computational layers and their average (red full line) compared to the measured SWC (black dashed line).

A sample diagram for one of the four calibration events, Fig. 10, shows the development of the mean SWC in the UZ and the measured SWC for five probe locations in the swale channel (OBS1=the closest to the swale inlet, OBS5 the closest to the outlet). Each of the simulated SWC is the depth-averaged SWC of eight computational layers of one UZ cell (where the SWC probe was located), which represents the top soil layer. Their θ_{sat} maximum limit of 0.455 m^3m^{-3}, corresponding to the highest observed saturation (measured at OBS1), was applied uniformly to all cells of the top UZ layers. Uniform θ_{sat} of the top UZ layers made simulated SWC, namely SIM2-SIM5, to be higher than observed. A θ_{sat} lower than the observed one would be in conflict with the initial SWC values, which were almost as high as θ_{sat} for high initial SWCs.

The different parameter sets also affect UZ water movement after the inflow stopped. While the SWC for *PS-Q↓SM↓*, *PS-Q↓SM↑ and PS-Q↑SM↑* stayed stagnant, the SWC for the *PS-Q↑SM↓* kept increasing.

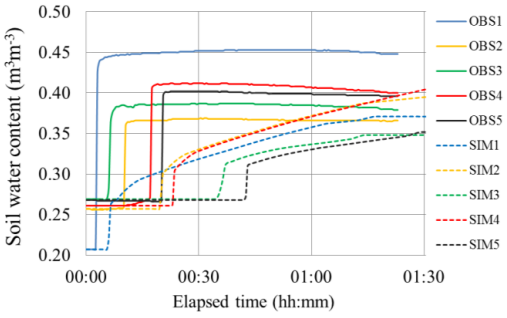

Figure 10 Observed (full line) and simulated (dashed line) development of the SWC for PS-Q↓SM↓.

Table 7 lists the RMSE between simulated and measured SWC at five probe locations, OBS1-5. The greatest residuals were found for simulations with low initial soil moisture, the smallest for high initial soil moisture. *PS-Q↓SM↑* simulates SWC with the least residuals, when focusing just on the UZ-layer averages. The reason for partly deviating agreement of the SWC can be explained by the limitation of having a single maximum SWC for the entire swale model, whereas in the field, the maximum reached SWC varied among probes.

Table 7 RMSEs between observed and simulated SWC for five points along the swale bottom.

PS	Stat	OBS-SIM 1	OBS-SIM **2**	OBS-SIM **3**	OBS-SIM **4**	OBS-SIM **5**	**Average**
PS-Q↓SM↓	RMSE	1.613	0.564	1.023	0.795	1.084	1.016
PS-Q↓SM↑		0.107	0.524	0.259	0.374	0.144	0.281
PS-Q↑SM↓		1.331	0.634	0.563	0.591	0.569	0.738
PS-Q↑SM↑		0.226	0.607	0.151	0.379	0.375	0.348

4. Discussion

Simulation runs with the calibrated Mike SHE confirm that a grass swale exposed to significant inflows functions mainly as a conveyance channel with minor attenuation of flow volumes and peaks. Due to the nature of irrigation experiments, Mike SHE was tested with respect to simulating the filling of swale channel soil storage and flow routing on gently inclined grass surfaces, for block-type inflow hydrographs. The outlet discharge could be reproduced by the model applied with high spatial and temporal resolutions, mostly with high agreements (NSE>0.8) between the observed and simulated hydrographs. In general, better agreement was achieved for runs with wet antecedent conditions and high inflow rates, but limited model sensitivity to changes in swale SWC was noted, as none of the applied model parameter sets produced satisfactory outlet discharges for increasingly dry antecedent conditions. Because of the relatively high hydraulic loading, the role of the unsaturated zone was of minor importance and consisted in controlling the supply of infiltration/saturation excess to the overland flow. After the swale inflow started, relatively fast soil saturation and the attainment of K_s infiltration rates could be reproduced in model simulations, with some storage in the upper UZ.

A systematic manual calibration was favoured over an automatic calibration, which is available for Mike SHE (DHI´s AUTOCAL) for the following reasons: the limited number of calibration parameters; a relatively homogeneous and simple swale structure in the form of a grass channel, and the interest in effects of soil-water calibration parameters needed for a better understanding of the results. In this regard, the calibration procedure strove to increase the validity of the calibration results and mitigate uncertainties which are associated with potential modeller's subjectivity (related to pre-selecting parameter values, selection of model simplifications, selection of model internal numeric engines, etc.) by performing four event-based calibrations for representative events for the four inflow conditions. In general, the automatic calibration is beneficial when applied in multi-event calibration and for long time series, which was not the case in our study. Using typical parameter values from the literature and especially the previously obtained model parameters, K_{sat} and saturated soil water content describing the swale soil (Rujner et al. 2017, under review), focussed the calibration efforts mainly on those parameters that regulate initial runoff infiltration (parameters of the retention curve and relative hydraulic conductivity of the top soil layer) and the hydraulic roughness/flow velocity of the overland flow, described by Manning n and depression storage. Because the swale acted as a conventional drainage channel at high flows, and a quasi-block shape of the inflow hydrograph, it was relatively easy to reproduce the peak outflow and the timing

of the outflow hydrograph. Most of the calibration effort was spent on finding satisfactory agreements of the rising and falling hydrograph limbs, between the observed and simulated hydrographs. The goodness of fit between the observed and simulated hydrographs benefited from the inflow hydrograph shape with a constant peak flow.

Typically, the capturing of spatial heterogeneity in modelling is limited by the number of field measurement points and further simplifications in the model will lead to a loss of information (Beven, 2012). Input data to our model were provided in different spatial resolutions. The inputs measured in an earlier study (Rujner et al. 2017, under review) were either represented by a single value (K_s, θ_s), or were spatially averaged in (five) model subsections (initial SWC), or given in a high spatial detail, like the near-surface irrigation and the topography. Such spatially defined inputs were then used in calculations for each of the 7,680 computational cells. Potential effects of the level of topographical detail on flow modelling in a vegetative filter were addressed by Helmers and Eisenhauer (2006) who noted significant effects on the simulated discharge hydrograph and recommended the use of an accurate spatial representation of the filter. Our simulation results confirm that recommendation.

Water ponding occurring in the swale channel depressions was observed in the field and contributed to a better agreement between the observed and simulated hydrographs. With an exact cell-based assignment of the inflow and its direction, and the relative topographical accuracy, the locations of ponding could be well reproduced in simulations. Such a feature would be of particular interest when modelling the sedimentation or pollutant removal performance of LIDs with overland runoff. The vertical resolution of the soil profile into three soil layers was less relevant when dealing with high inflows, but served as a useful reference for soil moisture measurements. More important seemed to be the thicknesses of the upper computational layers. According to the Mike SHE user manual (DHI, 2017) increased detail will contribute to generation of surface runoff, which could be confirmed in the initial testing with thicker computational layers leading to less, or even no overland flow.

Beside swale channel depressions, the parameters describing the swale roughness and influencing the time of concentration the most, Manning n and depression storage, had to be adjusted. Before proceeding with the systematic calibration, spatially variable Manning n was tested, but its effect was negligibly low. Thus, both Manning n and depression storage were assumed uniform over the entire swale length. Different modelling outcomes were obtained for low and high inflow rates, showing that both parameters depended on the inflow rate. While under dry initial conditions the calibrated Manning n was larger for low inflows (0.26) than for high inflows (0.2), under wet initial conditions, the opposite was true (n = 0.18, compared to n = 0.11). The calibrated Manning n´s were in the range also found by other authors like Deletic and Fletcher (2006) reporting n's for a grass swale of 0.05 to 0.2, Helmer and Eisenhauer (2006) reporting n = 0.1 for a grass strip, and Rossman (2009) reporting n = 0.24 for a grass swale.

The depression storage calibrated for dry initial conditions in the range from 3.1 to 10 mm was considered rather high. However, such values are comparable to those reported by Palla et al. (2015), who applied SWMM in modelling a LID unit, assumed 5 mm storage as representative for green areas. Krebs et al. (2014) calibrated SWMM in a relatively high-spatial resolution of urban catchments with LIDs and for lawn surfaces found the depression storage values ranging from 2.5 to 5 mm. In this study, much smaller values of calibrated depression storage were found for wet initial conditions, 0.5 mm for low inflow rates and 0.05 mm (~0 mm) for high inflow rates. Low depression storage was in agreement with the observed early generation of runoff in the swale. The applied multi-cell method considered a higher resolution of the topography (0.1x0.1 instead of 0.2x0.2) to adjust overland flow among cells. It was deemed beneficial

considering channel irregularities, the occurring ponding and the resulting flow attenuation, which would have been ignored by the coarser grid.

The calibrated Van-Genuchten parameters greatly varied: $\alpha_{c,r}$ = 0.004-0.11 and $n_{c,r}$ = 1.28 -4.85, and similar variations were also reported in the literature, with respect to the values derived from soil samples from a particular soil class and the subsequent fitting of the soil water retention curve. For loamy sand, Ghanbarian-Alavijeh et al. (2010) reported $0.024 \leq \alpha_{c,r} \leq 0.045$ and $1.33 \leq n_{c,r} \leq 2.56$, and Stephens et al. (1987) reported for various sands $2.01 \leq n_{c,r} \leq 5.15$ and $0.018 \leq \alpha_{c,r} \leq 0.11$. Parameters α_r and n_r, in particular, change the ability of the soil to retain or release certain amounts of infiltrated water, whereas α_c and n_c , which are required for calculating the relative hydraulic conductivity, regulate how fast the soil saturation is reached. Therefore, sample values related to LIDs/Swales could not be found directly in the literature, although the soil water retention and relative hydraulic conductivity appear to be meaningful values for understanding the hydrology at the plot scale. The initial soil water content varied in space, both horizontally (in seven subsections) and vertically (in three depths). Uniform K_{sat} and θ_{sat}, together with the distributed initial SWC resulted in the attainment of soil saturation in swale sections after various flow durations, which followed various durations of water ponding; however, these sequences had no significance for the generation of outlet discharge. Concerning the peak flow and discharge volume, the simulations showed that the model was hardly sensitive to spatial variations of SWC, which resulted in higher volumetric residuals for events with low initial SWC. When looking at the average Nash-Sutcliffe model efficiencies of evaluation events, the parameter sets adjusted for wet conditions yielded slightly better performance values than those for dry conditions, supporting the finding that hydraulic processes prevail at this stage and that calibration/simulation for soils with higher hydraulic conductivities or initial dryness is more challenging. In this study the integrated effect of the unsaturated zone can be, therefore, described as a flow attenuation layer for the incoming block rainfall/runoff. The above discussion implies that in Mike SHE simulations, the routing of known quantities of inflow is well reproducible, but the underlying calibration process produced just a minor gain in understanding the role of the unsaturated zone and its potential effects of water retention and redistribution, and the antecedent soil moisture on the discharge hydrograph.

Swale modelling is becoming more important with the increasing use and implementation of such facilities. Simulations of LID flows are in general as important as their monitoring studies, because they provide alternative insights into the performance of these practices with respect to hydrologic and water quality benefits (Ahiablame, 2012). To improve the confidence in model predictions, the understanding of physical processes in such facilities and of the applicable models is required. Besides the conceptual models, Mike SHE performed well in coupling main hydrological processes in high temporal and spatial resolutions. The two selected design storms of 2-month and 3-years return periods were too large to evaluate the hydrological features of a LID (grass swale) in detail; infiltration and retention testing on a continuous, multi-event basis with smaller rain intensities, would be required to take full advantage of the distributed Mike SHE model and to further assess the swale hydrology. The results of this study can, therefore, be perceived as an initial point for simulating small-scale LIDs with a process-oriented approach.

5. Conclusions

The feasibility of using Mike SHE for simulating the hydrological response of a grass swale to irrigation inflows was tested on a set of data for 12 swale irrigation experiments. Within the limitations of the

specific data set used and the small size of the tested runoff catchment, the following conclusions may be drawn:

- Simulations with Mike SHE confirm that a grass swale exposed to significant inflows functions mainly as a conveyance channel with minor attenuation of flow volumes and peaks. The model reproduced the outlet hydrographs with good agreements (NSE>0.8) between the observed and simulated hydrographs.
- Relatively high inflow rates to the swale revealed relatively minor importance of the unsaturated zone in swale flow formation, shown by the predominant adjustments for infiltration/saturation excess for generating overland flows (by reducing infiltration with relative hydraulic conductivity and soil retention curve parameters).
- Four model calibrations with discrete events indicated that the soil parameters influencing the soil water content dependant hydraulic conductivity are the critical parameters for generation of surface runoff.
- Model calibrations for events with low antecedent soil moisture conditions reduced the predictive efficiency of the model for other events with higher AMC, and calibrations against the events with high AMC resulted in better agreement between the observed and simulated discharge hydrographs. The highest Nash-Sutcliffe model efficiencies were found for calibration parameter sets reflecting high inflow and AMC values.
- Good accuracy of modelled topography was beneficial for predicting locations of water ponding in the swale, which would be of interest when dealing with modelling sedimentation and pollutant removal performance of swales.
- The model output was little sensitive to spatial variations of the soil water content, which resulted in larger residuals in simulated runoff peak flows and volumes, especially for dry AMC. This suggests that calibrations / simulations for soils with higher hydraulic conductivities or very low initial soil moistures will be more challenging.
- The presented study findings for modelling grass swale flows indicate a good potential of distributed hydrological models, like Mike SHE, to be applied in process-oriented simulations of swales and similar small-scale LIDs.

Acknowledgement

This study was conducted under the research cluster Stormwater & Sewers, supported by the Swedish Water and Wastewater Association (Svenskt Vatten), and within the framework of the GreenNano project partially funded by FORMAS (grant 2015-151) and VINNOVA.

References

Ackerman, D. and E.D. Stein (2008). Evaluating the effectiveness of best management practices using dynamic modeling. J. Environ. Eng. 134(8): 628 – 639.

Ahiablame, L. M., Engel, B. A., & Chaubey, I. (2012). Effectiveness of low impact development practices: Literature review and suggestions for future research. Water, Air, and Soil Pollution, 223(7), 4253-4273.

Beven, K.J. (2012). Rainfall–runoff modelling-The Primer.2nd Edition. Chichester: JohnWiley & Sons Ltd

Bicknell, B.R., Imhoff, J.C., Kittle, J.L., Jr., Donigian, A.S., Jr., and Johanson, R.C. (1997). Hydrological Simulation Program--Fortran: User's manual for version 11: U.S. Environmental Protection Agency, National Exposure Research Laboratory, Athens, Ga., EPA/600/R-97/080, 755 p.

Dahlström, B. (2010). Regnintensitet–en molnfysikalisk betraktelse. [Rain Intensity – a cloud physical contemplation] (in Swedish). Report 2010-05, Swedish Water and Wastewater Association, Svenskt Vatten AB, Stockholm.

Davis, A. P., Stagge, J. H., Jamil, E., & Kim, H. (2012). Hydraulic performance of grass swales for managing highway runoff. Water Research, 46(20), 6775-6786.

Deletic, A. (2001). Modelling of water and sediment transport over grass areas, Journal of Hydrology, 248(1-4), 168-182.

Deletic A., Fletcher T.D. (2006). Performance of grass filters used for stormwater treatment - A field and modelling study. Journal of Hydrology 317 : 261-75. DOI: 10.1016/j.jhydrol.2005.05.021.

DHI (2017). MIKE SHE User Manual. Hørsholm, Denmark: Danish Hydraulic Institute.

DHI (Danish Hydraulic Institute) (2016). Mike URBAN User Manual.

Dietz, M. E. (2007). Low impact development practices: A review of current research and recommendations for future directions. Water, Air, and Soil Pollution, 186(1-4), 351-363.

Dietz, M. E., & Clausen, J. C. (2008). Stormwater runoff and export changes with development in a traditional and low impact subdivision. Journal of Environmental Management, 87(4), 560-566.

Eriksson, B. (1981). Den "potentiella" evapotranspirationen i Sverige. [The potential evapotranspiration in Sweden] (in Swedish). RMK 28, RHO27, SMHI, Norrköping

Flanagan, K., Branchu, P., Ramier, D., & Gromaire, M. C. (2017). Evaluation of the relative roles of a vegetative filter strip and a biofiltration swale in a treatment train for road runoff. Water Science and Technology, 75(4), 987-997.

García-Serrana, M., Gulliver, J. S., & Nieber, J. L. (2017). Non-uniform overland flow-infiltration model for roadside swales. Journal of Hydrology, 552, 586-599.

Ghanbarian-Alavijeh, B., Liaghat, A., Huang, G. H., & Van Genuchten, M. T. (2010). Estimation of the van Genuchten soil water retention properties from soil textural data. Pedosphere, 20(4), 456-465.

Helmers, M. J., & Eisenhauer, D. E. (2006). Overland flow modeling in a vegetative filter considering non-planar topography and spatial variability of soil hydraulic properties and vegetation density. Journal of hydrology, 328(1), 267-282.

Imteaz M.A., Ahsan A., Rahman A., Mekanik F. (2013). Modelling stormwater treatment systems using MUSIC: Accuracy. Resources, Conservation and Recycling 71 : 15-21.

Krebs, G., Kokkonen, T., Valtanen, M., Setälä, H., & Koivusalo, H. (2014). Spatial resolution considerations for urban hydrological modelling. Journal of hydrology, 512, 482-497.

Li, J., Orland, R., & Hogenbirk, T. (1998). Environmental road and lot drainage designs: Alternatives to the curb-gutter-sewer system. Canadian Journal of Civil Engineering, 25(1), 26-39. //doi.org/10.1016/j.resconrec.2012.11.007.

Mualem, Y. (1976). A new model for predicting the hydraulic conductivity of unsaturated storm-water infiltration. J. Irrig. Drain Eng. 134(5): 652 – 658.

Nash, J. E.; Sutcliffe, J. V. (1970). "River flow forecasting through conceptual models part I — A discussion of principles". Journal of Hydrology. 10 (3): 282–290. doi:10.1016/0022-1694(70)90255-6

Niazi, M., Nietch, C., Maghrebi, M., Jackson, N., Bennett, B. R., Tryby, M., & Massoudieh, A. (2017). Storm water management model: performance review and gap analysis. Journal of Sustainable Water in the Built Environment, 3(2), 04017002.

Palla, A., Gnecco, I., & La Barbera, P. (2017). The impact of domestic rainwater harvesting systems in storm water runoff mitigation at the urban block scale. Journal of Environmental Management, 191, 297-305.

Pitt, R., S. Chen, S.E. Clark, J. Swenson, and C.K. Ong. (2008). Compaction's impacts on urban porous media. Water Resour. Res. 12 (3), 513‑522.

Rawls, W., Brakensiek, D., & Saxtonn, K. (1982). Estimation of soil water properties. Transactions of the ASAE, 25(5), 1316-1320.

Refsgaard J.C., Storm B. (1990). Construction, calibration and validation of hydrological models. . In Distributed hydrological modelling. Springer; 41-54.

Richards, L.A. (1931). Capillary conduction of liquids through porous mediums. J. Appl. Phys. 1 (5), 318‑333.

Rossman, L.A. (2009). Stormwater management model: User´s manual version 5.0. United States Environmental Protection Agency (USEPA), EPA/600/R-05/040, Cincinnati, OH.

Rossman L.A. 2010. Modeling low impact development alternatives with SWMM. Journal of Water Management Modeling.

Rujner, H., Leonhardt, G., Marsalek, J., & Viklander, M. (under review). The effects of initial soil moisture conditions on swale flow hydrographs. Submitted to Hydrological Processes Journal (October 2017).

Sahoo, G.B, C. Ray, and E.H. De Carlo. (2006). Calibration and validation of a physically distributed hydrological model, MIKE SHE, to predict streamflow at high frequency in a flashy mountainous Hawaii stream. Journal of Contaminant Hydrology. In Press.

Stephens D.B., Lambert K., Watson D. (1987). Regression models for hydraulic conductivity and field test of the borehole permeameter. Water Resources Research 23 : 2207-14. DOI: 10.1029/WR023i012p02207.

Van Genuchten, M. T. (1980). A Closed-Form Equation for Predicting the Hydraulic Conductivity of Unsaturated Soils. Soil Science Society of America Journal, 44(5), 892-898.

Wong, T.H.F., Fletcher, T.D., Duncan, H.P. and G.A. Jenkins (2006). Modelling urban stormwater treatment – A unified approach, Ecological Engineering, 27(1), 58-70(2004).

Zimmerman, M.J., Waldron, M.C., Barbaro, J.R., Sorenson, J.R. (2010). Effects of Low-impact-development (LID) Practices on Streamflow, Runoff Quality, and Runoff Quality in the Ipswich River Basin, Massachusetts: A Summary of Field and Modeling Studies, US Department of the Interior, US Geological Survey.

Zölch, T., Henze, L., Keilholz, P., & Pauleit, S. (2017). Regulating urban surface runoff through nature-based solutions–An assessment at the micro-scale. Environmental Research, 157, 135-144.